UNIVERSITY OF ALBERTA

Block Shear Behaviour of Bolted Gusset Plates

by

Bino Baljit Singh Huns

A thesis submitted to the Faculty of Graduate Studies and Research in partial fulfillment of the requirements for the degree of Master of Science

in

Structural Engineering

Department of Civil and Environmental Engineering

Edmonton, Alberta

Spring 2003

National Library of Canada
Acquisitions and Bibliographic Services
395 Wellington Street
Ottawa ON K1A 0N4
Canada

Bibliothèque nationale du Canada
Acquisitions et services bibliographiques
395, rue Wellington
Ottawa ON K1A 0N4
Canada

Your file Votre référence

Our file Notre référence

The author has granted a non-exclusive licence allowing the National Library of Canada to reproduce, loan, distribute or sell copies of this thesis in microform, paper or electronic formats.

L'auteur a accordé une licence non exclusive permettant à la Bibliothèque nationale du Canada de reproduire, prêter, distribuer ou vendre des copies de cette thèse sous la forme de microfiche/film, de reproduction sur papier ou sur format électronique.

The author retains ownership of the copyright in this thesis. Neither the thesis nor substantial extracts from it may be printed or otherwise reproduced without the author's permission.

L'auteur conserve la propriété du droit d'auteur qui protège cette thèse. Ni la thèse ni des extraits substantiels de celle-ci ne doivent être imprimés ou autrement reproduits sans son autorisation.

0-612-82292-3

Canada

UNIVERSITY OF ALBERTA

LIBRARY RELEASE FORM

NAME OF AUTHOR:	BINO BALJIT SINGH HUNS
TITLE OF THESIS:	BLOCK SHEAR BEHAVIOUR OF BOLTED GUSSET PLATES
DEGREE:	MASTER OF SCIENCE
YEAR THIS DEGREE GRANTED:	2003

Permission is hereby granted to the University of Alberta Library to reproduce single copies of this thesis and to lend or sell such copies for private, scholarly or scientific research purposes only.

The author reserves all other publication and other rights in association with the copyright in the thesis, and except as herein before provided, neither the thesis nor any substantial portion thereof may be printed or otherwise reproduced in any material form whatever without the author's prior written permission.

10923-81 Street
Edmonton, Alberta T5H 1L6

Date: Dec 9, 2002

UNIVERSITY OF ALBERTA

FACULTY OF GRADUATE STUDIES AND RESEARCH

The undersigned certify that they have read, and recommend to the Faculty of Graduate Studies and Research for acceptance, a thesis entitled BLOCK SHEAR BEHAVIOUR OF BOLTED GUSSET PLATES submitted by BINO BALJIT SINGH HUNS in partial fulfillment of the requirements for the degree of Master of Science in Structural Engineering.

Dr. G. Y. Grondin, Co-Supervisor

Dr. R. G. Driver, Co-Supervisor

Dr. P.-Y. Ben Jar, External Examiner

Date: Dec. 7, 2002

ABSTRACT

Despite the large database of test results on block shear in gusset plates, the exact progression of the failure mechanism is not clear. Although current design equations predict the block shear capacity of gusset plates fairly well, it is important for a design equation not only to predict the capacity reliably, but also to predict accurately the failure mode. Current research at the University of Alberta makes use of a non-linear finite element model to study the block shear behaviour in gusset plates. The model was designed to predict the sequence of events that leads to the tear-out of a block of material from a gusset plate in tension. The model is developed to provide a useful tool to study block shear failure not only in gusset plates, but also in other members such as coped beams. This thesis presents the development of the finite element procedure for prediction of block shear failure in gusset plates and presents an assessment of several design equations for block shear in gusset plates. A limit states design equation that predicts well the observed failure mode and provides an adequate level of safety is proposed.

ACKNOWLEDGEMENTS

Collaboration is a higher value than independence.

Writing a thesis is a major undertaking, which could not be accomplished without the love and support of family. First and foremost, I would like to thank my Father and Mother, Charan Huns and Faithful Lo Formigoni for instilling in me the confidence to believe in myself and all I set forth to accomplish. To my wife, Livia, for her endless love, support and encouragement. You sheltered me with a place of comfort yet inspired me with the will to succeed. To the Huns and the Formigoni family for their continued love and reassurance every step of the way. And to my wife's family, the Gortva family, for their complete faith and adoration.

I thank my supervisor, Dr. Gilbert Grondin, for his encouragement, guidance, and wisdom throughout this project. I thank you for always having the time to see me even with your busy schedule. I also thank you for your commitment to my project from the very beginning to the very end.

To my supervisor, Dr. Robert Driver, for your wisdom and advice through this project. I thank you for giving me the opportunity to present my project in the 4th Structural Specialty Conference in Montreal, Quebec.

To my colleagues Clinton Miller, Anthony Ng and Peter Song for always lending a helping hand whenever I needed help studying for exams. To Anthony Ng and Angus Lam for assisting with assembling and dismantling my test assembly.

To the Mary Louise Imrie Graduate Student Award and to the Graduate Student Association for providing travel assistance to the 4th Structural Specialty Conference in Montreal, Quebec. To the Steel Structures Education Foundation, the C. W. Carry Chair for Research of the University of Alberta, and the Natural Sciences and Engineering Research Council of Canada for their financial support in this project.

This thesis is dedicated to the
loving memory of my Grandfather

Gurdial Singh Huns

who always believed in me and
who inspired me to succeed in life.

And to my wife

Livia Huns

for her love, support
and encouragement

TABLE OF CONTENTS

1. INTRODUCTION

1.1. General 1

1.2. Objectives and Scope 2

1.3. Organization of Thesis 3

2. LITERATURE REVIEW

2.1. Introduction 4

2.2. Block Shear in Gusset Plate 5

2.2.1 Bjorhovde and Chakrabarti (1983, 1985) 5

2.2.2 Hardash and Bjorhovde (1984) 6

2.2.3 Gusset Plate Research at University of Alberta 7

2.2.4 Epstein and Chamarajanagar (1994) 9

2.2.5 Udagawa and Yamada (1998) 9

2.2.6 Aalberg and Larsen (1999) 10

2.2.7 Menzemer, Fei and Srivatsan (1999) 10

2.2.8 Swanson and Leon (2000) 11

2.2. Design Standards 11

*2.3.1 CAN/*CSA–*S16.1–94* 11

2.3.2 CSA–S16–01 12

2.3.3 AISC 1999 12

2.3. Summary 13

3. EXPERIMENTAL PROGRAM

3.1. Introduction 15

3.2. Description of Test Specimens, Test Assembly and Instrumentation 15

3.3. Material Properties 16

3.4. Testing Procedure 17

3.5. Experimental Results 18

3.5.1 Specimen T1A 18

3.5.2 Specimen T1B 19

3.5.3 Specimen T1C 19
3.5.4 Specimen T2A 20
3.5.5 Specimen T2B 20
3.5.6 Specimen T2C 21
3.6 Summary 22

4. FINITE ELEMENT ANALYSIS AND RESULTS
4.1. Introduction 47
4.2. Finite Element Model 47
4.3. Mesh Refinement Study 49
4.4. Modelling of Fracture on the Tension Face 50
4.5. Modelling of Fracture on the Shear Planes 52
4.6. Comparison of Finite Element Analysis with Test Results 53
4.6.1 Nast et al. (1999) 54
4.6.2 Hardash and Bjorhovde (1984) 54
4.6.3 Mullin (2002) 55
4.6.4 Udagawa and Yamada (1998) 56
4.6.5 Gusset Plates from Current Investigation 57
4.7 Parametric Study 58
4.7.1 Plate 1 - Long and Narrow Connection 59
4.7.2 Plate 2 - Long and Wide Connection 59
4.7.3 Plate 3 - Short and Narrow Connection 60
4.7.4 Plate 4 – Short and Wide Connection 60
4.7.5 Plate 5 – Long Bolt Spacing and Wide Connection 60
4.8 Summary 61

5. STATISTICAL ANALYSIS OF TEST RESULTS
5.1. Introduction 103
5.2. Background to Limit States Design 103
5.3. Professional Factor 104
5.3.1 CAN/CSA–S16.1–94 105
5.3.2 CSA–S16–01 106

5.3.3 AISC 1999 Specification 106
5.3.4 Hardash and Bjorhovde (1984) 107
5.3.5 Kulak and Grondin (2001) 108
5.3.6 Proposed New Equation 108
5.4 Material Factor 109
5.5 Geometric Factor 110
5.6 Calculation of Resistance Factor 110

6. SUMMARY, CONCLUSIONS AND RECOMMENDATION

6.1. Summary 116
6.2. Conclusions 117
6.3. Recommendations 118

REFERENCES 119

APPENDIX A - Published Gusset Plate Test Results 124

APPENDIX B - Summary of Predicted Gusset Plate Capacities 132

LIST OF TABLES

Table		Page
3-1	Ancillary test results	23
3-2	Block shear test results	23
4-1	Definition of the plastic portion of the true stress vs. true strain curve for the finite element analysis	62
4-2	Comparison of finite element predicted capacity with test results	63
4-3	Range of parameters for all gusset plates investigated experimentally	64
4-4	Gusset plates used in the parametric study	64
5-1	Calculation of resistance factor	112
A-1	Summary of gusset plate specimens	126
B-1	Summary of measured and predicted capacities of published test data	134
B-2	Test to predicted ratios for various resistance equations	139

LIST OF FIGURES

Figure		Page
2-1	Definition of dimensional parameters	14
3-1	Test specimens T1A, T1B, and T1C	24
3-2	Typical bolt layout and numbering for test specimens T1A, T1B and T1C	24
3-3	Test specimen T2A	25
3-4	Typical bolt layout and numbering for test specimen T2A	25
3-5	Test specimens T2B and T2C	26
3-6	Typical bolt layout and numbering for test specimens T2B and T2C	26
3-7	Test set-up	27
3-8	Diagram of test set-up	28
3-9	Side view of test set-up	29
3-10	Instrumentation of test specimen	30
3-11	Connection of the aluminium bar at the displacement point	31
3-12	Connection of the aluminium bar at the displacement point	31
3-13	Load vs. deformation curve for specimen T1A	32
3-14	Specimen T1A at 2 mm displacement	32
3-15	Specimen T1A at 11 mm displacement	33
3-16	Specimen T1A at 12 mm displacement	34
3-17	Specimen T1A at 19 mm displacement	35
3-18	Specimen T1A at the end of testing	35
3-19	Specimen T1B at end of test	36
3-20	Load vs. deformation curve for specimen T1B	36
3-21	Load vs. deformation curve for specimen T1C	37
3-22	Specimen T1C at 9 mm displacement	37
3-23	Specimen T1C at 10 mm displacement	38
3-24	Specimen T1C at 12 mm displacement	38
3-25	Specimen T1C at 22 mm displacement	39
3-26	Specimen T1C at 27 mm displacement	39

Figure		Page
3-27	Specimen T1C at end of testing	40
3-28	Specimen T2A at end of testing	40
3-29	Load vs. deformation curve for specimen T2B	41
3-30	Specimen T2B at 600 kN	41
3-31	Specimen T2B at 690 kN	42
3-32	Specimen T2B at 660 kN	42
3-33	Specimen T2B at 403 kN	43
3-34	SpecimenT2B at 331 kN	44
3-35	Specimen T2B at end of testing	45
3-36	Specimen T2C at end of testing.	45
3-37	Load vs. deformation curve for specimen T2C	46
4-1	Gusset plate T-2 tested by Nast *et al.* (1999)	65
4-2	Stress vs. strain curve of gusset plate material from Nast *et al.* (1999)	65
4-3	Meshes used for the mesh refinement study	66
4-4	Convergence of strains along the tension face (Nast *et al.* Specimen T-2)	67
4-5	Tension portion of cyclic loading curve for gusset plate T-2 tested by Nast *et al.* (1999)	67
4-6	Load vs. deformation from fine mesh	67
4-7	Predicted load vs. deformation response (100% maximum principal strain criterion)	68
4-8	Predicted load vs. deformation response (maximum shear strain criterion)	68
4-9	Predicted load vs. deformation response (130% shear strain criterion)	68
4-10	Progression of block shear failure in gusset plate T-2 tested by Nast *et al.* (1999)	69
4-11	Gusset plate 1 tested by Hardash and Bjorhovde (1984)	70
4-12	Stress vs. strain curve used for the analysis of gusset plate 1 tested by Hardash and Bjorhovde (1984)	71
4-13	Load vs. deformation curve for gusset plate 1 tested by Hardash and Bjorhovde (1984)	71

Figure		Page
4-14	Gusset plate 11 tested by Hardash and Bjorhovde (1984)	72
4-15	Load vs. deformation curve for gusset plate 11 tested by Hardash and Bjorhovde	73
4-16	Gusset plate 4U tested by Mullin (2002)	73
4-17	Stress vs. strain curve used in the analysis of gusset plate 4U tested by Mullin (2002)	75
4-18	Load vs. deformation curve for 4U	75
4-19	Gusset plate 8U tested by Mullin (2002)	76
4-20	Definition of bolt element	77
4-21	Stress vs. strain curve used in the analysis of gusset plate 8U tested by Mullin (2002)	78
4-22	Load vs. deformation curve for 8U	78
4-23	Gusset plate 224.4 tested by Udagawa and Yamada (1998)	79
4-24	Stress vs. strain curve used in the analysis of gusset plate 224.4 tested by Udagawa and Yamada (1998)	80
4-25	Load vs. deformation curve for gusset plate 224.4	80
4-26	Gusset plate 23F.4 tested by Udagawa and Yamada (1998)	81
4-27	Stress vs. strain curve used in the analysis of gusset plate 23F.4 tested by Udagawa and Yamada (1998)	82
4-28	Load vs. deformation curve for gusset plate 23F.4	82
4-29	Gusset plate 423.4 tested by Udagawa and Yamada (1998)	83
4-30	Stress vs. strain curve used in the analysis of gusset plate 423.4 tested by Udagawa and Yamada (1998)	84
4-31	Load vs. deformation curve for gusset plate 423.4	84
4-32	Gusset plate T1 from current investigation	85
4-33	Stress vs. strain curve used in the analysis of gusset plate T1 from current investigation	86
4-34	Load vs. deformation curve for T1	86
4-35	Progression of block shear failure in gusset plate T1 from current investigation	87
4-36	Gusset plate T2 from current investigation	88

Figure		Page
4-37	Stress vs. strain curve used in the analysis of gusset plate T2 from current investigation	89
4-38	Load vs. deformation curve for T2	89
4-39	Progression of block shear failure in gusset plate T2 from current investigation	90
4-40	Gusset plate 1 from the parametric study	91
4-41	Load vs. deformation curve for gusset plate 1 (Finite Element Analysis)	92
4-42	Progression of block shear failure in gusset plate 1 from the parametric study	93
4-43	Gusset plate 2 from the parametric study	95
4-44	Load vs. deformation curve for gusset plate 2 (Finite Element Analysis)	96
4-45	Gusset plate 3 from the parametric study	97
4-46	Load vs. deformation curve for gusset plate 3 (Finite Element Analysis)	98
4-47	Gusset plate 4 from the parametric study	99
4-48	Load vs. deformation curve for gusset plate 4 (Finite Element Analysis)	100
4-49	Gusset plate 5 from the parametric study	101
4-50	Load vs. deformation curve for gusset plate 5 (Finite Element Analysis)	102
5-1	Test capacity vs. predicted capacity based on CAN/CSA–S16.1–94	113
5-2	Test capacity vs. predicted capacity based on CSA–S16–01	113
5-3	Test capacity vs. predicted capacity based on AISC 1999	114
5-4	Test capacity vs. predicted capacity based on Hardash and Bjorhovde (1984)	114
5-5	Test capacity vs. predicted capacity based on Kulak and Grondin (2001)	115
5-6	Test capacity vs. predicted capacity based on proposed new equation	115
A-1	Definition of dimensional parameters	125

LIST OF SYMBOLS

A	-	instantaneous cross-sectional area
A_{gt}	-	gross tension area
A_{gv}	-	gross shear area
A_{nt}	-	net tension area
A_{nv}	-	net shear area
A_o	-	initial cross-sectional area
C_L	-	connection length factor
E	-	modulus of elasticity
F_Y	-	specified minimum yield strength
F_u	-	specified minimum tensile strength
F_{eff}	-	effective tensile stress
L	-	connection length
P_r	-	factored block shear resistance of gusset plate
P_n	-	nominal block shear resistance of gusset plate
R	-	nominal resistance
R_t	-	constant used to account for non-uniformity of normal stresses on the tension area
S	-	specified load effect
S_{net}	-	net distance between the outside bolt lines
t	-	plate thickness
V_G	-	coefficient of variation for the geometric factor
V_M	-	coefficient of variation for the material factor
V_P	-	coefficient of variation for the professional factor
V_R	-	coefficient of variation for the resistance
α	-	load factor

β	-	safety index
$\varepsilon_{\ln}^{e}$	-	elastic component of the total strain
$\varepsilon_{\ln}^{p}$	-	plastic component of the total strain
$\varepsilon_{\ln}^{tot}$	-	total strain
ε_{nom}	-	engineering strain
ε_{ln}	-	logarithmic (or true) strain
ϕ	-	resistance factor
Φ_{β}	-	correction factor for the resistance factor
ρ_G	-	bias coefficient for the cross-sectional geometry
ρ_M	-	bias coefficient for the material properties
ρ_R	-	bias coefficient for the resistance
ρ_P	-	bias coefficient for the design equation
σ_{nom}	-	engineering stress
σ_{true}	-	true stress
σ_u	-	measured tensile strength
σ_Y	-	measured yield strength

CHAPTER 1

INTRODUCTION

1.1 General

Gusset plates are widely used in steel structures such as trusses and braced buildings to transfer forces from axially loaded members to adjacent members. The design of gusset plates is well established both for the transfer of tension and compression forces (Nast *et al.*, 1999). One of the failure modes in gusset plates loaded in tension is block shear tear out. This mode of failure is characterized by tearing of a block of material and it presumes a combination of tension rupture and shear yield or rupture. Although this mode of failure can occur in welded or bolted connections, it is more common in the latter because of the reduced area that results from the presence of the bolt holes.

Block shear failure started to receive attention in the 1970s when the allowable bearing stress in high-strength bolted joints was increased based on a bearing strength model proposed by Fisher and Struik (1974). The bearing stress was increased from 1.34 times the minimum specified yield strength, F_Y, to 1.5 times the specified tensile strength, F_u, (Research Council on Riveted and bolted Structural Joints, 1976), which prompted experimental investigations to investigate the new requirements as applied to the simple beam connection. Tests reported by Birkemoe and Gilmor (1978) exposed the block shear mode of failure in coped beams. Birkemoe and Gilmor proposed that the block shear capacity of a coped beam could be estimated as the sum of the ultimate shear strength along a vertical plane through the bolt holes and the tensile strength along the net tension area at right angle to the line of bolts. Further testing on coped beam connections at the University of Texas (Yura *et al.*, 1982; Ricles and Yura, 1983) showed that the proposed strength calculation based on simultaneous shear and tension fracture overestimated the capacity of the connections. It was noted that the vertical plane of the connections exhibited gross yielding, but no shear fracture. A modified block shear model was proposed whereby the block shear capacity consisted of the sum of the yield strength on the gross shear area and the net tension section rupture strength (assuming a linearly varying tensile stress) on the tension area.

Following the work on block shear in coped beams, an evaluation of test results from gusset plates by Bjorhovde and Chakrabarti (1985) suggested a model in which the ultimate shear resistance was developed along the shear planes and the ultimate tensile strength was developed along the last row of bolts. Work by Hardash and Bjorhovde (1984) lead to the development of a model where the ultimate strength is used on the tension area and an effective shear stress, which takes a value between the shear yield and the shear ultimate, is used on the shear surfaces.

A significant amount of testing on gusset plates followed, with contributions coming from Canada (Yam and Cheng, 1993; Nast *et al.*, 1999), Japan (Udagawa and Yamada, 1998) and Norway (Aalberg and Larsen, 1999). From these tests it became clear that tension fracture between the last bolts in a connection is the first step in the block shear failure process. The failure process on the shear planes has remained misunderstood.

A recent review of North American design practice for block shear design (Kulak and Grondin, 2001) indicated that, although the block shear equations in design standards generally give a good prediction of the block shear capacity of gusset plate connections, the models did not predict the failure mode reliably. A model consisting of rupture on the net tension area and yielding on the gross shear area of the block of material tearing out was proposed. A modified version of this model, where the shear capacity is limited to the shear rupture strength on the net shear areas was recently adopted in CSA–S16–01. Such an approach, borrowed from the procedure for design of tension members, may not fully describe the true block shear behaviour of gusset plates. Although several block shear tests on gusset plates have been reported, our understanding of the sequence of events that lead to block shear failure is still lacking.

1.2 Objectives and Scope

The main objective of the research work presented in the following is to develop a finite element procedure to predict the behaviour of block shear failure from initial yielding of the gusset plate to rupture along the tension face and subsequent rupture along the shear faces. Such a model would provide a better understanding of the block shear behaviour of

gusset plates and would be valuable for the investigation of block shear failure in other members such as coped beams and angle and tee sections in tension.

The main objectives of this investigation are as follows:

- Through an examination of all the test data on block shear of gusset plate, identify the areas where more research is required;
- Develop a finite element procedure to investigate the block shear failure process and validate the model through a comparison with test results;
- Investigate the failure mechanism of block shear and the associated load carrying capacity using the finite element model;
- Conduct a limited number of full-scale tests on gusset plates to examine closely the progression of block shear failure;
- Expand the database of test results on gusset plates through a parametric study using the finite element model;
- Assess the current design equations for block shear in gusset plates and propose an equation for application in limit states design.

The investigation presented in the following is limited to gusset plates with bolted connections.

1.3 Organization of Thesis

The thesis is divided into six chapters. Chapter 2 reviews research previously completed on block shear failure of gusset plates. Capacity equations proposed by others for the general case of block shear are presented, as are the equations prescribed by current design standards in North America. The experimental portion of this research is discussed in Chapter 3. Details of the test specimens, material properties, test apparatus, instrumentation, test procedure, and test results are presented. Chapter 4 presents the development and validation of a finite element model and the procedure for the study of block shear in gusset plates. The results of a parametric study designed to expand the database of test results are then presented. An analysis of all the test results and a critical assessment of a number of design equations, with a proposal for a suitable limit states design equation for block shear resistance, is presented in Chapter 5. A summary of the research, conclusions and recommendations are presented in Chapter 6.

CHAPTER 2

LITERATURE REVIEW

2.1 Introduction

Gusset plates are commonly used in steel structures such as trusses and industrial buildings to transfer forces from bracing and truss members to other members in a structure. The design of gusset plates for compression and tension is well established (Nast *et al.*, 1999).

Whitmore (1952) conducted experiments on gusset plates using scale models of plates made of materials such as bakelite, aluminium, and gypsum compounds. Through these experiments he demonstrated that the design of gusset plates based on beam theory was unreliable. Based on the results of his investigation, Whitmore proposed a method for predicting the peak stress in a gusset plate for a given brace load, which consisted of dividing the brace load by an area equal to the plate thickness times what later became known as the "Whitmore effective width". The Whitmore effective width is defined as the distance between two lines radiating outward at 30-degree angles from the first row of bolts in the gusset-to-brace connection along a line running through the last row of bolts. Whitmore showed that the predicted stress agreed well with test results. This method is still widely used today for design of gusset plates to transfer loads from tension members.

Since this early work on gusset plates, many researchers have investigated the behaviour of gusset plates in tension. Irvan (1957) and Hardin (1958) used elastic model tests, which were similar to those of Whitmore, but with gusset plates of different material and with minor modifications compared to those tested by Whitmore. Their work confirmed the earlier results of Whitmore. Hardin (1958), Davis (1967) and Varsarelyi (1971) also investigated the stresses in gusset plates loaded in the elastic range. Hardin's experimental investigation confirmed Irvan's conclusions regarding the inaccuracy of beam theory to predict stresses in gusset plates and supported Irvan's method for determining the magnitude of the peak stress in gusset plates. Davis and Varsarelyi

carried out finite element investigations of the elastic stresses in gusset plates. In general, these investigations confirmed the findings of the experimental investigations regarding the stresses in gusset plates loaded in the elastic range.

In 1976, the Research Council on Structural Connections increased the allowable bearing stress in high strength bolted joints from 1.35 times the yield strength to 1.5 times the tensile strength of the material in the connected parts. This drastic increase in allowable bearing stress prompted significant changes to design practice. For example, for ASTM A36 steel, the most commonly used grade of steel at that time, the bearing stress was increased from 335 MPa to 600 MPa, nearly an 80% increase in bearing stress. At about the same time, Canada was adopting Limit States Design for steel structures and research was conducted at the University of Toronto (Birkemoe and Gilmor, 1978) on the shear resistance of coped beam webs and the effect of the increase in bearing stress on coped and uncoped beam bolted connections. The research involved one full-scale test on coped beams. A failure mode consisting of shearing out of a block of the web was observed. This led to the development of the concept of block shear failure and a model was proposed to predict the resistance of bolted connections to block shear failure.

This early research on block shear in coped beams was followed by several other research programs on block shear in gusset plates, which are summarized in the following section.

2.2 Block Shear in Gusset Plates

2.2.1 Bjorhovde and Chakrabarti (1985)

Bjorhovde and Chakrabarti (1985) investigated the strength and behaviour of gusset plates using full size corner gusset plates connected to a beam and column and a tensile load applied through a bracing member. A total of six specimens were tested: two different thicknesses (3 mm and 9 mm) and three brace member orientations (30°, 45°, and 60° measured relative to the beam axis). The test results showed that the 3 mm plate buckled and tore at the bottom bolts (the bolts farthest from the brace load). The tearing propagated from the edge of the bottom bolt holes on the tension side of the hole group, towards the free edge of the gusset plate, thus developing combined shear and tension on

the failure planes. Because of insufficient capacity of the loading apparatus, the 9 mm plate specimens were not tested to failure. Since block shear failure was not observed in the tests, their test results are not used for the work presented in the following chapters.

Based on their investigation, Bjorhovde and Chakrabarti (1985) concluded that a yield criterion based on Whitmore's method was appropriate for the design of gusset plates. Recommendations for future work included further study of the influence of plate boundaries, including the use of stiffeners along the free edges.

In addition to their experimental program, Bjorhovde and Chakrabarti (1985) used a non-linear finite element analysis (including geometric and material non-linearities) to predict the structural response of gusset plates. Quadrilateral and triangular plate elements were used in the finite element model. Bolts and gusset plate–to–boundary members framing angles were also modeled using spring elements and the properties for these spring elements were derived from tests to determine appropriate load-deformation curves. The finite element analysis results were generally found to be in good agreement with the test results.

2.2.2 Hardash and Bjorhovde (1984)

Hardash and Bjorhovde (1984) tested gusset plates in which block shear failure was the observed failure mode. The test specimens consisted of 6 mm plates of ASTM-A36 steel and used 12.7 mm (1/2 in) diameter A325 bolts placed in punched 14.3 mm (9/16 in) diameter holes. In their 28 tests, Hardash and Bjorhovde investigated the effect of gauge distance over a range of 50 to 100 mm, bolt spacing of 38.1 mm and 50.8 mm, and from two to five bolts in a line. Figure 2-1 provides definitions of dimensional parameters. A description of the specimens tested by Hardash and Bjorhovde is presented in Appendix A. Although Hardash and Bjorhovde also reported the results of tests conducted at the University of Illinois, these tests are not presented in Appendix A because the majority of these specimens did not fail in a block shear failure mode.

The test results from Hardash and Bjorhovde (1984) showed that once the gusset plate fractured in tension between the bolts in the last row, a significant drop in load carrying capacity occurred and the load either kept decreasing or increased only a small amount

thereafter. Fracture on the tension portion of the block shear failure surface always occurred before fracture in shear. Using the results of their investigation and those of other researchers, Hardash and Bjorhovde derived an equation for the calculation of the block shear capacity, P_u, of bolted gusset plate connections as follows:

$$P_u = (F_u S_{net} + 1.15 F_{eff} L)t \tag{2-1}$$

where F_{eff} is an effective stress on the shear planes of the block shear failure surface, given as:

$$F_{eff} = (1 - C_L)F_Y + C_L F_u \tag{2-2}$$

The empirical constant C_L is given as:

$$C_L = 0.95 - 0.047L \tag{2-3}$$

The terms in the above equations are defined as follows:

P_u : nominal tensile resistance of the gusset plate,

F_u : ultimate tensile strength of the material,

S_{net} : net distance between the outside bolt lines,

F_{eff} : effective tensile stress,

L : connection length from edge of gusset plate to last bolt row (inches)

t : plate thickness,

F_Y : tensile yield strength of the material,

C_L : connection length factor.

Equation 2-1 indicates that the block shear capacity of a bolted gusset plate connection is reached when the ultimate tensile strength is reached on the net tension area and an effective shear stress has developed on the gross shear area. The proposed shear stress on the shear planes usually has a magnitude between the yield and ultimate shear strength.

2.2.3 Gusset Plate Research at University of Alberta

Rabinovitch and Cheng (1993) extended earlier University of Alberta work on gusset plates in compression (Hu and Cheng, 1987; Yam and Cheng, 1993) to include gusset plate connections under cyclic loading. A series of five tests on full-scale gusset plates connected to a joint between a beam and column was tested under cyclic loading. Tests

on stiffened and unstiffened gusset plates showed that the latter behaved better under cyclic loading, showing a more stable post-buckling behaviour. Five of the test specimens were loaded to failure in tension after cycling under fully reversed loading. All five specimens failed by block shear tear out.

Walbridge *et al.* (1998) developed finite element models to predict the behaviour of gusset plates loaded monotonically in compression and cyclically in compression and tension. Their models were validated by comparison with test results from Yam and Cheng (1993) and Rabinovitch and Cheng (1993). The models incorporated the effect of the beam and column boundary members, bolt slip in the splice plates to brace member connection, and material yielding. The work also expanded the earlier test programs by studying the effect of gusset plate–brace member interaction. Although the finite element models did not include specifically the bolt holes in the gusset plates, they were able to predict accurately the tension failure load reported by Rabinovitch and Cheng. The good prediction of the block shear capacity despite the absence of the bolt holes in the finite element models is probably attributable to the use of an elastic–perfectly plastic material model, ignoring any strain-hardening effects.

Nast *et al.* (1999) studied the effect of gusset plate–brace member interaction on stiffened and unstiffened gusset plates using four full-scale tests. Four specimens were tested: two gusset plates with free edge stiffeners and two gusset plates without stiffeners. The gusset plate dimensions and bolt layout were identical in all tests. Both sets of specimens were tested with a short brace member and with a long brace member. The short brace members were designed to buckle the gusset plate before buckling of the brace. The long brace members were designed to buckle before buckling of the gusset plate. Nast *et al.* (1999) also used finite element modelling developed by Walbridge *et al.* (1998) to determine the size of the free edge stiffeners to include in the testing program.

Mullin (2002) studied the behaviour of reinforced and unreinforced gusset plates using five full-scale tests only differing by the number of bolts in the connection. All the gusset plates had the same gauge distance of 102 mm, end distance of 38 mm, plate thickness of 6.4 mm, bolt hole diameter of 20.6 mm, and bolt spacing of 76 mm. The number of bolts

ranged from four to 16. These gusset plates were loaded in tension until fracture on the tension face occurred.

A description of the gusset plate test specimens from the University of Alberta that failed in a block shear mode is presented in Appendix A.

2.2.4 Epstein and Chamarajanagar (1996)

Epstein and Chamarajanagar (1996) conducted a numerical investigation of block shear in bolted angles with staggered and non-staggered holes. The angles were modeled using a solid element with large deformation capability. Thirteen single angle connections with different stagger patterns were modeled. The angles were modelled using a coarse mesh and failure was assumed to take place when the maximum calculated normal strain had reached a value five times the yield strain. Although the finite element analysis showed a reasonably good correlation with test results, the authors suggested that much improvement was still needed in the finite element model and the failure criterion. It is the opinion of the writer that the finite element mesh used by Epstein and Chamarajanagar was too coarse to reach convergence and the critical strain used as a failure criterion was unrealistically small. This is discussed further in Chapter 4.

2.2.5 Udagawa and Yamada (1998)

In 1998, Udagawa and Yamada tested 219 splice plates with different gauge distances ranging from 40 mm to 81 mm, end distances ranging from 23 mm to 63.5 mm, edge distances ranging from 23 mm to 101 mm, number of bolts (ranging from two to 12), number of lines of bolts (ranging from one to four), and different steel grades with yield strengths varying from 400 MPa to 780 MPa. These test specimens are described in detail in Appendix A. The objective of the test program was to investigate the effect of the bolt pattern in connections on the ultimate tensile strength and mode of failure. It was shown that as these parameters vary, the mode of failure varies among block shear failure, net tension failure and bearing failure. The test specimens were loaded in tension only and 73 specimens failed by block shear tear out.

2.2.6 *Aalberg and Larsen (1999)*

Aalberg and Larsen (1999) investigated block shear in tension members and coped beams made of I-shaped members with nominal steel yield strengths of 235 MPa and 700 MPa. The bolted connections were made on the web of the wide flange members. In their first series of tests, Aalberg and Larson used double lap splice joints with three lines and two rows of 20 mm bolts in 21 mm diameter holes. In the second series, the test specimens had two lines by two to four rows of 18 mm bolts in 19 mm holes. The tension area in two of the test specimens in the first series was removed in order to examine specifically the behaviour along the shear planes. A description of the test specimens tested in tension with the tension area intact is presented in Appendix A. It was noted that shear fracture occurs on the gross shear area, tangent to the edge of the holes. A comparison of the test specimens with and without the tension area removed indicated that about 90 percent of the shear capacity was mobilized by the time the tension area fractures. In all the cases investigated, the capacity of the shear planes alone did not exceed the capacity of the connection just prior to rupture on the tension plane. Aalberg and Larsen (1999) compared their test results with AISC Specification (AISC, 1995). It was noted that in all cases the equation that governed was the one that would predict shear rupture plus tension yield. They noted that this was inconsistent with the observed behaviour. Predictions using CAN/CSA–S16.1–89 (CAN/CSA–S16.1–89 provisions for block shear are the same as the provisions in CAN/CSA–S16.1–94 described below) showed consistent underestimation of the test results (predicting 72 to 87 percent of the observed capacity). A comparison of the test specimens made of high strength steel with those made of lower strength steel indicated that the prediction models using the yield strength on the gross shear area tend to overestimate block shear capacity in high strength steel gusset plates. This is a direct consequence of the high yield strength to tensile strength ratio of 0.96 observed in their test specimens.

2.2.7 *Menzemer, Fei and Srivatsan (1999)*

Menzemer, Fei and Srivatsan (1999) investigated block shear failure of aluminium gusset plates under tensile loading. A total of 23 gusset plates were tested; 20 plates were 6.25 mm thick and made of aluminium alloy 6061-T6 and three were 6.25 mm thick and

made of aluminium alloy 5083-H321. The investigated parameters were the gauge distance and connection length. All test specimens were loaded to fracture on the tension face. Menzemer, Fei and Srivatsan (1999) proposed that the failure load can be determined as the sum of the net tension area rupture strength and the gross shear area yield strength.

2.2.8 Swanson and Leon (2000)

Swanson and Leon (2000) performed tests on bolted T-stubs and clip angle connections. Fifty-eight tests were conducted and only one test specimen failed in block shear (a description of this test specimen is presented in Appendix A). The parameters that were investigated were bolt diameter, gauge distance, and bolt spacing. Two bolt diameters were used: 22 mm and 25 mm. The gauge distance ranged from 76 mm to 203 mm and the bolt spacing of 63.5 mm and 76 mm. The specimen with the smallest bolt spacing of 63.5 mm failed in block shear. This specimen was loaded cyclically until total failure occurred. Swanson and Leon (2000) observed that failure started as rupture on the net tension area and progressed until the tear out of the block was complete.

2.3 Design Standards

2.3.1 CAN/CSA–S16.1–94

The block shear provisions in CAN/CSA–S16.1–94 are based on the assumption that the ultimate tensile strength and the ultimate shear strength are reached simultaneously. The resulting equation for calculating the block shear capacity is:

$$\phi P_u = 0.85\phi[F_u A_{nt} + (0.6F_u)A_{nv}] \tag{2-4}$$

where P_u is the nominal block shear capacity, F_u is the ultimate tensile strength of the material, A_{nt} is the net tension area, A_{nv} is the net shear area, and the resistance factor as 0.85ϕ where ϕ is 0.9. The shear strength of the material is taken as 0.6 times the tensile strength. The equation therefore makes the assumption that there is sufficient ductility on the tension surface to develop the full capacity of the shear planes.

2.3.2 CSA–S16–01

CSA–S16–01 proposed that the capacity of gusset plates should be the lesser of:

$$\phi P_u = \phi[F_u A_{nt} + (0.6F_Y)A_{gv}] \quad (2\text{-}5)$$

$$\phi P_u = \phi[F_u A_{nt} + (0.6F_u)A_{nv}] \quad (2\text{-}6)$$

where A_{gv} is the gross shear area, F_y is the yield strength of the material, and the other variables are as defined above.

In Equation 2-5, the block shear resistance is taken as the sum of the tensile resistance on the net section and shear yield resistance on the gross shear area. This reflects the observation from many tests that fracture on the tension area occurs before fracture on the shear area. The standard also states that the shear yield resistance on the gross shear area cannot exceed the ultimate shear strength on the net shear area. This is not consistent with the observed failure mode, which shows rupture on an area close to the gross area.

2.3.3 AISC 1999

The Load and Resistance Factor Design (LRFD) equations in the 1999 AISC Specification assume that there are two possible block shear failure modes: rupture on the net tension area along with shear yielding on the gross shear area and rupture on the net shear area with yielding on the gross tension area. The shear yield or rupture strength is taken as 0.6 times the tensile yield or rupture strength, respectively. These conditions are expressed as follows:

When $F_u A_{nt} \geq 0.6F_u A_{nv}$:

$$\phi P_u = \phi[0.6F_Y A_{gv} + F_u A_{nt}] \leq \phi[0.6F_u A_{nv} + F_u A_{nt}] \quad (2\text{-}7)$$

When $F_u A_{nt} < 0.6F_u A_{nv}$:

$$\phi P_u = \phi[0.6F_u A_{nv} + F_Y A_{gt}] \leq \phi[0.6F_u A_{nv} + F_u A_{nt}] \quad (2\text{-}8)$$

Equation 2-7 applies if the tensile strength on the net tension area is larger than or equal to the shear strength on the net shear area. In this case the block shear capacity is taken as the sum of the yield strength on the gross shear area and ultimate strength on the net tension area. The shear capacity, however, is limited to the ultimate strength on the net shear area. If the condition for Equation 2-7 is not met, the block shear capacity is taken

as the sum of the ultimate resistance on the net shear area and the yield resistance on the gross tension area. The tensile capacity is limited to ultimate on the net tension area. This is summarized in Equation 2-8. Aalberg and Larsen (1999) and Kulak and Grondin (2001) observed that Equation 2-8 does not describe a condition that would be observed in practice. However, the equation seems to govern the calculated block shear capacity in many cases.

2.4 Summary

Several experimental and numerical investigations of block shear on gusset plates have been conducted by a number of researchers over the past 25 years. Although the database of test results for block shear in gusset plates and tension members is large, the exact sequence of block shear failure seems still to remain misunderstood. There seems to be a consensus among researchers that the design provisions in certain standards do not reflect the mode of failure observed in the laboratory. Furthermore, the experimental data available have been collected on relatively short connections. Therefore, more research on block shear in gusset plates is needed to provide a better understanding of the block shear process and to expand the database of test results to include long connections.

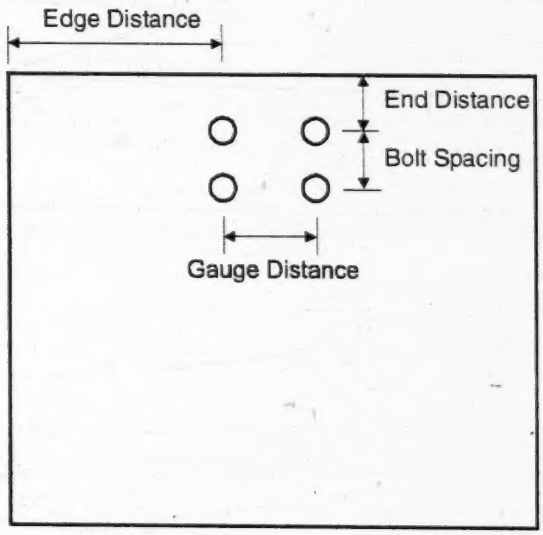

Figure 2-1 Definition of dimensional parameters

CHAPTER 3

EXPERIMENTAL PROGRAM

3.1 Introduction

Many laboratory experiments have been conducted to study block shear failure of gusset plates. These experiments did not directly observe the mechanisms leading to block shear failure. The purpose of this experimental program is to observe the failure progression in block shear failure and to reach a better understanding of what happens as block shear occurs. This chapter describes the test specimens used in the experimental program, the test set-up, the instrumentation, the testing procedure, and the test results.

3.2 Description of Test Specimens, Test Assembly and Instrumentation

Two connection configurations were investigated, namely, a long and narrow connection and a short and wide connection. The long and narrow connection, illustrated in Figures 3-1 and 3-2, consists of six 19 mm (3/4 inch) bolts and uses the minimum gauge distance allowed in CSA–S16–01, namely 2.7 times the bolt diameter (51 mm). The test plates had an average measured thickness of 6.6 mm and the bolt pitch was 76 mm. The test specimens from this series were designated as T1A, T1B, and T1C. One configuration of the short and wide connection, shown in Figures 3-3 and 3-4, consists of four bolts and uses a gauge distance equal to eight times the bolt diameter, namely, 152 mm. The test plate had a thickness of 6.5 mm and the bolt pitch was 51 mm. This test specimen is designated as T2A. Because the tension plane of the potential block shear failure surface had a capacity substantially greater than that of the shear planes, this connection did not fail in block shear. The connection was therefore modified by adding a row of four bolts as shown in Figures 3-5 and 3-6. The modified connection had eight bolts with gauge and pitch dimensions of 51 mm. The measured plate thickness for the two specimens of this connection configuration was 6.6 mm. The two specimens were designated as T2B and T2C.

An overall view of a test specimen placed in the testing machine is shown in Figure 3-7 and a description of the test set-up is shown in Figures 3-8 and 3-9. In all the connections, 584×203×15.9 mm plates were used as splice plates. The width of the splice plates was

reduced to 95 mm where it connected to the load transfer plates. The width and thickness of the load transfer plates corresponded to the maximum gripping width and thickness of the grips in the testing machine. Because the thickness of the load transfer plates and the gusset plate were not the same, 229×203×12.7 mm filler plates were used between the splice plates and the gusset plate. All holes were match drilled in the gusset plate, splice plates, and filler plates in order to ensure that all the bolts would be in bearing from the beginning of the tests.

A test specimen assembly, as shown in Figures 3-7, 3-8 and 3-9, consisted of one gusset plate, four splice plates, four filler plates, and top and bottom load transfer plates. The bolts between the gusset plate and the splice plate were 19 mm (3/4 inch) diameter A325 bolts and bolts at the joints between the splice plates and the load transfer plates were 12.7 mm (½ inch) diameter A325 bolts. All the bolts were installed to snug tight, as defined in CSA–S16–01.

The load response of the gusset plate during testing was taken as the deformation between the free unloaded end of the gusset plate and the middle of the plate as shown in Figure 3-10. This deformation was measured using Linear Variable Displacement Transformers (LVDTs). A plexi-glass bracket, held by two 6.4 mm (1/4 inch) bolts to the middle of the gusset plate was used to mount the LVDTs as shown in Figure 3-10. A 25 mm aluminium channel, fastened at midpoint of the end of the test plate served as the reference line for the deformation measurements (see Figures 3-11 and 3-12). An average reading from the two LVDTs provided an accurate measurement of the deformation of the gusset plate in the shear block area. The output of the LVDTs and the applied load was monitored using a data acquisition system controlled using Lab View®.

3.3 Material Properties

The material properties for the gusset plates were required to calculate the predicted block shear capacity of the test specimens and to define the material model in the finite element analysis. Tension coupons from the gusset plates were obtained in accordance with CAN/CSA–G40.20–98 and testing was performed as per the specifications outlined in ASTM A370–97a (ASTM, 1997). Since all the gusset plates were cut from the same

plate, only one set of three coupons was tested. The gusset plates, splice plates and the spacers were grade 350W steel. A summary of the material properties obtained from the gusset plate material is presented in Table 3-1.

3.4 Testing Procedure

The load on the test assembly was applied using a MTS 1000 universal testing machine under stroke control at 1 mm/min. The intent of the tests was to examine closely the process of block shear failure from the yielding stage to fracture of the block of material along the tension and shear faces. This required the removal of the splice plates at various intervals during testing to observe the progression of block shear failure. Before the tests, finite element models of the test specimens were developed and analysed to determine the expected behaviour of the specimens from the T1 series and specimen T2A. Test specimens T2B and T2C were not analysed prior to testing. The load vs. deformation curve predicted using the finite element analysis described in Chapter 4 was used to help determine when to remove the splice plates for visual inspection of the test specimens. The finite element analysis indicated that fracture in the specimens of the T1 series would not start until the deformation over the length of the joint would reach 2 mm. Therefore, it was decided that a close examination of the test specimens at 1 mm intervals would be sufficient to capture the fracture process. After tension fracture was observed, two more observations at 1 mm increments were performed to examine initiation and progression of shear cracks. The subsequent examinations of the block shear failure progression were made at 5 mm increments until failure of the connection.

For specimen T2A, the expected displacement at first fracture was only 0.35 mm. Since this displacement is considerably smaller than the displacement from the T1 series, examinations of the gusset plate were conducted at predetermined load levels. The specimens were first loaded to 450 kN. Examination of the gusset plate was then performed at every 20 kN increments. The 450 kN load was chosen so that first fracture would not be missed since the assumed first fracture occurs at 696 kN. The 20 kN increment was arbitrarily chosen to observe the connection until first tension fracture occurs. The process of observing the connection at every 20 kN was continued two more times thereafter, observing the connection at every 50 kN increments until total failure of

the connection occurred. An analysis of test specimen T2B was not conducted prior to testing because of time constraint in the laboratory. Therefore, the splice plates were removed at the same intervals used for specimen T2A.

In order to determine the effect of removing the splice plates during testing on the block shear capacity, specimens T1B and T2C were tested continuously to failure without removing the splice plates.

3.5 Experimental Results

A summary of the test results is presented in Table 3-2. Each of the test specimens were tested to failure on the shear planes. A description of the tests follows.

3.5.1 Specimen T1A

The load vs. deformation curve for test specimen T1A is shown in Figure 3-13. At every displacement increment the specimen was unloaded and the splice plates removed to examine the gusset plate. The part of the load vs. deformation curve shown as a dotted line indicates a portion of the response for which the test data was accidentally lost during testing. The first examination of the gusset plate was made when the displacement reached approximately 1 mm (load of 522 kN). At this stage no cracks were detected, but some deformation of the holes had already taken place. At 2 mm (load of 586 kN) the bolt holes had elongated further and mill scale was starting to flake off along the tension and shear planes as shown in Figure 3-14. At 6 mm displacement (load of 676 kN), the tension plane, between holes 5 and 6, was beginning to show signs of necking. At a displacement of 8 mm (load of 692 kN), minor cracks were first noted at the edge of holes 5 and 6 on the tension face. These cracks seemed to penetrate about 0.1 mm below the surface and were about 1 mm long. At 9 mm displacement (load of 696 kN) necking over the full width of the tension face was observed. At a displacement of 11 mm and load of 681 kN, a fine crack was apparent along the tension plane as shown in Figure 3-15. Once loading was resumed, the maximum load reached only 595 kN at a displacement of 12 mm. This corresponds to a decrease in load capacity of 13 percent from the load reached at a displacement of 11 mm. At this point the tension plane had completely fractured as shown in Figure 3-16 and a 2 mm long crack was emanating

from the bottom right of Hole 5 on shear plane. Following the fracture of the tension plane, the load carrying capacity of the connection remained relatively constant. At a displacement of 14 mm the data acquisition system failed and the data for that increment were lost. The portion of the load vs. displacement curve in the 13 to 19 mm range was therefore approximated as indicated by the dotted line in Figure 3-13. At a displacement of 19 mm (load of 540 kN), shear cracks had only formed on the right side of the connection, as shown in Figure 3-17. The shear cracks on the right shear plane were 17 mm and 22 mm below holes 5 and 3, respectively, and 22 mm above hole 1. At a load of 250 kN, fracture of the right shear plane was observed (Figure 3-18) and the test was terminated.

3.5.2 Specimen T1B

Specimen T1B was loaded continuously from the beginning of the test to block shear failure at a displacement rate of 1 mm/min. Figure 3-19 shows the test specimen at the end of the test and the load vs. deformation curve is shown in Figure 3-20. A comparison of the curve shown in Figure 3-20 with that in Figure 3-13 shows that the capacity of T1B within 1% of T1A, but tension fracture occurred at a smaller displacement than for T1A. The reason for this difference in ductility between the two tests is not well understood, but it is possible that it is caused by the periodic unloading and removal of the splice plates during testing of T1A. Figure 3-20 shows a marked drop in load carrying capacity when fracture occurred on the tension plane. A slight increase in load was observed following tension fracture, but the capacity never exceeded the load level at which tension fracture occurred. At a displacement of approximately 18 mm the load started to drop until fracture of the connection occurred.

3.5.3 Specimen T1C

The load vs. deformation curve for specimen T1C is shown in Figure 3-21. As for specimen T1A, the test specimen was unloaded at preset intervals to remove the splice plates and examine the gusset plate closely. As for T1A, the specimen was first unloaded at a displacement of 1 mm (load of 520 kN). It was observed that all holes were deformed, but no tension cracks or shear cracks were observed. At a displacement of 5 mm (load of 668 kN), necking had started at the edge of holes 5 and 6 on the tension

face. At a displacement of 9 mm (load of 712 kN), necking of the tension face was observed as shown in Figure 3-22. Necking was evident across the entire tension face between bolt holes 5 and 6. At a displacement of 10 mm (load of 621 kN), a crack was observed across the full tension face as shown in Figure 3-23. Although the displacement at tension fracture is about 12% lower than the corresponding displacement for T1A, it is about 27% greater than the displacement at tension fracture observed in T1B. This is supported by the data shown in Table 3-2. It is possible that the larger displacement at fracture is due to the loading process. At a displacement of 12 mm (load of 638 kN), the tension crack had fully opened, as shown in Figure 3-24, and no shear cracks were noted. At a displacement of 22 mm (load of 489 kN) a 12 mm long shear crack was observed under hole 6 and a 15 mm long shear crack was observed under hole 5 as shown in Figure 3-25. Short shear cracks were also observed under holes 2 and 4 and under hole 1 a shear crack had propagated to the free edge of the plate. At a displacement of 27 mm (load of 289 kN), cracks under holes 5 and 6 had grown to approximately 30 mm at both holes, as shown in Figure 3-26. Shear cracks, approximately 20 mm long, had developed under hole 3 and hole 4. The crack under hole 2, had propagated to the end of the gusset plate. Loading was then continued until total fracture of the connection. The experiment was terminated when the load dropped below 200 kN. Figure 3-27 shows the connection at the end of the test.

3.5.4 Specimen T2A

Because of technical problems encountered in this test, no records of displacement were collected during this test. The test specimen reached a maximum capacity of 512.5 kN. Bolt bearing failure, shown in Figure 3-28, was the mode of failure. It was noted that the tension face did not yield. Since block shear failure was not the mode of failure observed, the connection was modified for the remaining two tests (T2B and T2C). It was decided that additional bolts were needed to reduce the effective area on the tension plane. Four additional bolts were added to the existing connection as shown in Figure 3-5. This effectively decreased the net tension area and increased the shear area.

3.5.5 Specimen T2B

The load vs. deformation curve for test specimen T2B is shown in Figure 3-29. As for

two earlier tests in the T1 series, T2B was unloaded at predetermined displacement intervals to examine the gusset plate. The specimen was unloaded and splice plates removed to examine the gusset plate a total of 34 times during the test. Examination of the gusset plate at a load of 450 kN and 470 kN indicated progressive elongation of the bolt holes. Since there was no visual change in the gusset plate from 450 kN to 570 kN, except for elongation of the bolt holes, the load increment was increased from 20 kN to 30 kN. The bolt hole elongation at a load of 600 kN is shown in Figure 3-30. The mill scale was flaking off, indicating that the gusset plate connection had started to yield. At a load of 690 kN, necking along the tension plane was observed, as shown in Figure 3-31. Cracking along the tension plane was first observed from bolt holes 5 to 7 at a load of 660 kN (see Figure 3-32). The tension plane between holes 7 and 8 had necked, but had not fractured. At a load of 403 kN, the remaining portion of the tension plane fractured as shown in Figure 3-33. Short shear cracks were observed near the bottom of holes 1 and 2. By the time that the load had reached 331 kN shear cracks were observed at the bottom of holes 5 and 8 and from the end of the plate to the edge of hole 1, as shown in Figure 3-34. A 4 mm crack at the bottom of hole 2 that started at the end of the gusset plate was also observed at this load stage. The test was terminated when the load dropped below 100 kN. Figure 3-35 shows the test specimen at end of testing.

3.5.6 Specimen T2C

Specimen T2C was loaded continuously from the start of testing until to failure at a displacement rate of 1 mm/min. Figure 3-36 shows the test specimen at the end of testing and the load vs. deformation curve is presented in Figure 3-37. The curve shows a 55 percent drop in load after tension fracture, this is due to the fact that the area on the tension plane is larger than the area along the shear planes. After tension fracture, the curve shows only a very small increase in capacity. This is due to the fact that most of the shear capacity had been mobilized by the time fracture took place on the tension face of the block shear failure surface. A comparison of the load vs. deformation curve for T2C with that of T2B (Figure 3-28) shows that cyclic loading and periodic removal of the splice plates did not have a noticeable effect on the gusset plate strength and behaviour.

3.6 Summary

A total of six gusset plate test specimens were tested to examine the progression of tension and shear fracture in a block shear failure mode. Three specimen configurations were investigated: three specimens were designed with a large net shear to net tension area ratio of 9.2, two specimens had a small shear to tension area ratio of 1.7, and one specimen, the one with the smallest shear to tension area ratio of 0.69, was tested to demonstrate that block shear failure does not occur unless sufficient shear area is provided to develop the full strength of the net tension area.

In four of the six tests, the specimens were unloaded periodically and the splice plates were removed to examine the gusset plates at various stages of loading. In all cases of block shear failure, it was observed that fracture on the tension plane occurs well before rupture on the shear planes. Tension rupture followed necking of the net section and occurred over the tension plane (or a large portion of it) at once. The tests also indicated in all cases that most of the shear capacity had been mobilized by the time rupture on the tension plane occurred.

Table 3-1

Ancillary test results

	Modulus of Elasticity (MPa)	Mean Static Yield Stress σ_y (MPa)	Static Ultimate Stress σ_u (MPa)	Initial Cross-Sectional Area (mm^2)	Final Cross-Sectional Area (mm^2)	Strain at Strain Hardening (%)	Strain at Ultimate Stress (%)	Rupture Strain (%)
Coupon 1	201 980	337	437	84.3	24.5	5.2	17.6	30.9
Coupon 2	194 160	337	459	84.4	27.0	5.9	18.3	30.6
Coupon 3	196 520	335	455	83.8	30.3	5.1	17.8	28.9

Table 3-2

Block shear test results

Specimen	At Tension Fracture		At Peak Load	
	Load (kN)	Deformation (mm)	Load (kN)	Deformation (mm)
T1A	691	10.4	696.0	9.0
T1B	691	7.3	690.8	7.3
T1C	716	9.3	715.9	9.3
T2A	N/A	N/A	513.0	N/A
T2B	756	8.9	756.0	8.9
T2C	678	5.6	693.1	5.0

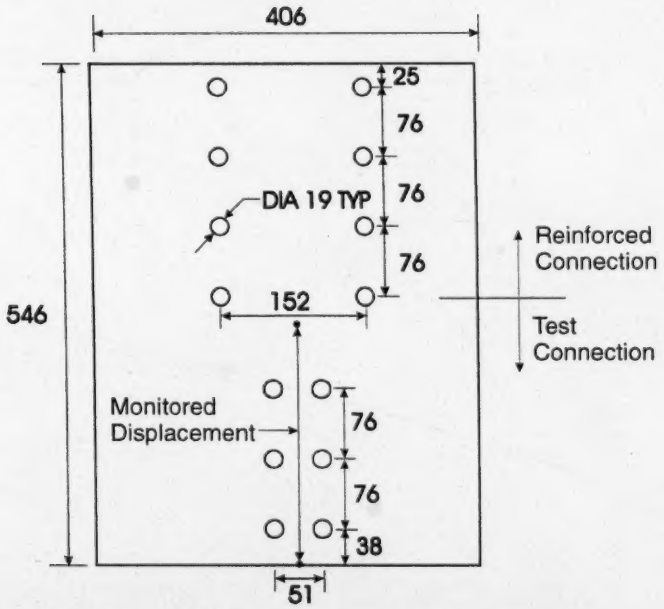

Figure 3-1 Test specimens T1A, T1B, and T1C

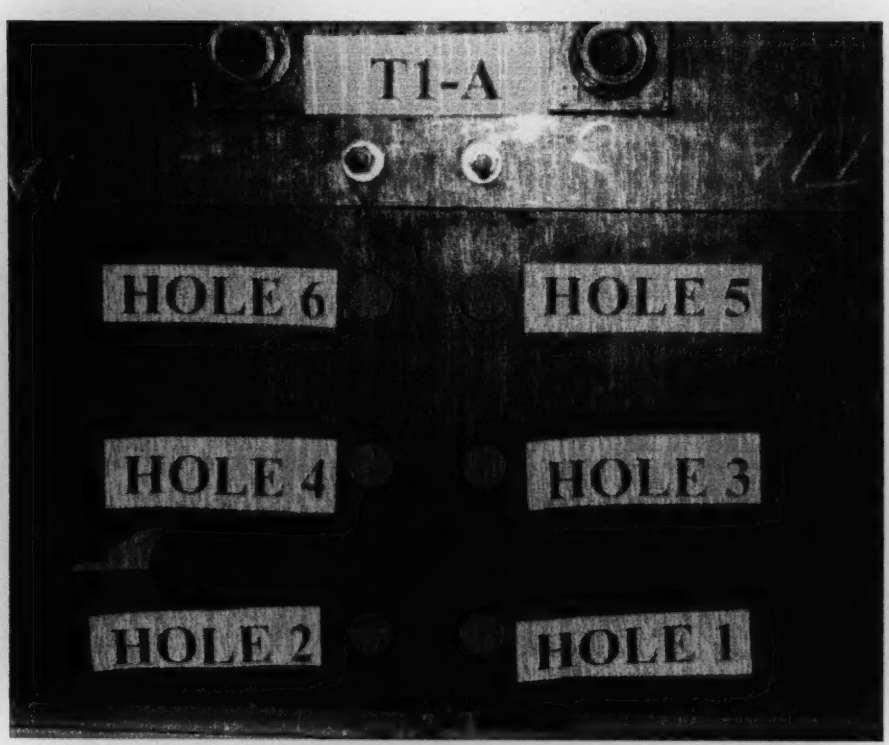

Figure 3-2 Typical bolt layout and numbering for test specimens T1A, T1B and T1C

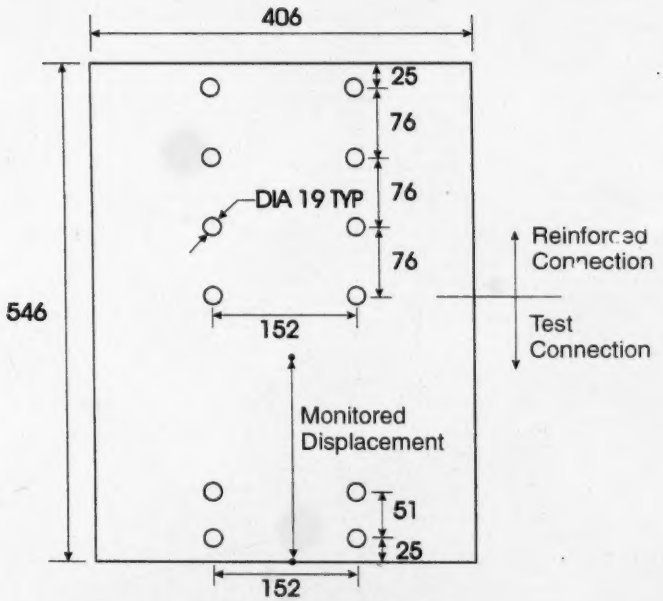

Figure 3-3 Test specimen T2A

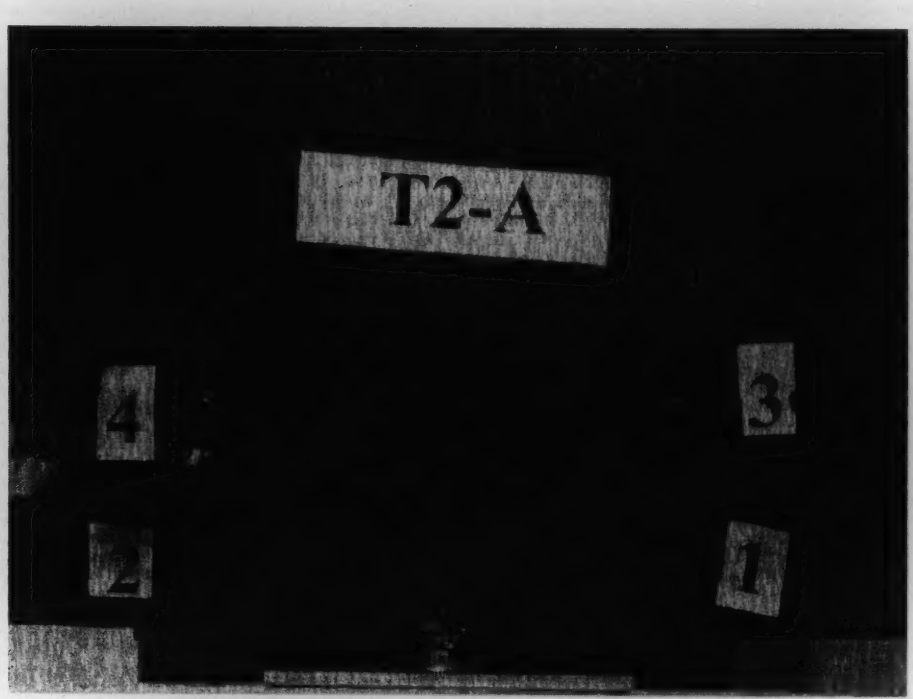

Figure 3-4 Typical bolt layout and numbering for test specimen T2A

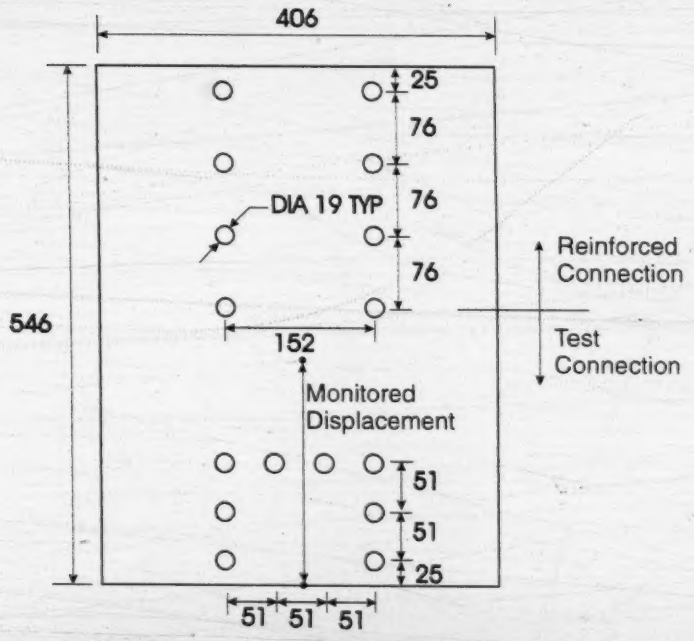

Figure 3-5 Test specimens T2B and T2C

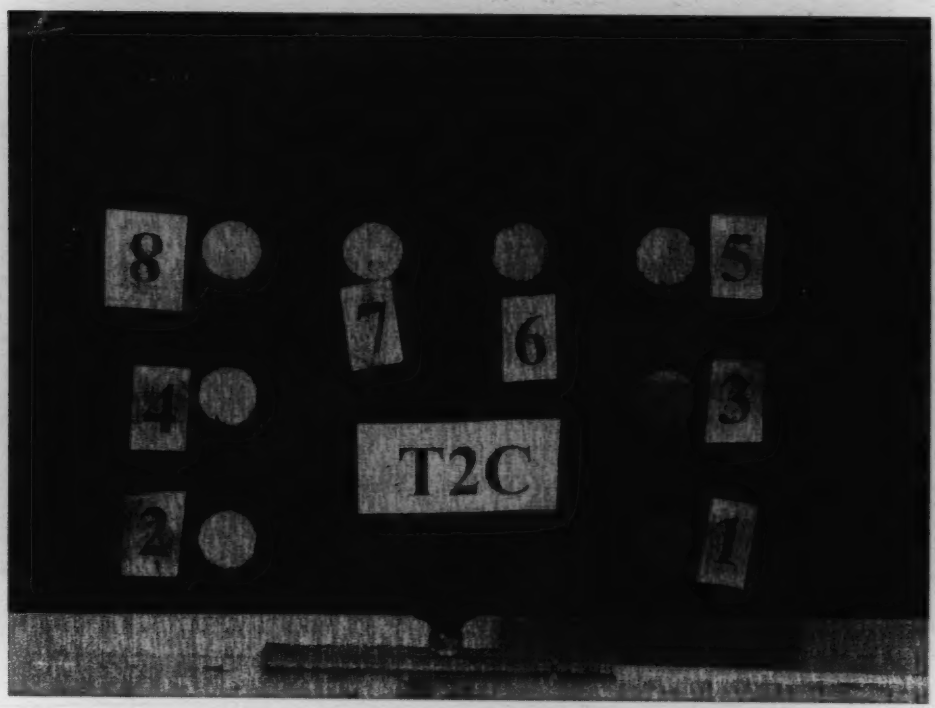

Figure 3-6 Typical bolt layout and numbering for test specimens T2B and T2C

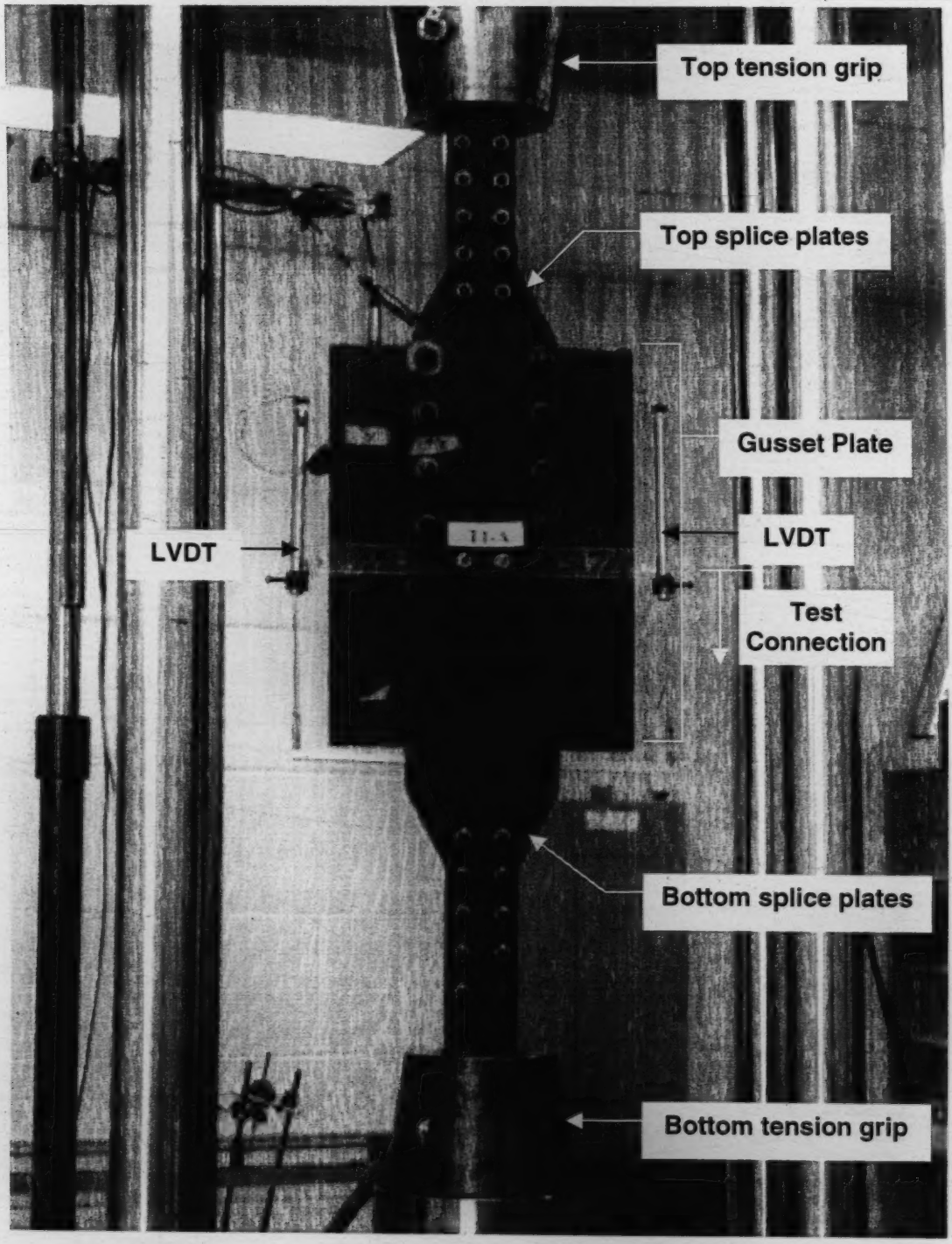

Figure 3-7 Test set-up

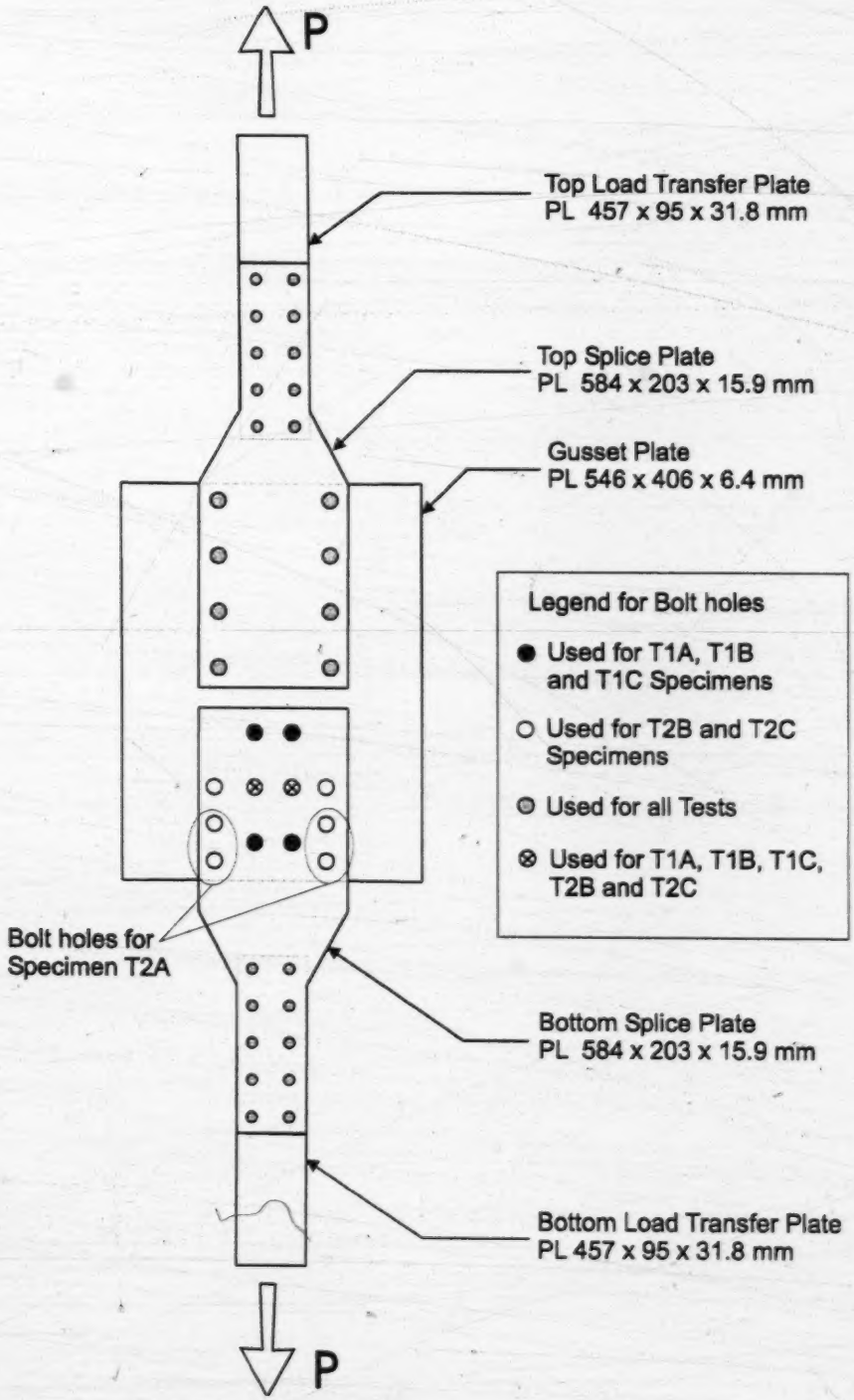
P
Top Load Transfer Plate
PL 457 x 95 x 31.8 mm
Top Splice Plate
PL 584 x 203 x 15.9 mm
Gusset Plate
PL 546 x 406 x 6.4 mm
Legend for Bolt holes
Used for T1A, T1B and T1C Specimens
Used for T2B and T2C Specimens
Used for all Tests
Used for T1A, T1B, T1C, T2B and T2C
Bolt holes for Specimen T2A
Bottom Splice Plate
PL 584 x 203 x 15.9 mm
Bottom Load Transfer Plate
PL 457 x 95 x 31.8 mm
P

Figure 3-8 Diagram of test set-up

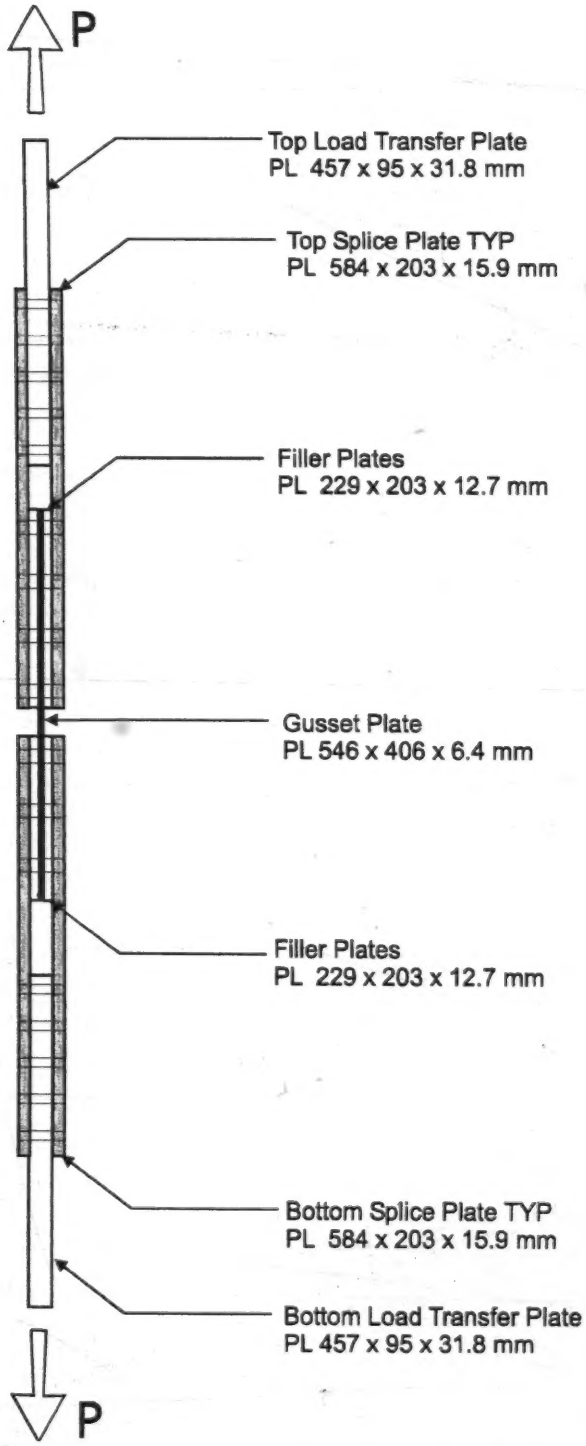
P
Top Load Transfer Plate
PL 457 x 95 x 31.8 mm
Top Splice Plate TYP
PL 584 x 203 x 15.9 mm
Filler Plates
PL 229 x 203 x 12.7 mm
Gusset Plate
PL 546 x 406 x 6.4 mm
Filler Plates
PL 229 x 203 x 12.7 mm
Bottom Splice Plate TYP
PL 584 x 203 x 15.9 mm
Bottom Load Transfer Plate
PL 457 x 95 x 31.8 mm
P

Figure 3-9 Side view of test set-up

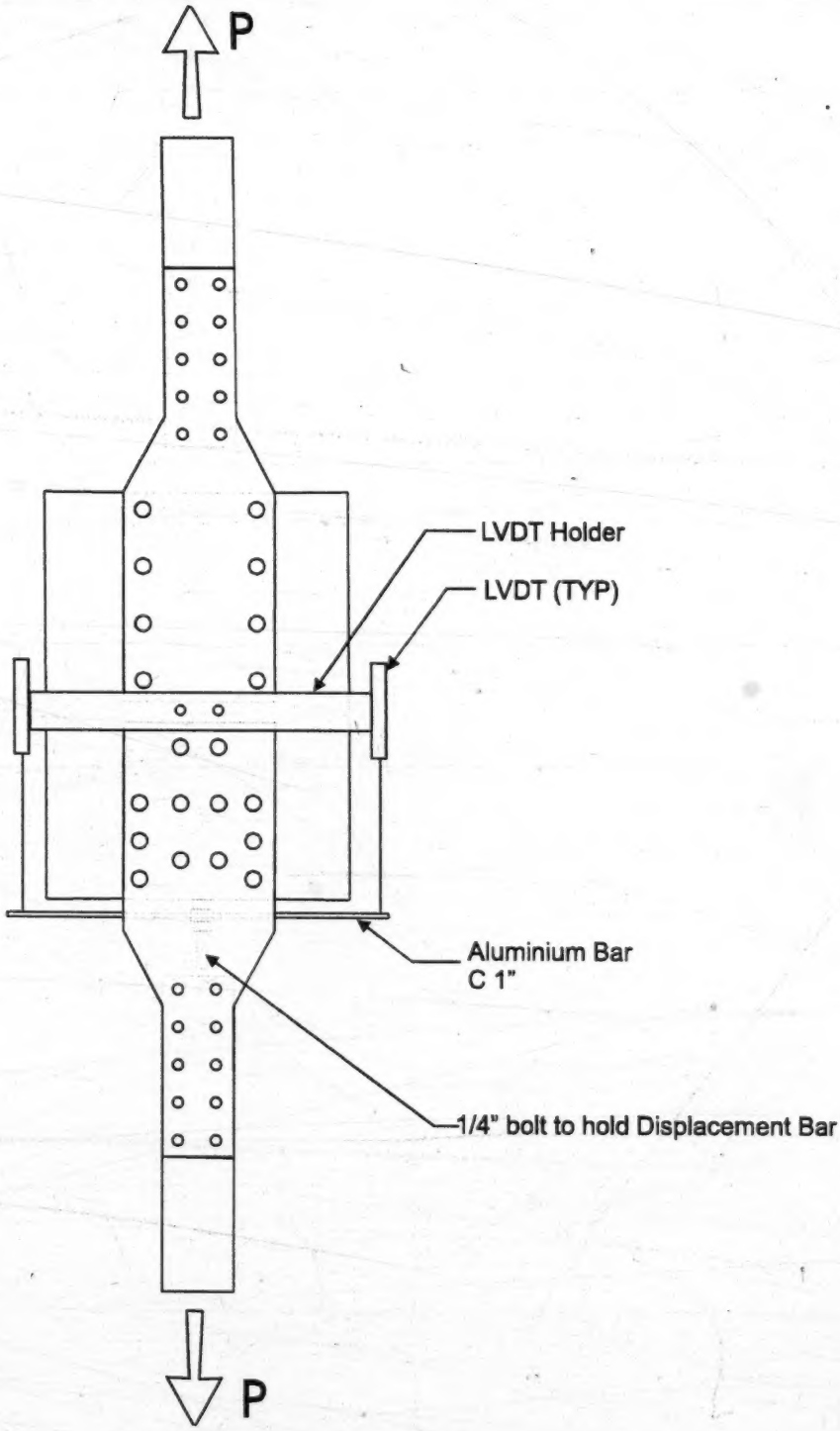

Figure 3-10 Instrumentation of test specimen

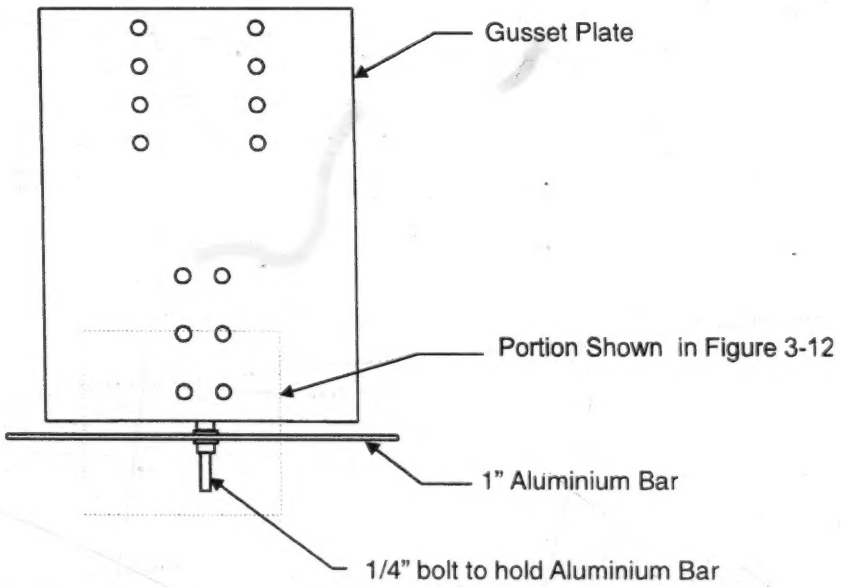

Figure 3-11 Connection of the aluminium bar at the displacement point

Figure 3-12 Connection of the aluminium bar at the displacement point

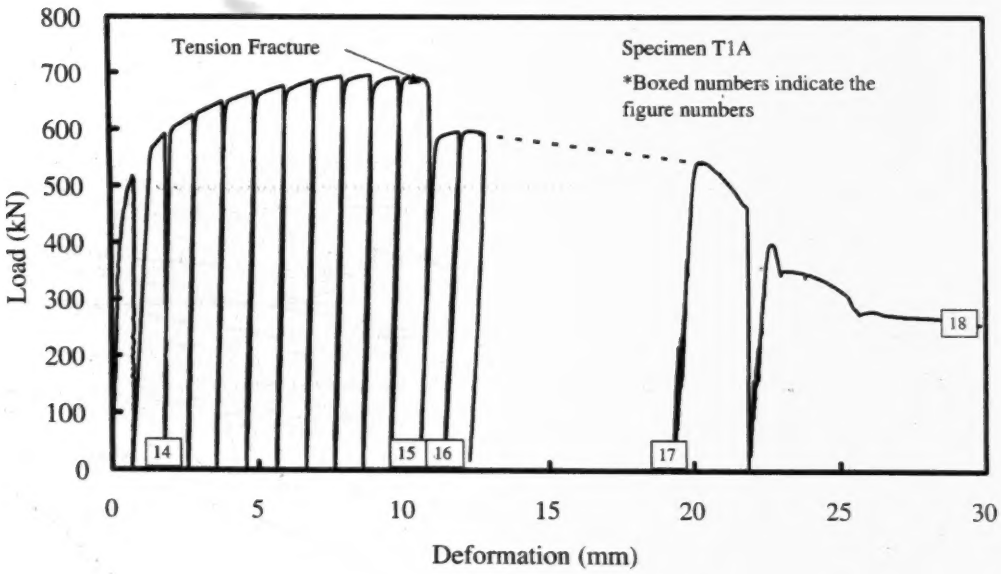

Figure 3-13 Load vs. deformation curve for specimen T1A

Figure 3-14 Specimen T1A at 2 mm displacement

a) Entire connection

b) Necking of tension face

Figure 3-15 Specimen T1A at 11 mm displacement

a) Entire connection

b) Tension fracture between holes 5 and 6

Figure 3-16 Specimen T1A at 12 mm displacement

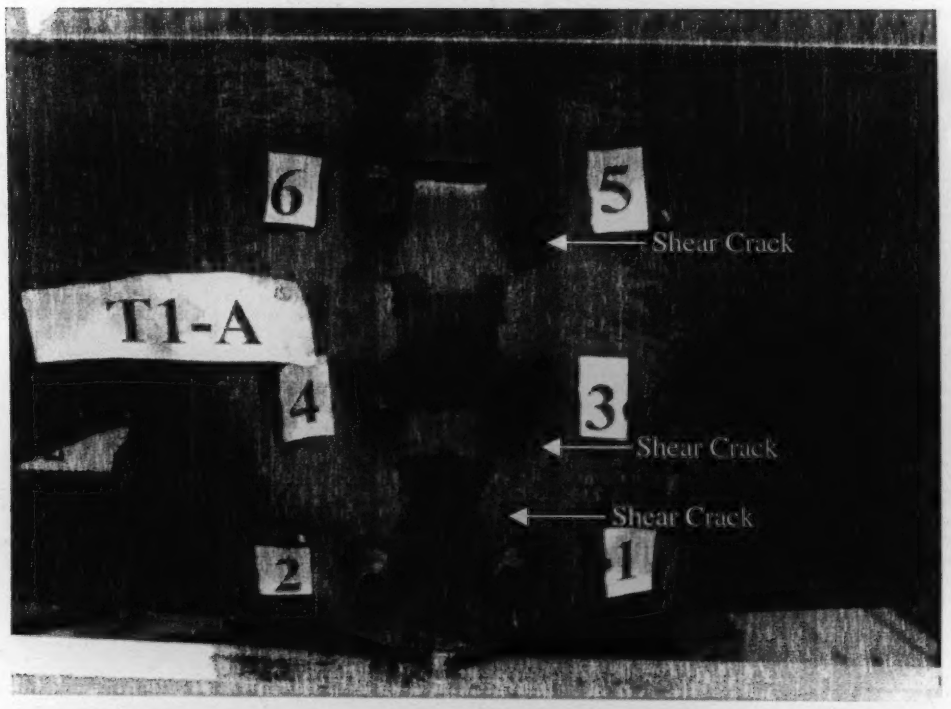

Figure 3-17 Specimen T1A at 19 mm displacement

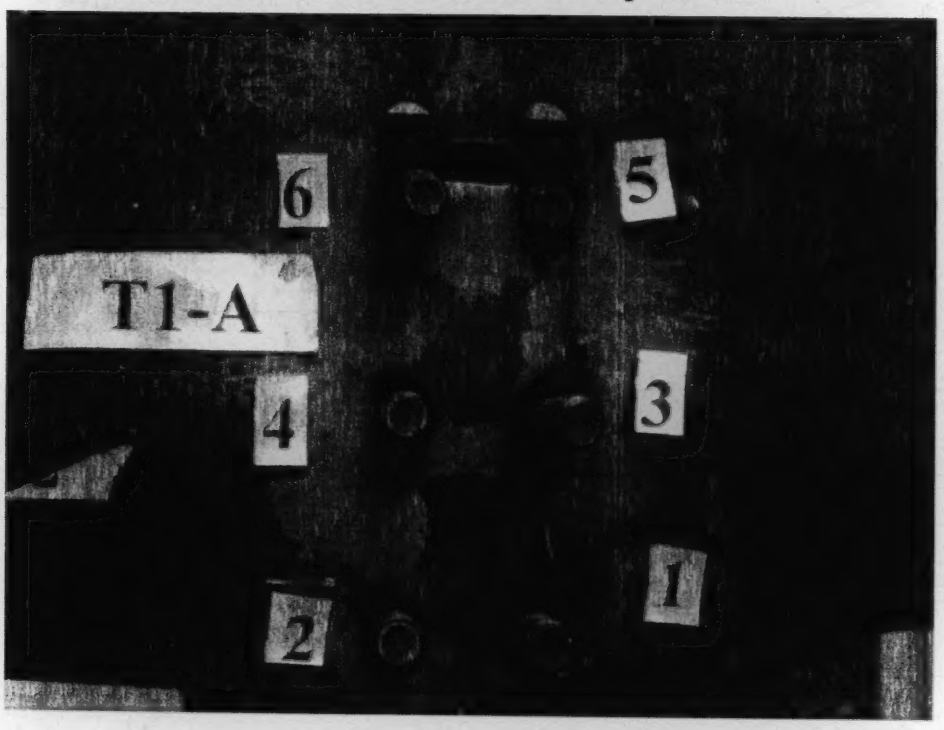

Figure 3-18 Specimen T1A at the end of testing

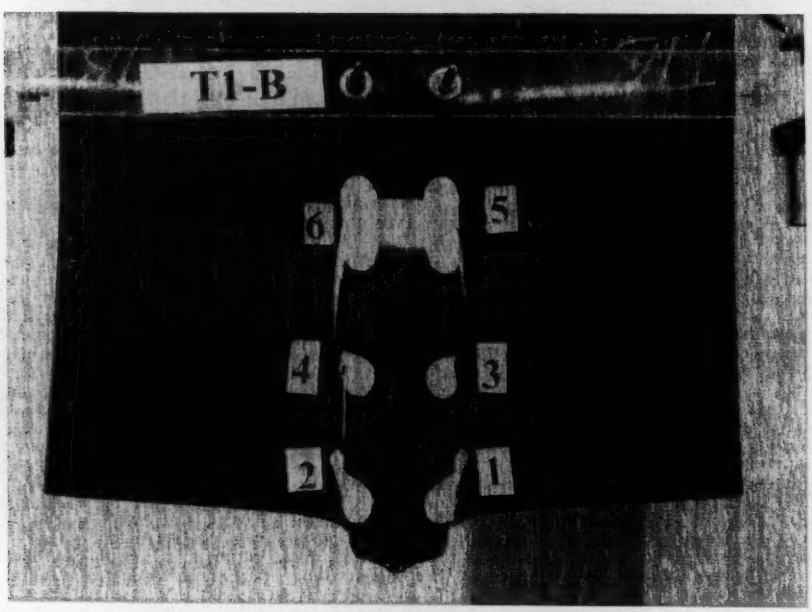

Figure 3-19 Specimen T1B at end of test

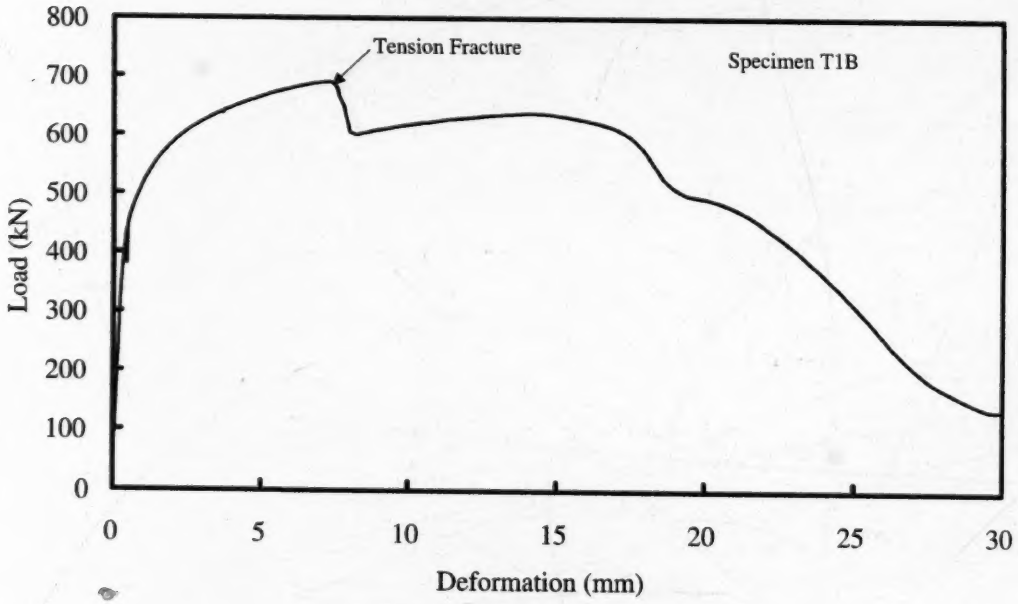

Figure 3-20 Load vs. deformation curve for specimen T1B

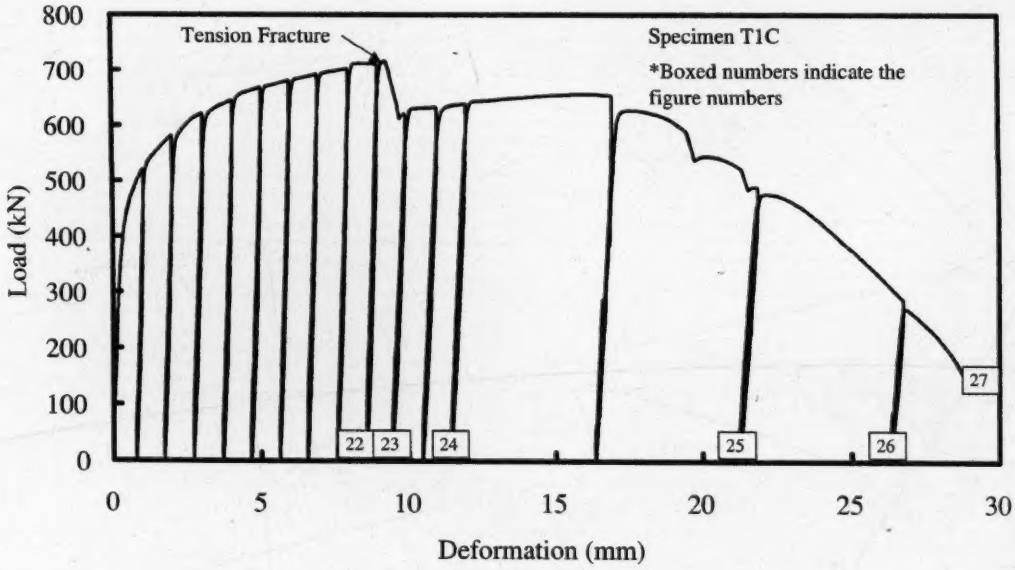

Figure 3-21 Load vs. deformation curve for specimen T1C

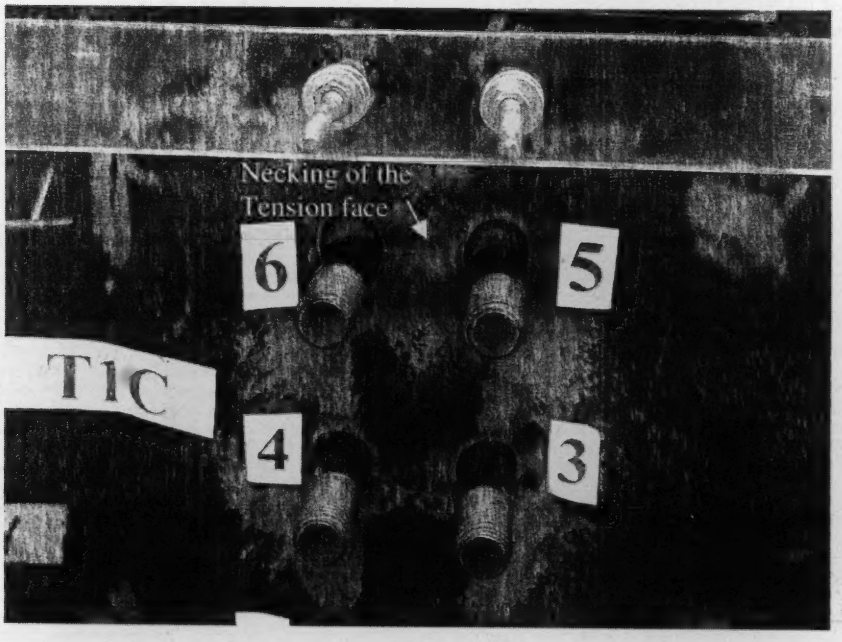

Figure 3-22 Specimen T1C at 9 mm displacement

Figure 3-23 Specimen T1C at 10 mm displacement

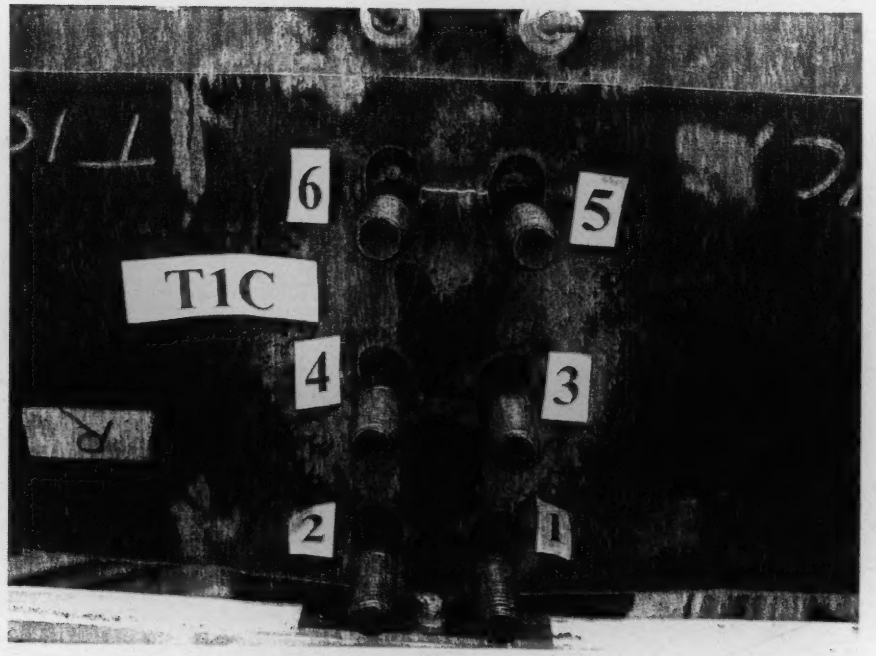

Figure 3-24 Specimen T1C at 12 mm displacement

Figure 3-25 Specimen T1C at 22 mm displacement

Figure 3-26 Specimen T1C at 27 mm displacement

Figure 3-27 Specimen T1C at end of testing

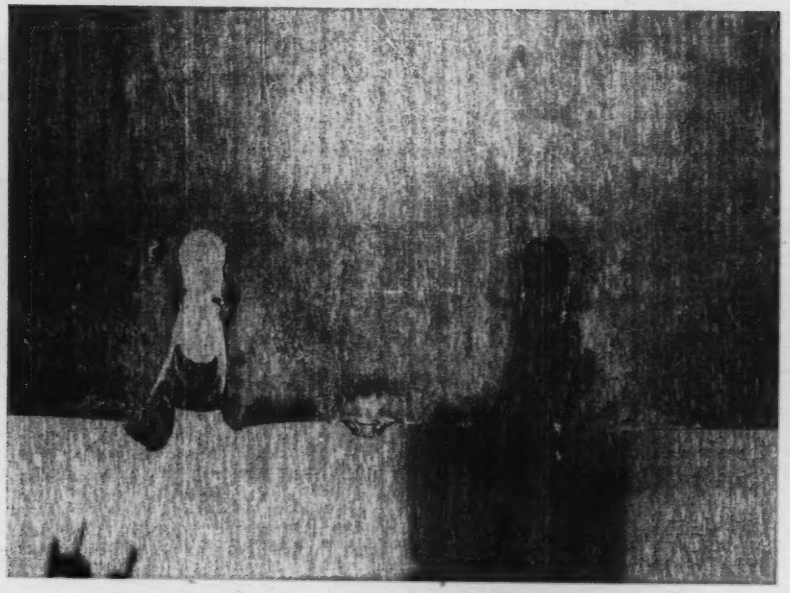

Figure 3-28 Specimen T2A at end of testing

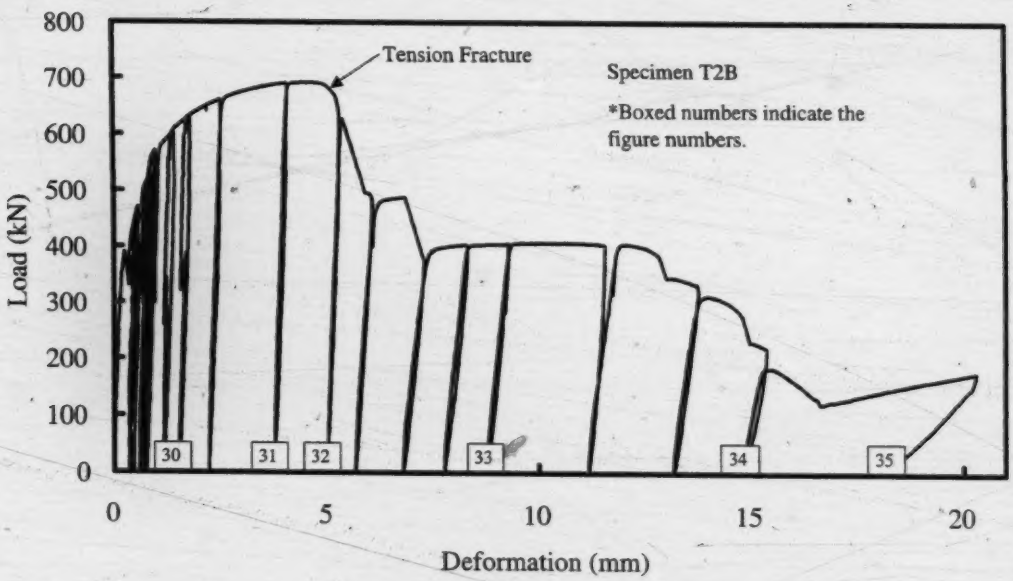

Figure 3-29 Load vs. deformation curve for specimen T2B

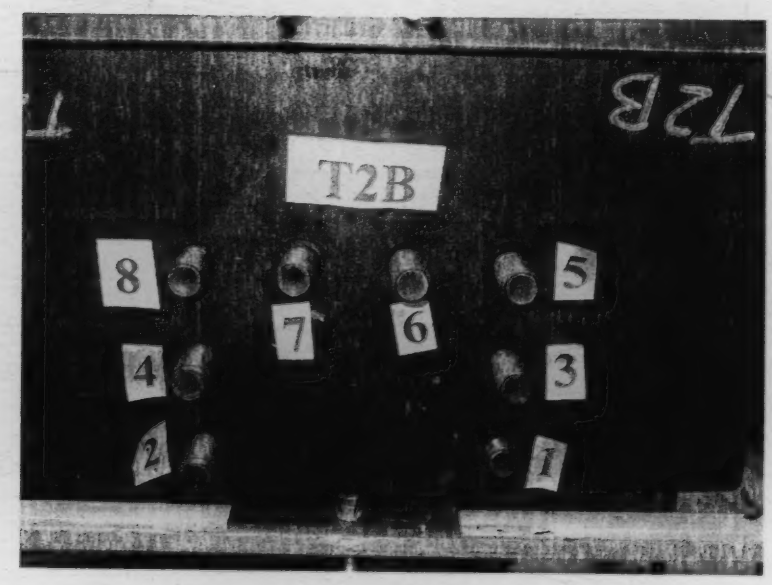

Figure 3-30 Specimen T2B at 600 kN

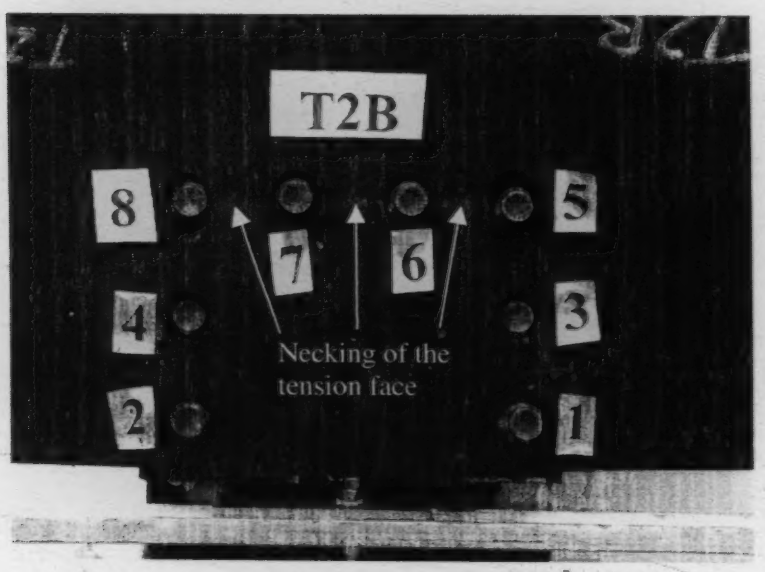

Figure 3-31 Specimen T2B at 690 kN

Figure 3-32 Specimen T2B at 660 kN

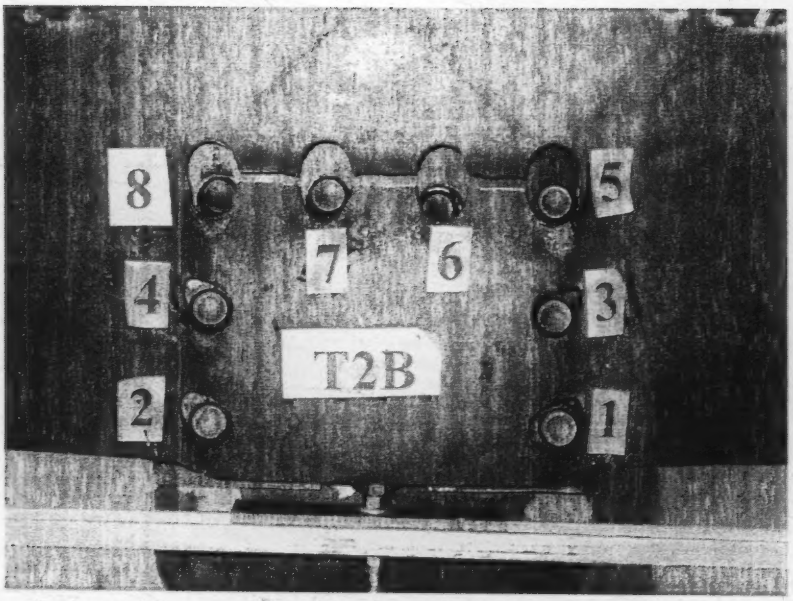

Figure 3-33 Specimen T2B at 403 kN

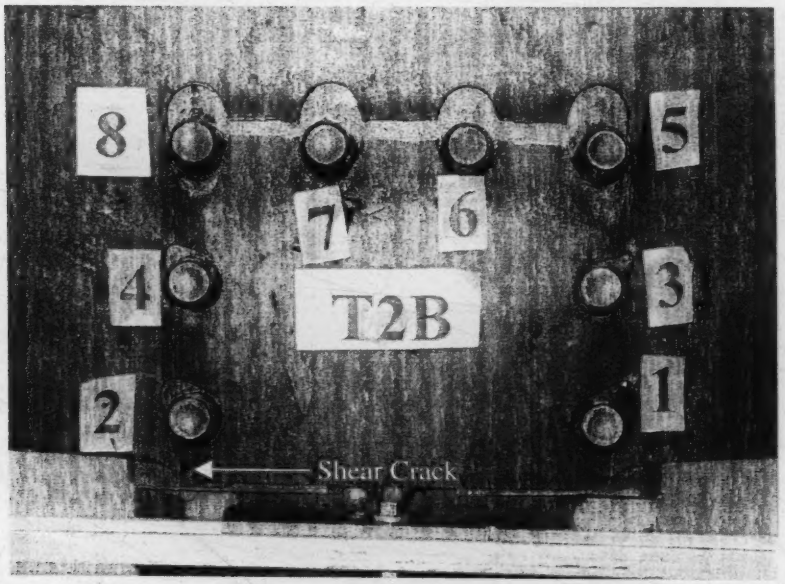

a) Entire connection

b) Crack at bottom of hole 1

Figure 3-34 SpecimenT2B at 331 kN

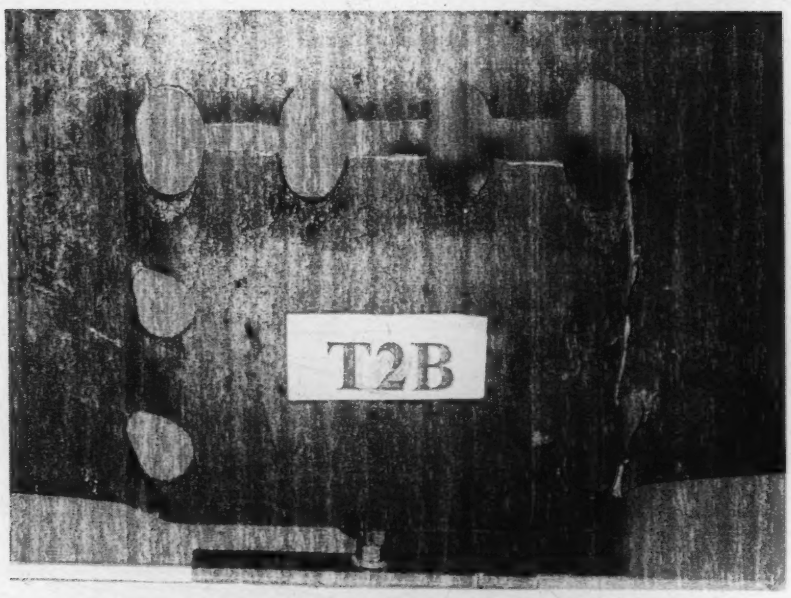

Figure 3-35 Specimen T2B at end of testing

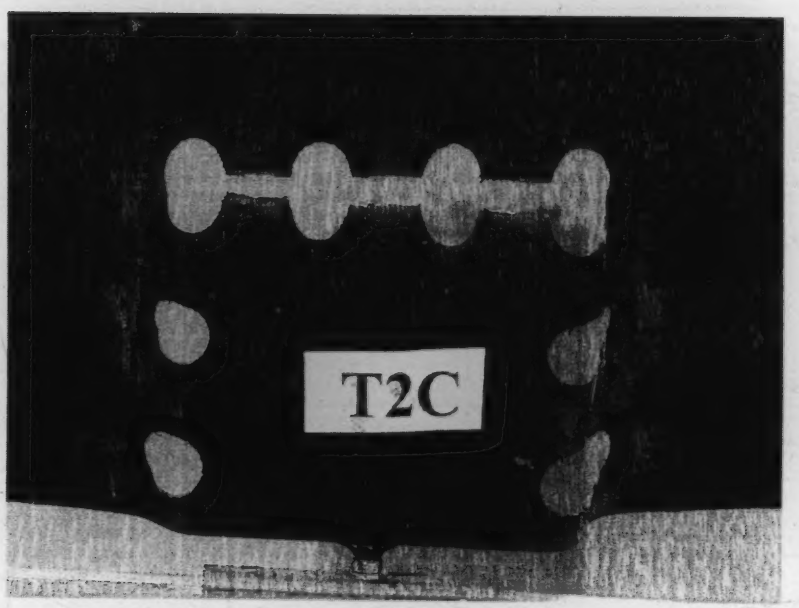

Figure 3-36 Specimen T2C at end of testing

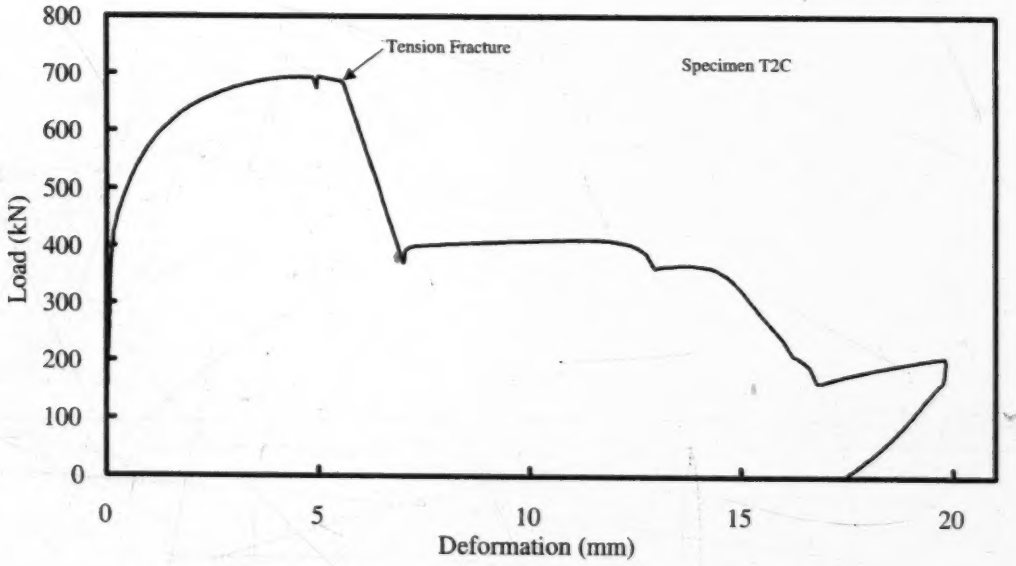

Figure 3-37 Load vs. deformation curve for specimen T2C

CHAPTER 4

FINITE ELEMENT ANALYSIS AND RESULTS

4.1 Introduction

The following describes a numerical investigation of block shear failure of gusset plates. The purpose of the finite element analysis is to develop a model that can predict the block shear behaviour of gusset plates so that the finite element model can be used to expand the database of test results on block shear in gusset plates. The general purpose non-linear finite element analysis program, ABAQUS (Hibbitt *et al.*, 1998), was used to conduct the analysis. The results of tests on ten gusset plates were used to validate the finite element model. The test specimens and the finite element models of these test specimens are discussed in detail in the following.

4.2 Finite Element Model

The finite element procedure used to investigate the strength and behaviour of gusset plates failing in block shear was validated by comparing the finite element predictions with test results. The general procedure and model for block shear investigation will be discussed using a model of gusset plate T-2 tested by Nast *et al.* (1999). Gusset plate T-2, shown in Figure 4-1, consists of a 550 mm×451 mm×9.6 mm plate of grade G40.21 350W steel. The bolted detail consisted of two lines of five 25 mm bolts, with a pitch and gauge distance of 70 mm. Differences between this model and models of other test specimens will be explained when predicted strength and behaviour are compared with test results.

Shell element S4R from ABAQUS was used to model the gusset plate. The S4R element is a four node doubly curved shell element that accounts for finite strains and allows for change in the element thickness. It has six degrees of freedom at each node (three displacement and three rotation components).

The analysis incorporated both geometric and material non-linearities. The material properties used in the finite element analysis were true stress and strain derived from the

engineering stress vs. strain curve obtained from tension coupon tests. The following equations were used to convert engineering stresses and strains to true stresses and strains (Hibbitt *et al.*, 1998):

$$\sigma_{true} = \sigma_{nom}(1 + \varepsilon_{nom}) \tag{4-1}$$

$$\varepsilon_{\ln} = \ln(1 + \varepsilon_{nom}) = \ln\left(\frac{A_o}{A}\right) \tag{4-2}$$

where,

σ_{true}: true stress,

σ_{nom}: engineering stress,

E : modulus of elasticity of the material,

ε_{nom} : engineering strain,

ε_{ln} : logarithmic (or true) strain,

A_o : initial cross-sectional area,

A : instantaneous cross-sectional area.

Equation (4-2) represents the total strain, which is the sum of the elastic strain and the plastic strain. This can be written as follows:

$$\varepsilon_{\ln}^{tot} = \varepsilon_{\ln}^{e} + \varepsilon_{\ln}^{p} = \frac{\sigma_{true}}{E} + \varepsilon_{\ln}^{p} \tag{4-3}$$

where $\varepsilon_{\ln}^{tot}$ is the total strain, $\varepsilon_{\ln}^{e}$ is the elastic component of the total strain, and $\varepsilon_{\ln}^{p}$ is the plastic component of the total strain. The plastic component of the strains and the corresponding stresses are summarized in Table 4-1 for the different finite element models described in the following.

An isotropic hardening material model was used in the inelastic range. To capture highly localized strains and stresses that develop after necking, an additional point (point B on the stress vs. strain curve shown in Figure 4-2) was needed on the stress vs. strain curve beyond the ultimate stress (point A in Figure 4-2). The slope of the stress vs. strain curve between points A and B was obtained from material properties of annealed A516 Steel presented by Khoo *et al.* (2000). The material modulus presented by Khoo *et al.* (2000) is

571 MPa. If the stress vs. strain curve is extrapolated to a true plastic strain of 120%, the resulting stress at point B varies between 1100 MPa and 1200 MPa for the various models presented in Table 4-1. Further discussion of the rupture strain used in the finite element analysis will be presented later.

Although the gusset plate tested by Nast *et al.* (1999) was mounted in a reaction frame that incorporated a beam and a column, only the gusset plate was included in the finite element model. The support provided to the gusset plate by the beam and column elements was modeled by a fixed boundary along the supported edges. Displacements were applied to the upper half of each bolt hole to simulate bearing of the bolts against the holes. In addition, to model the interaction between the splice plates and the gusset plate, all the nodes that would have been under the splice plate were restrained in the out-of-plane direction but were free to move in the plane of the plate.

Because of the large displacements and the large strains involved in the analysis, a non-linear analysis was used. The arc length method proposed by Riks and implemented in ABAQUS (Hibbitt *et al.*, 1998) was used for large deformation, large displacement analysis in the study. The procedure used to model fracture in tension and shear is explained in section 4.4.

4.3 Mesh Refinement Study

A mesh refinement study was conducted on the gusset plate model of Nast *et al.* test specimen T-2. The mesh refinement study was performed using three mesh sizes shown in Figure 4-3. The mesh size is defined by the number of elements placed between adjacent bolt holes. The coarse mesh has six elements between bolt holes, the intermediate mesh has 24 elements between bolt holes, and the fine mesh has 32 elements between bolt holes. In order to reduce the computation time, the fine mesh had elements that were fine near the bolt holes and coarser at some distance from the bolt holes as shown in Figure 4-3(c). Compatibility between the fine mesh portion and the coarse mesh portion of the model in Figure 4-3 was ensured by using constraint equations. Figure 4-4 shows the major principal strain distribution between the bolts in the last row of bolts when the gusset plate was subjected to a force of 1730 kN, corresponding to 95% of the

block shear capacity obtained in the test. The figure shows that convergence has not been reached with the coarse mesh. Because of material yielding, a high strain concentration was observed near the bolt holes, necessitating a very fine mesh to reach convergence. The two finer meshes show similar strain magnitudes and strain gradients near the bolt holes. Although the two strain distributions are not exactly the same, it was felt that a mesh finer than the one shown in Figure 4-3(c) would be impractical. Therefore, the fine mesh was adopted for the following analysis.

In order to validate the finite element model, the finite element results obtained with the fine mesh were compared to the test results presented by Nast *et al.* (1999). These tests were conducted under fully reversed cyclic loading. Figure 4-5 shows the test results on the tension portion of the cyclic loading curve (see dotted lines). In order to compare these test results to the finite element results, only the load vs. deformation envelope in the tension range (shown as a solid line in Figure 4-5) on the tension side of the loading history was used. The load vs. deformation curves, shown in Figure 4-6, shows a comparison between the finite element results and the test result. The deformation plotted on the horizontal axis corresponds to the monitored displacement identified in Figure 4-1. Since the stiffness and the behaviour predicted by the finite element model were in very good agreement with the test results, this mesh size was used for the remaining analyses.

4.4 Modelling of Fracture on the Tension Face

In order to model the progression of rupture during block shear failure, consistent failure criteria are required for the tension and shear faces of the block shear failure surface. It was felt that the failure criterion proposed by Epstein and Chamarajanagar (1994) would not be suitable for this study because the mesh size used in their investigation was much coarser than the mesh size found to be necessary to ensure convergence in the present investigation, and the rupture strain proposed (five times the yield strain) is much smaller than the rupture strain observed for structural steel. An investigation of the ductile fracture of steel by Khoo *et al.* (2000) showed that the localized rupture strain is approximately 80% to 120% for structural grade steel. The localized rupture strain was also obtained from tension coupon tests presented in Chapter 3. Measurement of cross-sectional areas before and after rupture and use of Equation 4-2 indicated a localized

rupture strain varying from 103% to 123%, with the average of three tension coupons at 113%. The work of Nast *et al.* (1999) and of other investigators cited below did not report cross-sectional area reduction from their material tests. Therefore, a rupture strain of 100% was assumed for the validation of the finite element analysis. This represents a lower bound of the test results for the plate specimens presented in Chapter 3, and represents an average of the values observed by Khoo *et al.* (2000).

In order to determine when fracture on the tension face would initiate, the major principal strain at the element integration points across the net tension face was plotted and extrapolated to the edge of the bolt holes using a sixth order polynomial. Rupture along the tension face was assumed to take place when the extrapolated major principal strain reached a value of 100%. As will be explained in section 4.5, a fracture criterion based on shear strain was also investigated. From the analysis of ten different gusset plate geometries presented below, the maximum shear strain coincident with a maximum principal strain of 100% varied from 110% to 140%. A value of 130% maximum shear strain was therefore adopted as one rupture criterion on the tension and the shear faces of the block shear failure plane. More details of this procedure are given in section 4.5.

Once the critical strain at the edge of the hole on the tension face was reached, all the elements on the tension face were removed from the model to simulate tension fracture. This sudden fracture of the tension face simulated in the analysis is consistent with the observations made during the tests described in Chapter 3. ABAQUS allows removal of elements in a model while the model is under load. This feature was used to enable creation of a crack-like feature in the model while the applied displacement on the gusset plate was maintained. The removal of elements is performed as a separate step in the loading process, thus allowing an equilibrium iteration to take place. Because the gusset plate is loaded under displacement control condition, the load vs. deformation curve shows a sudden decrease of load when elements along the tension plane are removed (see Figure 4-7).

4.5 Modelling of Fracture on the Shear Planes

Three shear fracture models were investigated. The first model consisted of using a maximum principal strain of 100% as the criterion for removing elements along the shear planes, as was done on the tension plane. The predicted load vs. displacement curve, shown in Figure 4-7, shows a small increase in load carrying capacity after tension rupture. As opposed to fracture on the tension plane, progression of fracture along the shear planes was observed to be gradual in the tests. Elements along the shear planes were therefore removed incrementally as the strain along the failure path reached the critical value. Removal of elements along the shear planes resulted in abrupt drops of load. The stepwise nature of the load vs. deformation curve beyond tension fracture is a feature of the discrete nature of the elements removal along the failure path. The test results presented in Chapter 3 indicated that the shear cracks were progressing gradually along the shear planes. This gradual fracture could not be modelled accurately in the finite element analysis by element removal due to the finite size of the elements. Rather, the element removal technique adopted for this investigation results in a stepwise load vs. displacement behaviour as observed in Figure 4-7. A lower bound estimate of the load vs. displacement curve can be obtained by joining the minimum load points. As the lower bound curve indicates, removal of elements was accompanied by a slight increase in load carrying capacity until a peak capacity was reached. In the Nast *et al.* specimen modelled herein a subsequent increase in capacity was observed after the load carrying capacity had started to decrease. This observed behaviour does not seem realistic, therefore another shear failure criterion was investigated.

The maximum shear strain was used as an alternative shear failure criterion. In order to establish the critical shear strain, the maximum shear strain distribution was plotted across the tension plane when the maximum principal normal strain had reached 100% on the tension plane. The shear strain distribution was then extrapolated to the edge of the bolt holes on the tension face to obtain the maximum shear strain associated with the 100% concentrated tension rupture strain. This critical maximum shear strain was then used as a rupture criterion on the shear planes. As for the previous shear rupture criterion, when an element along the shear plane reached the critical shear strain, the element and

as many as six other adjacent elements along the failure path were removed and an equilibrium iteration allowed the new equilibrium state to be reached before resuming loading. Load was further increased until the critical shear strain was reached once again in the next element along the maximum shear plane. The resulting load vs. deformation curve was a stepped curve, reflecting the stepwise nature of this crack propagation model. The loading and element removal process was repeated until the trend on the load vs. deformation curve showed a significant decrease in load carrying capacity as shown in Figure 4-8. Because of the method adopted to determine the critical shear strain, the value of this critical shear strain was different for different bolt hole layouts.

The third method was developed to obtain a critical shear strain common to all bolt hole layouts. The critical shear strain was therefore taken as the average critical shear strain obtained using the second method on ten different gusset plates. It was observed that the critical shear strain for ten gusset plates varied from 110% to 140%. A value of 130% shear strain was taken as the failure criterion. In contrast to the second method described above, the critical shear strain of 130% was also used as the fracture criterion on the tension plane. Once again, failure on the tension plane was modelled by removing all the elements on the tension plane when the maximum shear strain at the edge of a bolt hole on the tension plane had reached the critical value. Figure 4-9 shows the load vs. deformation curve obtained using this method for the gusset plate illustrated in Figure 4-1.

4.6 Comparison of Finite Element Analysis with Test Results

The gusset plates were loaded by imposing a displacement at each bolt hole on the 29 nodes closest to the loaded edge of the gusset plate. The 29 nodes were obtained by projecting the bolt diameter onto the bolt hole in the direction of the applied load. The only gusset plates that were not modelled in this manner were gusset plates tested by Mullin (2002). In these latter models, both the bolts and splice plates had to be modelled to capture yielding of the splice plates and bolt distortion. This was necessary because the measured displacements in these tests captured both the splice plate deformations and the bolt distortion. The following presents a short discussion of the finite element models of the 10 gusset plates used to validate the finite element procedure.

4.6.1 Nast et al. (1999)

Nast *et al.* (1999) conducted fully reversed cyclic tests on full-scale corner gusset plates. Figure 4-5 shows the tension portion of the cyclic response of the gusset plate and the test envelope, shown as a solid line. The response envelope was used for comparison with the finite element results shown in Figure 4-6. Since the test was stopped immediately after fracture on the tension face in the final load cycle, a comparison between the finite element analysis and test results cannot be made beyond rupture on the tension face. Figure 4-6 shows an excellent correlation between the experimental and the predicted load vs. deformation curves.

Modelling of shear rupture was discussed in section 4.5. The 130% maximum shear strain as the rupture criterion was found to provide a reasonable prediction of the block shear behaviour up to tension rupture. The predicted block shear failure progression after tension rupture is expected to fall between the curves designated as upper bound and lower bound in Figure 4-9. The lower bound curve is a function of the size and the number of elements removed in a particular step, which explains the slightly irregular shape of the lower bound curve. The expected behaviour of the gusset plate beyond tension rupture would be similar to the curve designated as the trend line, obtained using a regression analysis. The upper bound curve in Figure 4-9 shows that the tension rupture load was the peak capacity of this gusset plate.

The predicted progression of block shear failure in the gusset plate tested by Nast *et al.* is depicted in Figure 4-10. The sequence of events shown in the figure indicates that tension rupture occurs before onset of shear fracture, as observed in the test. The figure also shows that shear fracture takes place along the outside edge of the bolt holes, which suggests that shear fracture occurs on a surface area between the net shear area and the gross shear area of the connection, but much closer to the gross area.

4.6.2 Hardash and Bjorhovde (1984)

Two finite element models were developed for gusset plate specimens tested by Hardash and Bjorhovde (1984). One of the test specimens (Gusset Plate 1) is a 6.4 mm plate with

the bolt layout shown in Figure 4-11(a). The finite element mesh of gusset plate 1 is shown in Figure 4-11(b). The other test specimen from Hardash and Bjorhovde (Gusset Plate 11) was also a 6.4 mm plate. Its bolt layout is illustrated in Figure 4-14(a) and the finite element mesh is shown in Figure 4-14(b). A mesh density similar to that used for the test specimen by Nast *et al.* (1999) was adopted for these two models. Since a stress vs. strain curve was not provided, the stress vs. strain curve was assumed to have the same shape as that of Nast *et al.*, but was shifted to match the yield strength and ultimate strength reported by Hardash and Bjorhovde (1984). The stress vs. strain curve used for the analysis of the plates tested by Hardash and Bjorhovde is shown in Figure 4-12. The modulus of elasticity was taken as 204 000 MPa.

The load vs. deformation curve obtained from the finite element analysis of the Hardash and Bjorhovde specimens are shown in Figure 4-13 and Figure 4-15 for Gusset Plate 1 and Gusset Plate 11, respectively. The horizontal dashed line in these figures represents the reported test capacity. The capacity predicted from the finite element analysis is in very good agreement with the test capacity for Plate 1 and in reasonably good agreement with the test capacity for Plate 11. Once again it can be observed that the capacity of the gusset plate after tension fracture does not exceed the load level at tension rupture. The shear capacity after tension rupture increases by a very small amount, indicating that all or most of the shear capacity had been mobilized by the time fracture took place on the tension face of the block shear failure surface. For this reason, loading of Gusset Plate 11 in the finite element analysis was terminated at tension fracture. The predicted capacity is similar to that of the test capacity with a test-to-predicted ratio as shown in Table 4-2.

4.6.3 Mullin (2002)

Two finite element models were developed for gusset plate specimens tested by Mullin (2002). Specimen 4U is a 6.83 mm steel plate with bolt layout shown in Figure 4-16(a). The finite element mesh developed for 4U is shown in Figure 4-16(b). Specimen 8U was also a 6.83 mm plate. The bolt layout for this plate is shown in Figure 4-19(a) and the finite element mesh is shown in Figure 4-19(b). Once again, the test specimens were modelled using a mesh density similar to that used for the Nast *et al.* (1999) test specimen. Because the deformation reported by Mullin was measured on the splice

member at the position shown in Figures 4-16(a) and 4-19(a), the finite element model of the Mullin test specimens had to incorporate the splice member and the bolts as shown in Figure 4-16(c). The bolts were modeled as springs with an assumed non-linear spring stiffness of a 3/4" bolt load deformation curve provided in Kulak *et al.* (1987). Each bolt was modelled with eighteen spring elements. Figure 4-20 shows the load vs. deformation curve for a single spring element. To simulate bearing of the bolts on to the holes, eighteen spring elements were connected on the top half of each hole on the gusset plate and bottom half of each hole on the splice plates. The stress vs. strain curve used for the analysis was obtained from ancillary tests and is shown in Figure 4-17 and Figure 4-21 for specimens 4U and 8U, respectively. The modulus of elasticity was taken as 204 000 MPa and an isotropic hardening rule was used.

The test and predicted load vs. deformation curves for specimen 4U are presented in Figure 4-18. The analysis for this specimen was carried out beyond fracture on the tension surface and well into the shear fracture progression to confirm the trend of the load vs. deformation curve beyond fracture of the tension face. From the load vs. deformation curve, the finite element result shows a stiffness similar to that of the test result. The predicted capacity from the finite element analysis is in good agreement with the test results, with a test-to-predicted ratio of 1.10 as shown in Table 4-2. The load vs. deformation curve for specimen 8U is presented in Figure 4-22. The finite element analysis for this specimen was also carried out beyond tension fracture. The test-to-predicted ratio of 1.10 as shown in Table 4-2, shows that the test capacity and the predicted capacity are close. Analysis of specimen 8U was terminated when convergence could not be achieved.

4.6.4 Udagawa and Yamada (1998)

Finite element models were developed for three of the gusset plate specimens tested by Udagawa and Yamada (1998). All three plates had a thickness of 12 mm. The bolt hole patterns and finite element mesh for specimens designated as 224.4, 23F.4, and 423.4 are shown in Figures 4-23, 4-26 and 4-29, respectively. Since the stress vs. strain curve for the material was not provided, a stress vs. strain curve was developed using the method outlined above for the gusset plates from Hardash and Bjorhovde. The resulting stress vs.

strain curve is presented in Figures 4-24, 4-27 and 4-30 for specimens 224.4, 23F.4, and 423.4, respectively. The modulus of elasticity was taken as 204 000 MPa.

The load vs. deformation curves shown in Figure 4-25 (for specimen 224.4), Figure 4-28 (for specimen 23F.4) and Figure 4-31 (for specimen 423.4), show that the predicted capacities are very close to the actual test capacity in all three cases. The horizontal dashed line in these figures represents the test capacity. The test-to-predicted ratios for these three test specimens vary between 1.00 and 1.10 (see Table 4-2). The finite element models seem to predict the block shear capacity well in all three cases.

4.6.5 Gusset Plates from Current Investigation

Two finite element models were developed for the gusset plate specimens presented in Chapter 3. Since T1A, T1B and T1C had the same geometry, only one model, called T1, is necessary for these three specimens. Similarly, T2B and T2C are referred to at T2 in the following. The bolt pattern and finite element mesh used for T1 and T2 are shown in Figures 4-32 and 4-36, respectively. The stress vs. strain curve used for these models is presented in Figures 4-33 and 4-37 for T1 and T2, respectively. The stress vs. strain curves were derived from tension coupon test results and the procedure presented in section 4.2. As shown in Figure 4-34, the predicted capacity for specimen T1 is lower than the test capacity (Table 4-2 indicates a test-to-predicted ratio of 1.11). On the other hand, the predicted capacity for specimen T2 is greater than the test capacity as shown in Figure 4-37 (a test-to-predicted ration of 0.92 is obtained for this specimen). The progression of block shear failure is depicted in Figure 4-35 for specimen T1 and in Figure 4-39 for specimen T2. Although tension fracture occurred earlier in the finite element analysis there are strong resemblances to the failure progression photographs of the test specimens presented in Chapter 3.

For both gusset plates, the predicted ductility (expressed in terms of displacement) is significantly different from the ductility observed in the tests. One factor that could cause this significant difference in ductility would be that the bolt bearing condition for the finite element analysis is different from that obtained in the test specimens. The bolt bearing condition assumed in the finite element models is one where all the bolts are in

uniform bearing at the start of loading. In the test specimens, the bolt bearing condition is likely to be uneven, therefore resulting in different displacements from those predicted by the finite element analysis model at any given load level. This factor should not be a major consideration since the splice plates and gusset plates were matched drilled. Although load vs. deformation curves could not match the ductility exhibited in the tests, the finite element analysis models are successful at predicting the load carrying capacity and the general load response for all the gusset plates investigated in this validation process. The drop in load at tension fracture and the shear capacity observed after rupture of the net tension area are approximately the same magnitude as observed in the test specimens.

4.7 Parametric Study

The purpose of the parametric study was to expand the range of the gusset plate parameters that were not tested in previous laboratory experiments. A summary of all test result presented in the literature is presented in Table A-1 of Appendix A. This table lists the important geometric and material parameters for the gusset plates tested by various researchers. In order to define the geometry of gusset plates required to expand the database of test results, the range of each parameter affecting block shear capacity has been summarized in Table 4-3. The parameters that were considered in the analysis include plate thickness, number of bolts in the connection, bolt hole diameter, end distance, gauge distance, and pitch. Based on the data presented in Table 4-3, only five gusset plates were analysed for the parametric study. A summary table of connection parameters of each of the following gusset plates analysed for the parametric study is shown in Table 4-4. The number of bolts per line was expanded from a maximum of five in the experimental programs to eight in this investigation. The range of the gauge distance was expanded to 150 mm from a maximum of 101 mm in the pool of experimental data. Finally, the bolt pitch was doubled, thus pushing the 70 mm maximum pitch investigated experimentally to 140 mm. For all the gusset plates in the parametric study, material properties were assumed to be the same as those for the tension coupons presented in Table 3-1.

4.7.1 Plate 1 - Long and Narrow Connection

Plate 1 (6 mm thick) was analyzed to determine if the shear capacity developed after tension rupture would exceed the tension capacity prior to tension rupture, since the connection is very long and narrow. This connection has the largest number of bolts used in a connection, longest edge distance and the shortest gauge. Plate 1 used a total of 16 bolts with spacing of 70 mm, edge distance of 350 mm, and gauge distance of 35 mm, which corresponds to 2.7 times the bolt diameter (minimum allowed by the North American standards). Figure 4-40 shows the dimensions, bolt patterns and finite element mesh used for the analysis. Since the mesh is very fine and the gusset plate symmetrical, only half of the gusset plate was analyzed. The degrees of freedom along the axis of symmetry were all fixed, except for translation in the direction of the axis of symmetry. Figure 4-41, shows the load vs. deformation curve obtained from the finite element analysis. The load response indicates that tension fracture results in a relatively small reduction in load. The load response of the gusset plate after tension rupture indicates that most of the shear capacity was mobilized at the time tension fracture took place. This is to say that even with long narrow connections, the shear capacity would not exceed the tension capacity significantly. Figure 4-41 shows a capacity after tension rupture approximately 5% greater than the load carried at tension rupture. The capacity, taken conservatively at tension rupture, was noted at 1160 kN. The progression of block shear failure for this gusset plate is depicted in Figure 4-42 and shows that the shear failure plane develops along the outside edge of the boltholes.

4.7.2 Plate 2 - Long and Wide Connection

Plate 2 (6 mm thick) has the largest number of bolt holes, longest edge distance and the longest gauge distance. A total of 16 bolts are used with a pitch of 70 mm, edge distance of 350 mm, and gauge of 150 mm. Only half of the gusset plate was modeled to reduce the amount of time to generate the mesh and also to reduce the analysis time. Boundary conditions identical to those described for Plate 1 were also used for Plate 2. The gauge distance used in this specimen expands by almost 50% the maximum gauge distance investigated in a test program. Figure 4-43 shows the dimensions, bolt pattern, and finite element mesh used for the analysis. The analysis was conducted up to tension fracture.

Since the tension area of this connection is larger than for Plate 1, it is not expected that the capacity of the connection after tension fracture would exceed the load at tension fracture. Figure 4-44 shows the predicted load response of the gusset plate up to tension fracture. The capacity predicted by the finite element analysis is 1354 kN.

4.7.3 Plate 3 - Short and Narrow Connection

Plate 3 (20 mm thick) was analyzed using a mesh of the full connection. This connection has the shortest end distance, shortest gauge distance, and the smallest bolt spacing, all combined into one compact connection. The connection is a 4–bolt connection with a pitch of 35 mm, end distance of 17.5 mm, and gauge distance of 35 mm. Figure 4-45 shows the dimensions, the bolt pattern and the finite element mesh used for the analysis. The load response predicted by the finite element analysis is shown in Figure 4-46. The analysis was stopped at tension fracture. The predicted capacity for this gusset plate is 617 kN.

4.7.4 Plate 4 – Short and Wide Connection

The analysis of gusset plate 4 (12.7 mm thick) was also conducted using a mesh of the entire plate. With the exception of the plate thickness and the gauge distance, the dimensions of this gusset plate are the same as Plate 3. The gauge distance in Plate 4 is twice that in Plate 3, namely, 70 mm instead of 35 mm. Figure 4-47 shows the dimensions, bolt pattern, and finite element mesh used for this analysis. The load response of this gusset plate is illustrated in Figure 4-48. Despite the fact that the plate thickness is only 64% of that of Plate 3, the capacity is about 10% higher than that of Plate 3. This increased capacity is attributed to the increase in tension area resulting from the large increase in gauge distance.

4.7.5 Plate 5 – Large Bolt Spacing and Wide Connection

Plate 5 (6 mm thick) was also modelled in its entirety. This connection has a large gauge distance and the largest bolt spacing. A total of 4 bolts with a bolt spacing of 140 mm, edge distance of 150 mm, and gauge distance of 140 mm. The dimensions of the gusset plate and the finite element mesh are shown in Figure 4-49. The predicted capacity of the gusset plate, taken at fracture of the tension area, is 815 kN as shown in Figure 4-50.

4.8 Summary

A finite element procedure was developed for the investigation of block shear failure in gusset plates. The finite element analysis, performed using the commercial software ABAQUS, took into account the large plastic deformations taking place during the loading process to failure. It was found that convergence of strains at high strain magnitudes could only be achieved with a very fine mesh. A 'blunt crack' model was implemented by removing elements during the loading process to simulate the formation and progression of tears in the gusset plates. Element removal was performed when a critical strain was reach in an element. A critical value of the maximum shear strain of 130% was found to be an adequate failure criterion. The proposed finite element procedure was able to predict well the capacity of gusset plates and the trend of the load deformation curve after tension fracture. Although this approach cannot predict the true behaviour of the tearing process of block shear, it provides a useful tool to predict the block shear capacity of gusset plates. This finite element procedure was used to expand the database of test results to include gusset plates with longer connections, larger gauge distance, and longer pitch distance than investigated experimentally.

Table 4-1
Definition of the plastic portion of the true stress vs. true strain curve for the finite element analysis

Nast *et al.* (1999)		Hardash and Bjorhovde (1984)		Mullin (2002)		Udagawa and Yamada (1998)		Huns *et al.* (2002)	
True Stress (MPa)	True Strain (mm/mm)	True Stress (MPa)	True Strain (mm/mm)	True Stress (MPa)	True Strain (mm/mm)	True Stress (MPa)	True Strain (mm/mm)	True Stress (MPa)	True Strain (mm/mm)
421	0.000	229	0.001	306	0.000	278	0.001	337	0.000
428	0.011	234	0.012	313	0.018	293	0.012	337	0.004
443	0.021	247	0.021	405	0.054	317	0.021	338	0.011
489	0.040	289	0.041	448	0.084	372	0.040	429	0.047
523	0.063	319	0.063	480	0.115	413	0.063	472	0.075
547	0.086	338	0.087	504	0.150	446	0.086	536	0.161
595	0.151	377	0.152	537	0.211	517	0.151	1130	1.200
1194	1.200	975	1.200	1102	1.200	1116	1.200		

Table 4-2
Comparison of finite element predicted capacity with test results

Source	Test Specimen	Test Capacity (kN)	Predicted Capacity (kN)	Test/Predicted
Nast *et al.* (1999)	T-2	1815	1921	0.94
Hardash and Bjorhovde (1984)	Gusset Plate 1	243	252	0.96
	Gusset Plate 11	375	417	0.90
Mullin (2002)	4U	631	572	1.10
	8U	1078	984	1.10
Udagawa and Yamada (1998)	224.4	690	625	1.10
	23F.4	677	664	1.02
	423.4	685	687	1.00
Current Investigation	T1*	701	633	1.11
	T2*	692	756	0.92

* The test results reported here are the average results for each series.

Table 4-3
Range of parameters for all gusset plates investigated experimentally

	Plate Thickness (mm)	Number of Bolt Lines	Number of Bolts Per Line	Bolt Hole Diameter (mm)	End Distance (mm)	Gauge Distance (mm)	Bolt Pitch (mm)	Length of Connection (mm)
Minimum	6.0	2	2	14.3	19.0	39.8	38.1	63.2
Maximum	14.9	4	5	27.0	63.5	101.6	70.0	330.0

Table 4-4
Gusset plates used in the parametric study

Specimen	Plate Thickness (mm)	Number of Bolt Lines	Number of Bolts per Line	Bolt Hole Diameter (mm)	End Distance (mm)	Gauge Distance (mm)	Bolt Pitch (mm)
Plate 1	6.0	2	8	14.0	35.0	35.0	70.0
Plate 2	6.0	2	8	14.0	35.0	150.0	70.0
Plate 3	20.0	2	2	14.0	17.5	35.0	35.0
Plate 4	12.7	2	2	14.0	17.5	70.0	35.0
Plate 5	6.0	2	2	27.0	70.0	140.0	140.0

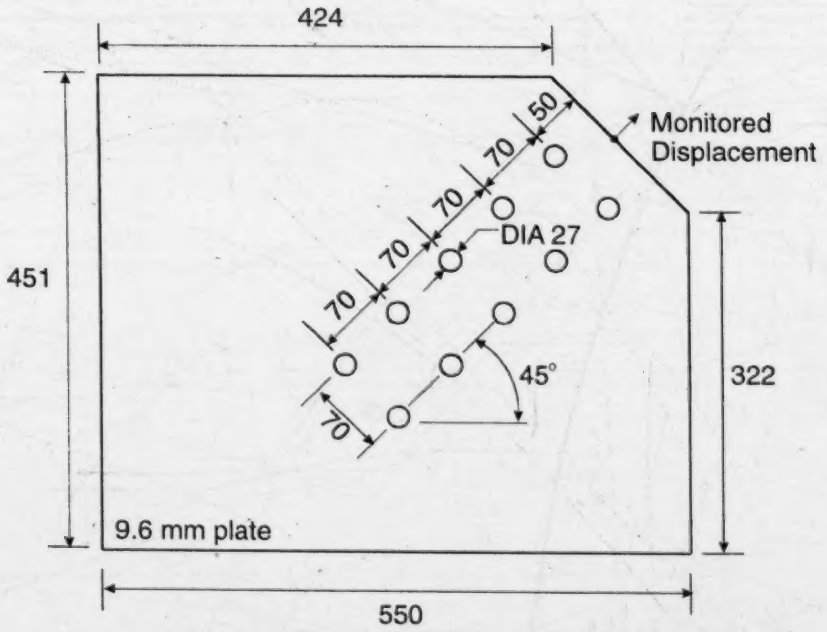

Figure 4-1 Gusset plate T-2 tested by Nast *et al.* (1999)

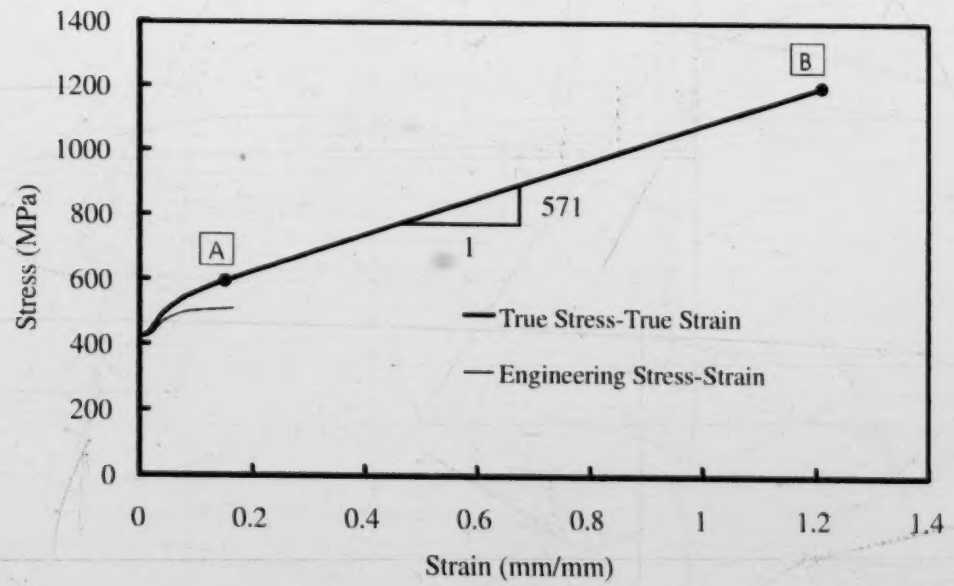

Figure 4-2 Stress vs. strain curve of gusset plate material from Nast *et al.* (1999)

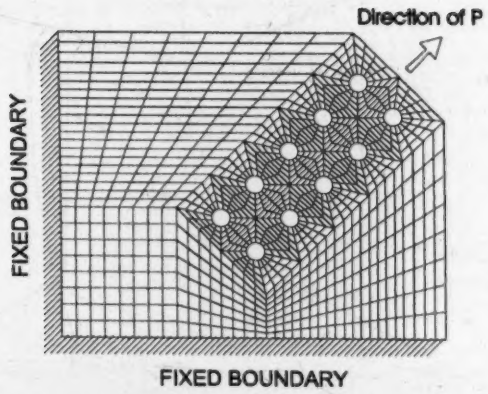

(a) Coarse mesh with 6 elements between bolt holes

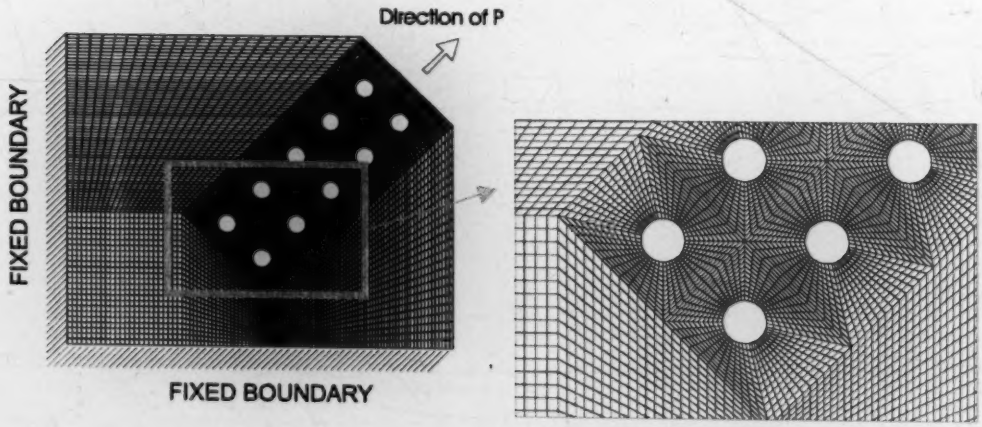

(b) Intermediate mesh with 24 elements between bolt holes

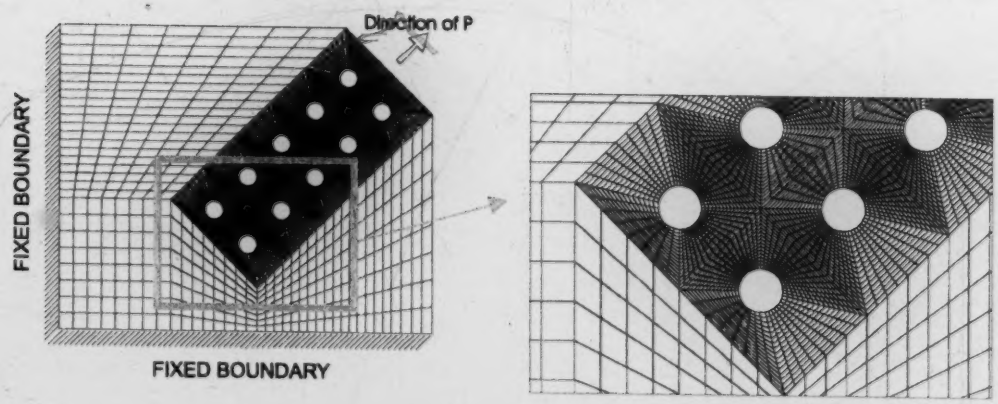

(c) Fine mesh with 32 elements between bolt holes

Figure 4-3 Meshes used for the mesh refinement study

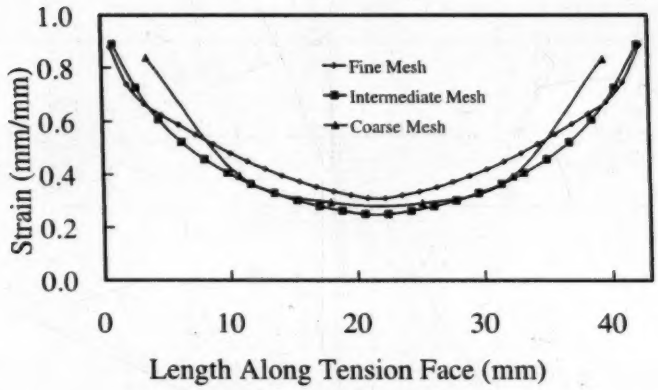

Figure 4-4 Convergence of strains along the tension face (Nast *et al.* Specimen T-2)

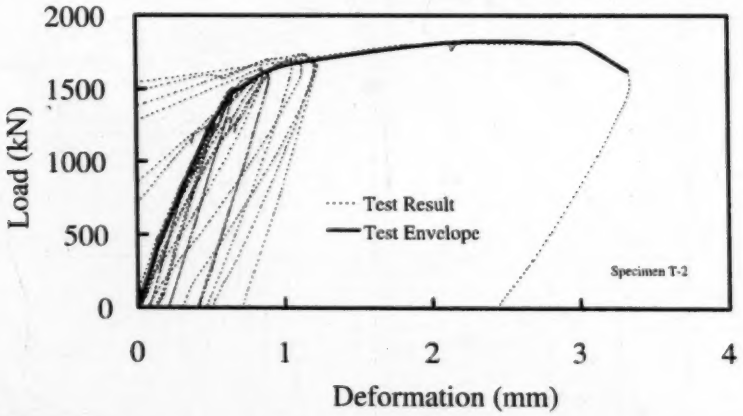

Figure 4-5 Tension portion of cyclic loading curve for gusset plate T-2 tested by Nast *et al.* (1999)

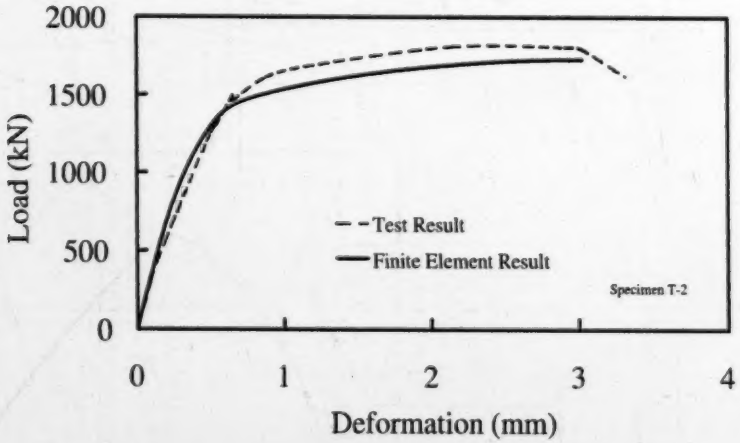

Figure 4-6 Load vs. deformation from fine mesh

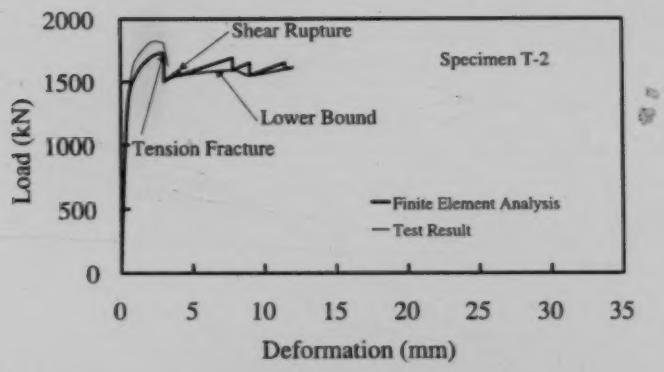

Figure 4-7 Predicted load vs. deformation response (100% maximum principal strain criterion)

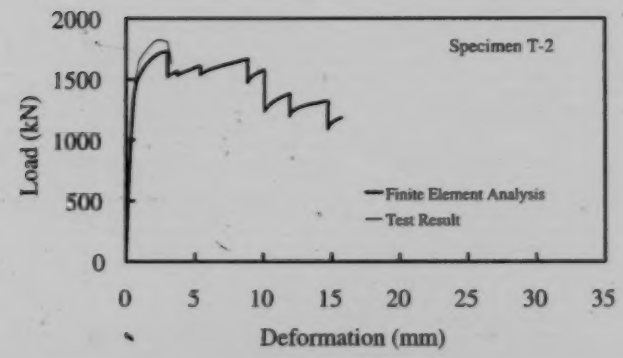

Figure 4-8 Predicted load vs. deformation response (maximum shear strain criterion)

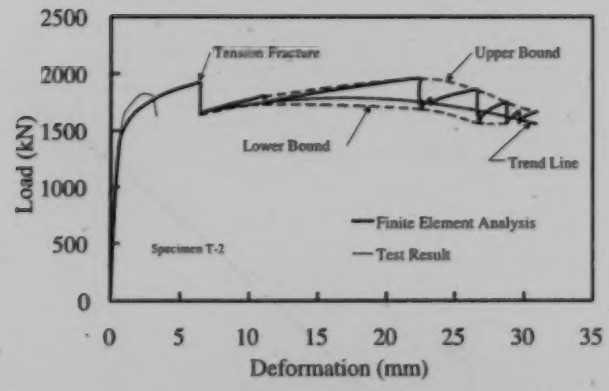

Figure 4-9 Predicted load vs. deformation response (130% shear strain criterion)

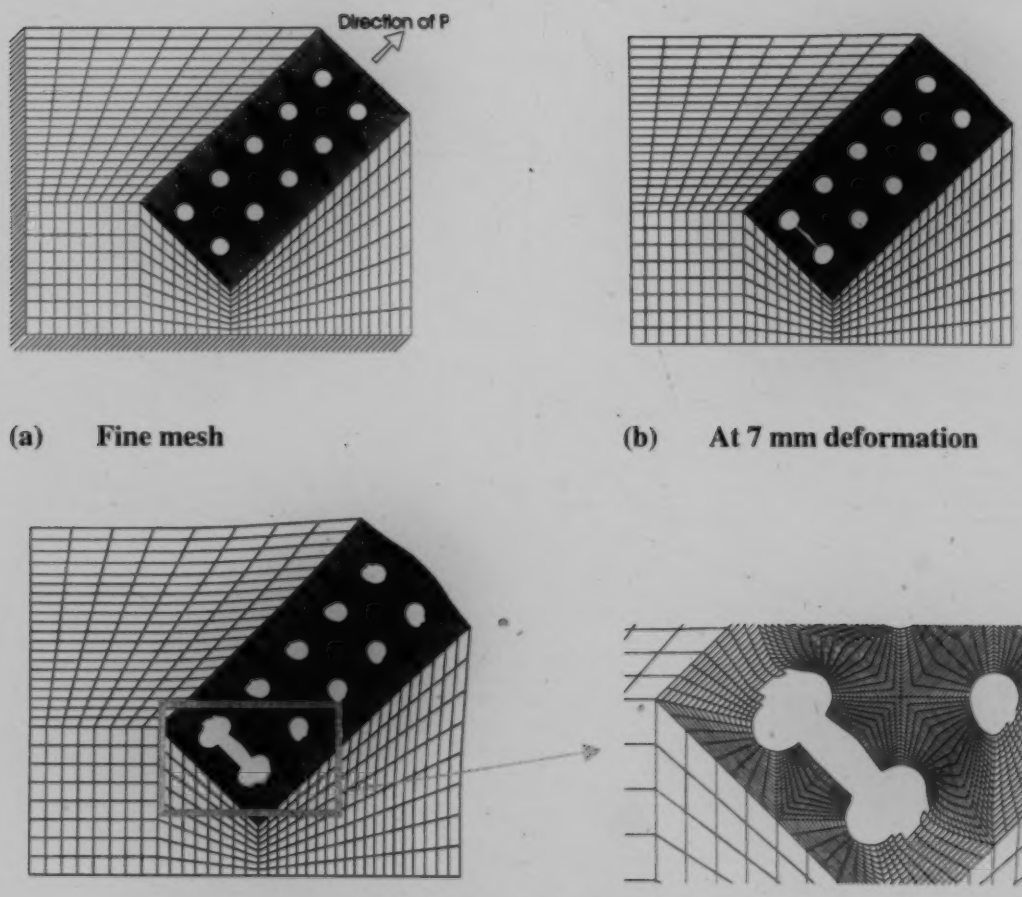

(a) Fine mesh

(b) At 7 mm deformation

(c) At 23 mm deformation

(d) At 30 mm deformation

Figure 4-10 Progression of block shear failure in gusset plate T-2 tested by Nast *et al.* (1999)

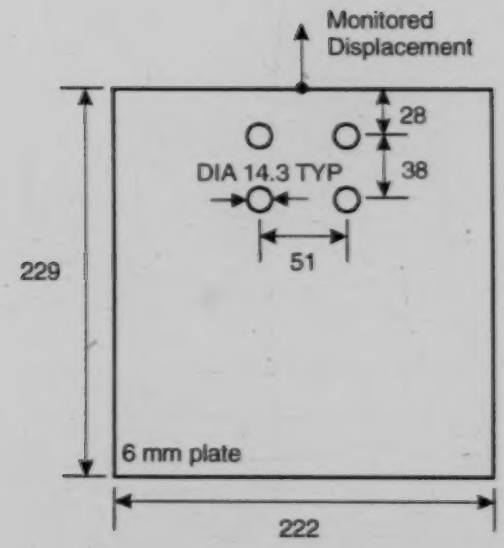

(a) Plate dimensions and bolt pattern

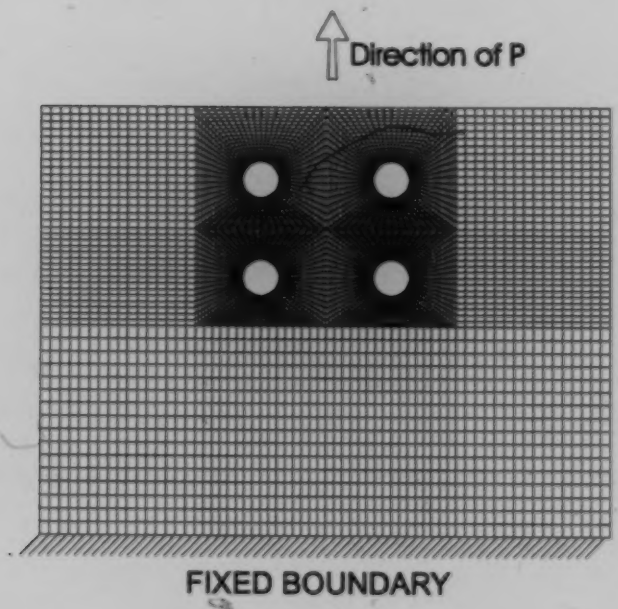

(b) Finite element mesh

Figure 4-11 Gusset plate 1 tested by Hardash and Bjorhovde (1984)

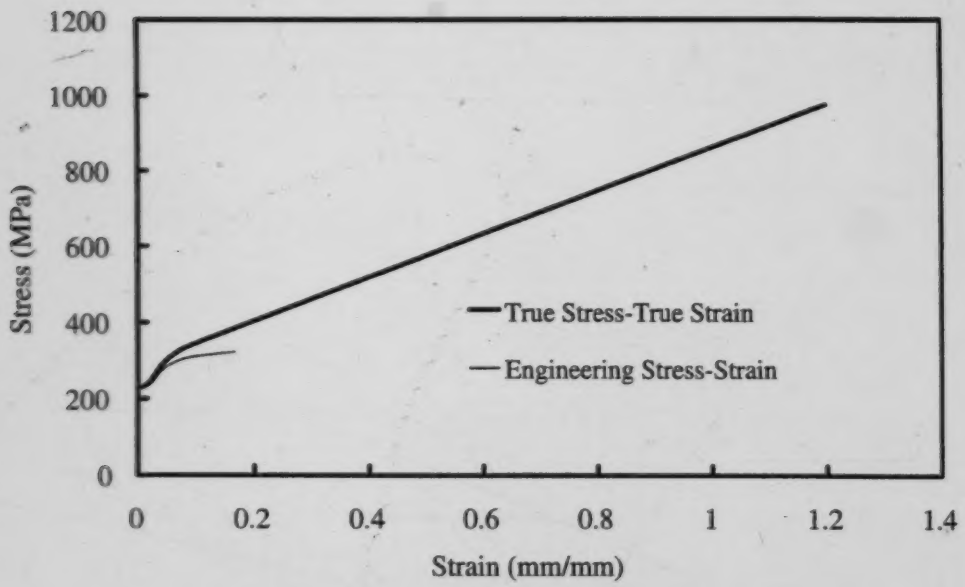

Figure 4-12 Stress vs. strain curve used for the analysis of gusset plate 1 tested by Hardash and Bjorhovde (1984)

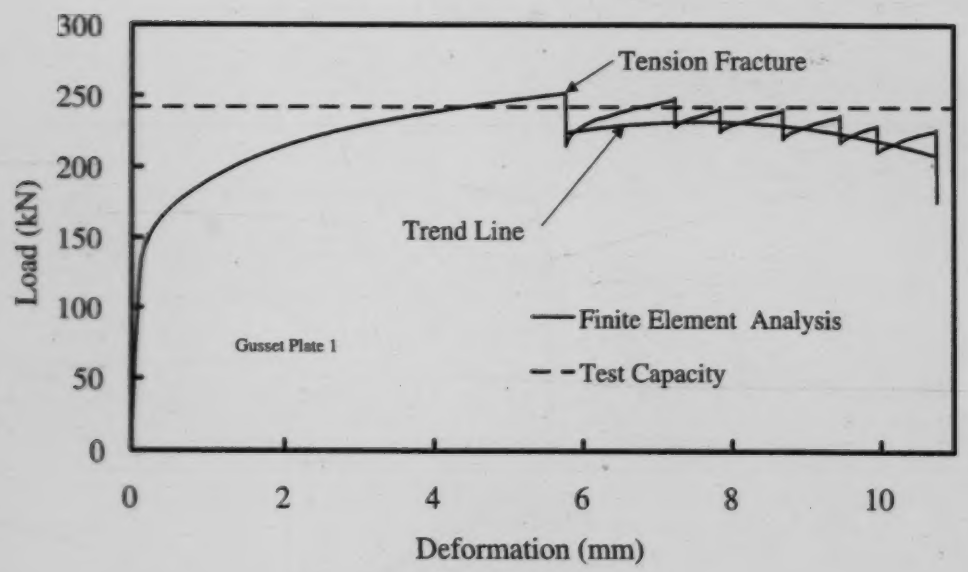

Figure 4-13 Load vs. deformation curve for gusset plate 1 tested by Hardash and Bjorhovde

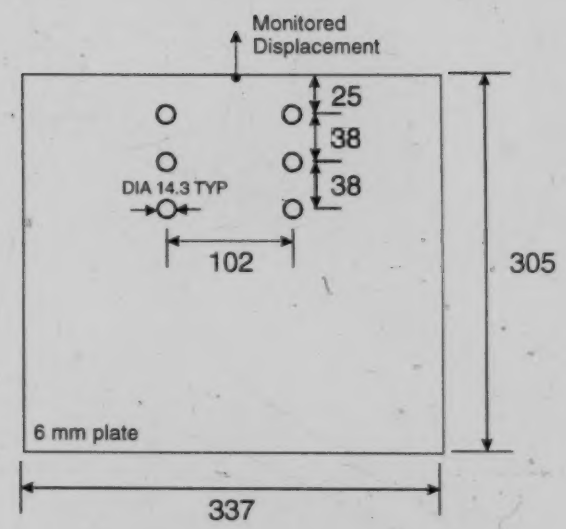

(a) Plate dimensions and bolt pattern

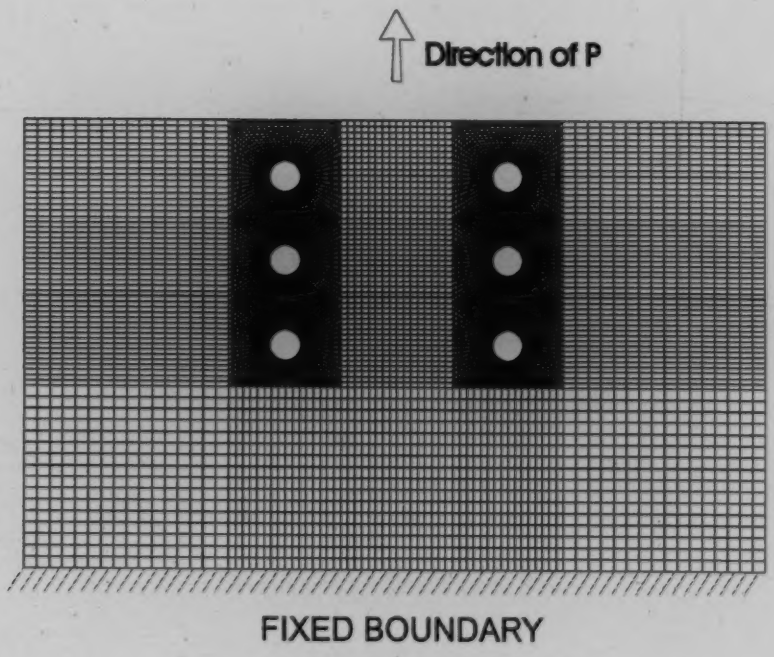

(b) Finite element mesh

Figure 4-14 Gusset plate 11 tested by Hardash and Bjorhovde (1984)

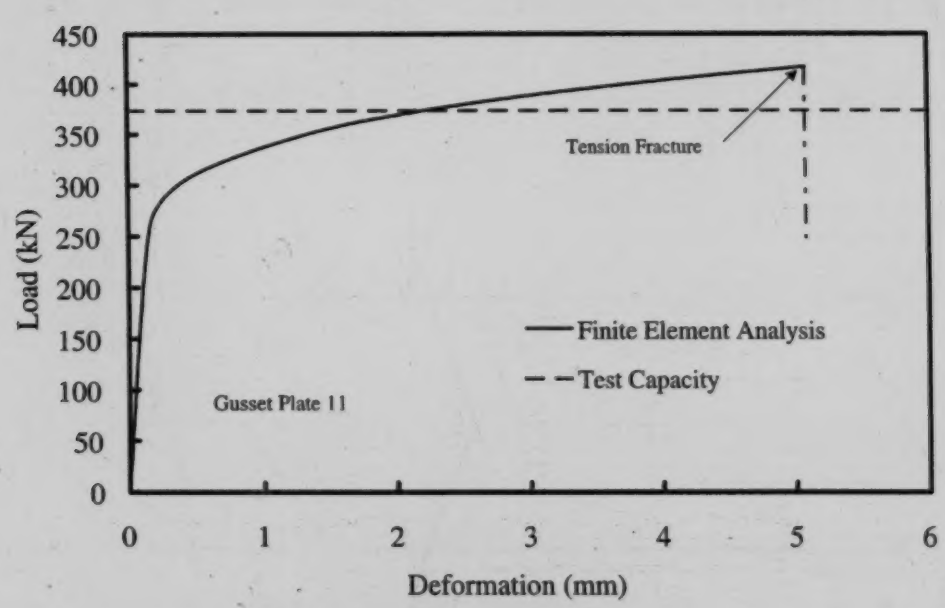

Figure 4-15 Load vs. deformation curve for gusset plate 11 tested by Hardash and Bjorhovde (1984)

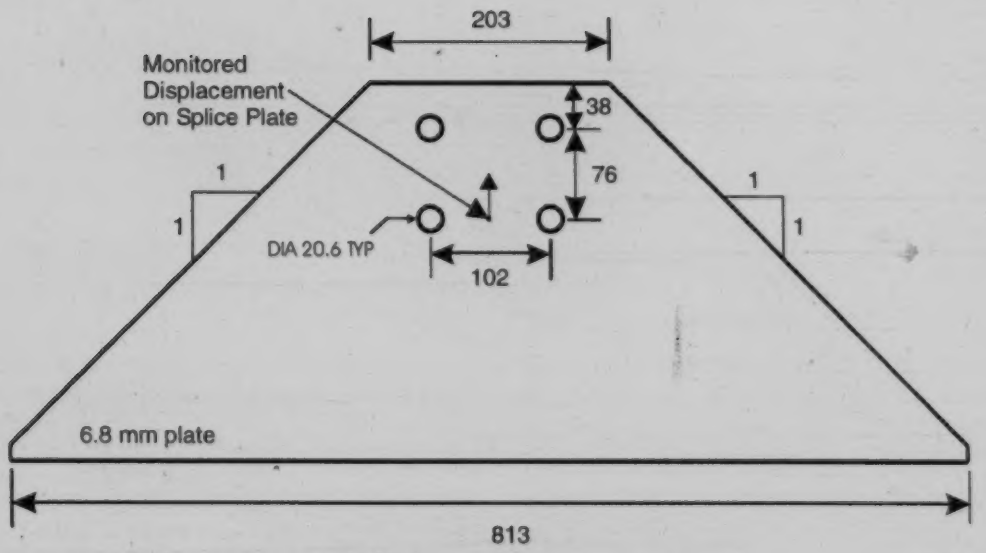

(a) Plate dimensions and bolt pattern

Figure 4-16 Gusset plate 4U tested by Mullin (2002)

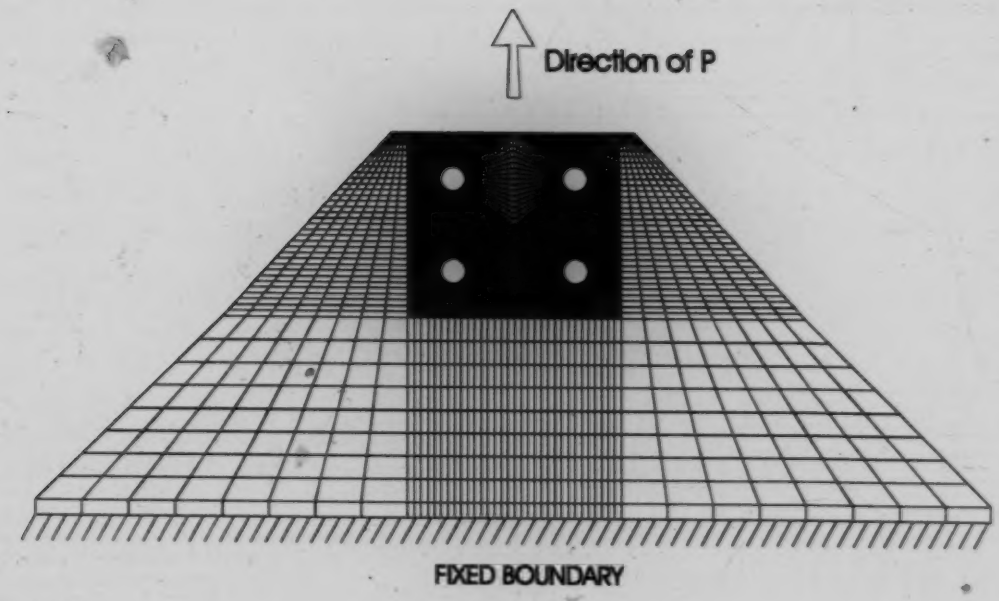

(b) Finite element mesh

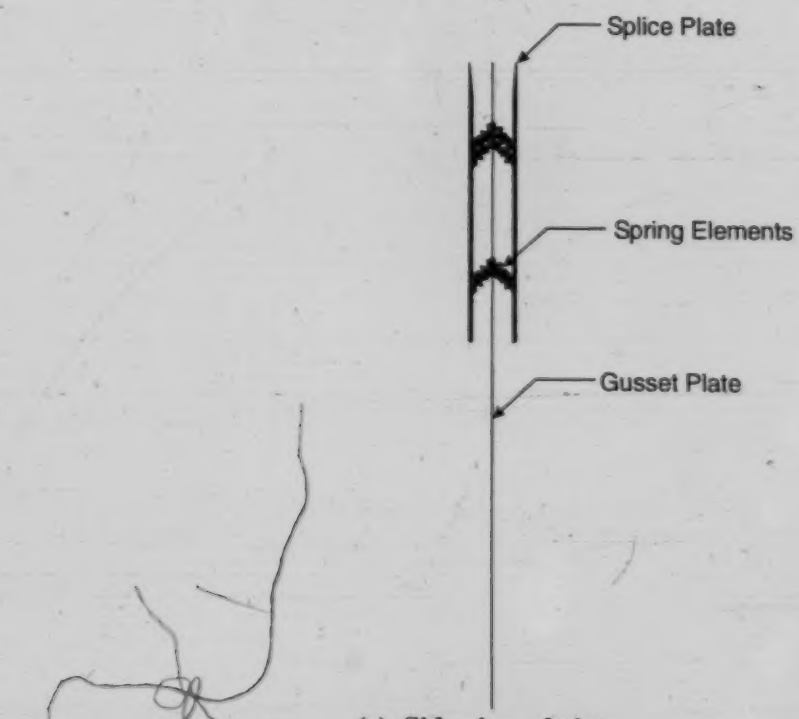

(c) Side view of plate

Figure 4-16 Cont'd

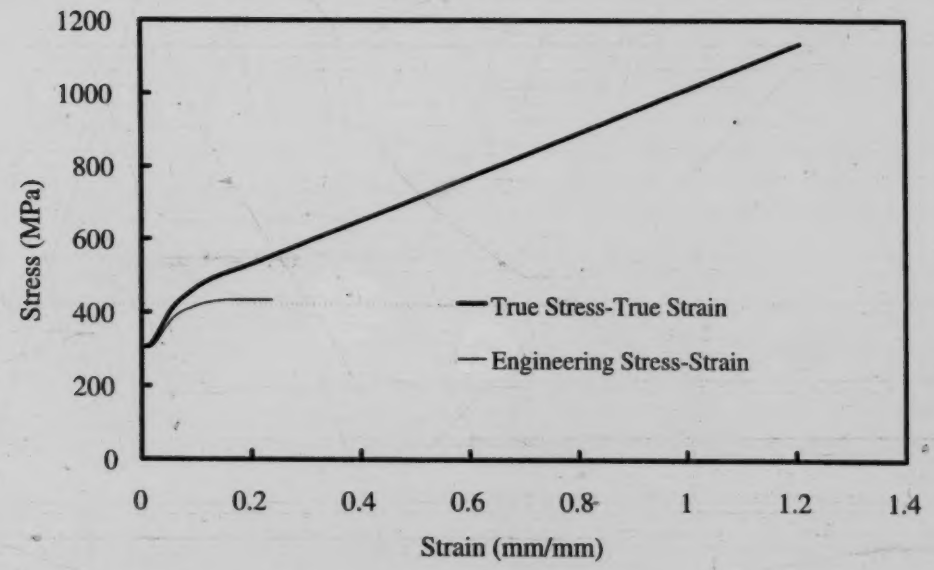

Figure 4-17 Stress vs. strain curve used in the analysis of gusset plate 4U tested by Mullin (2002)

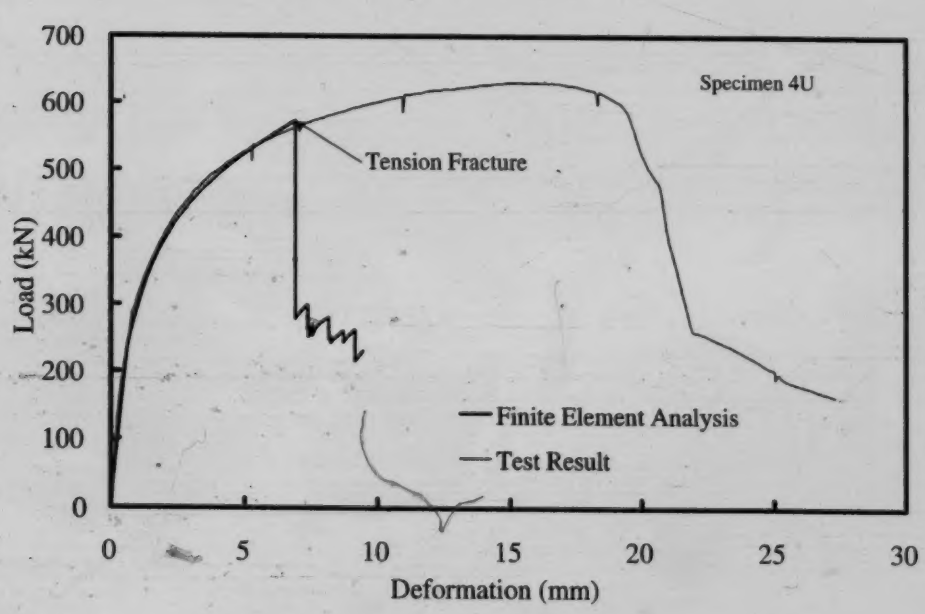

Figure 4-18 Load vs. deformation curve for 4U

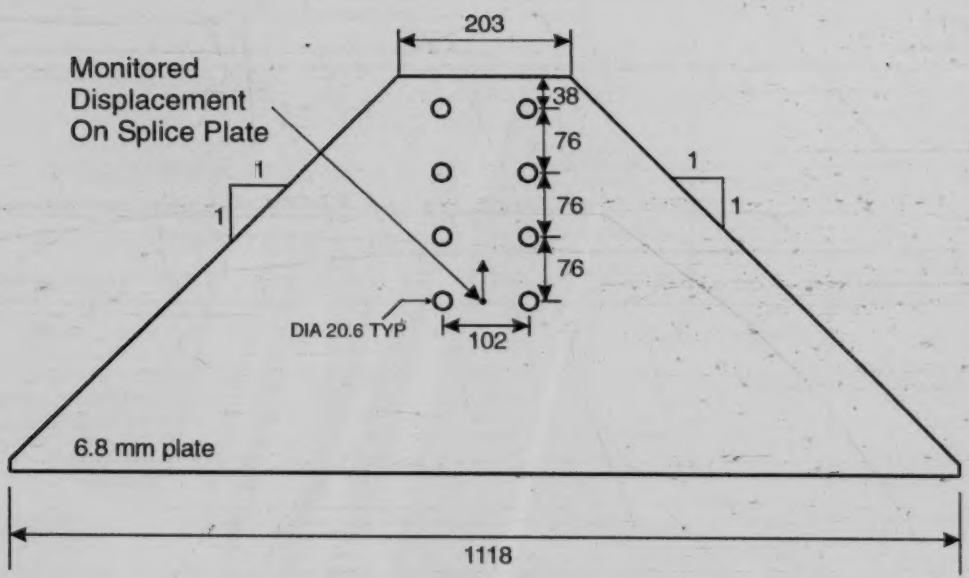

(a) Plate dimensions and bolt pattern

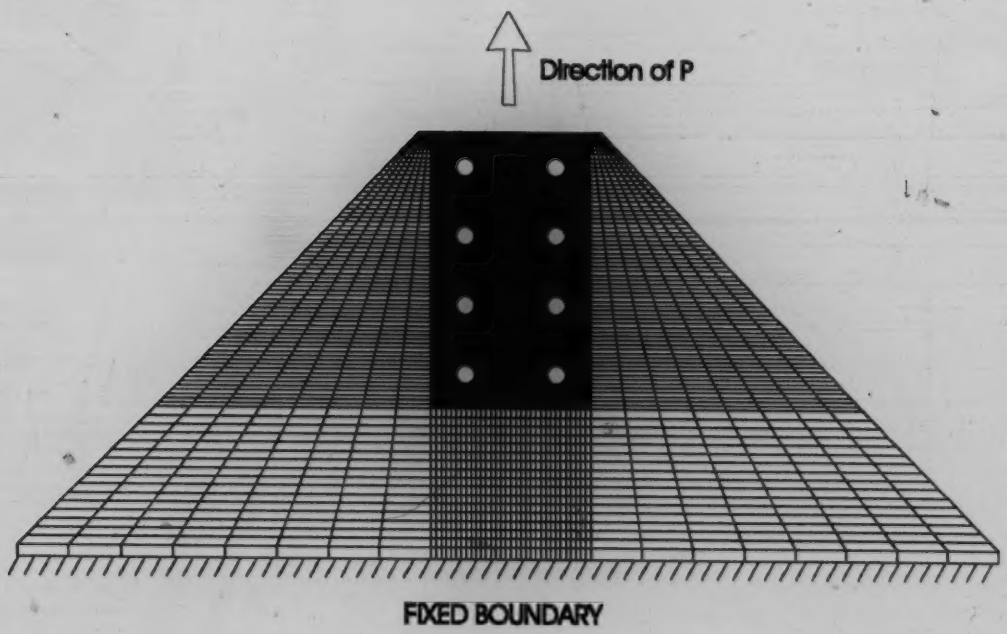

(b) Finite element mesh

Figure 4-19 Gusset plate 8U tested by Mullin (2002)

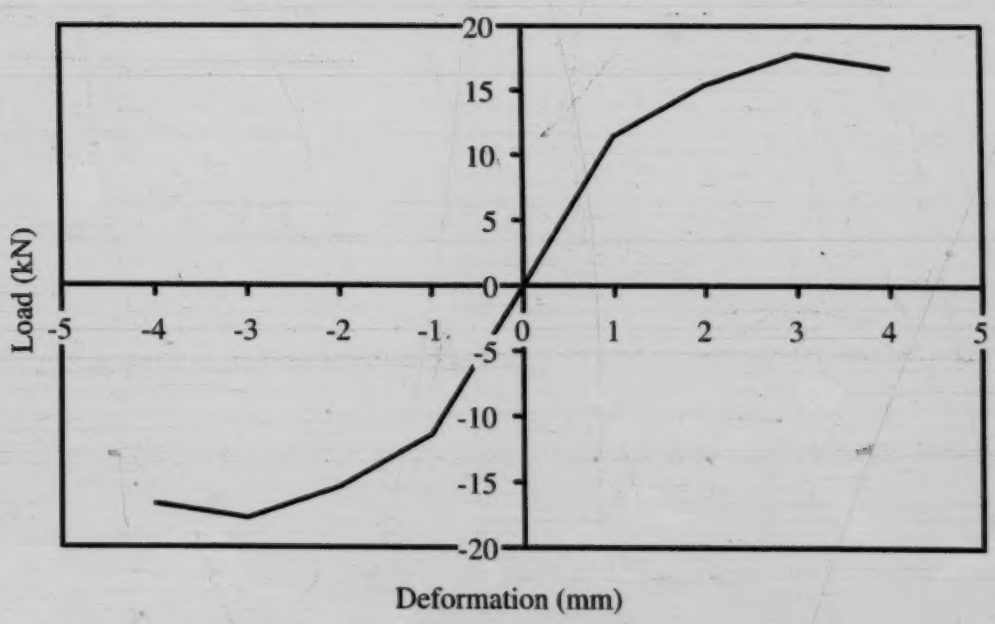

(a) Load vs. deformation response of a spring element

Load (kN)	Deformation (mm)
-16.7	-4
-17.8	-3
-15.4	-2
-11.4	-1
0	0
11.4	1
15.4	2
17.8	3
16.7	4

(b) Definition of the load response

Figure 4-20 Definition of bolt element

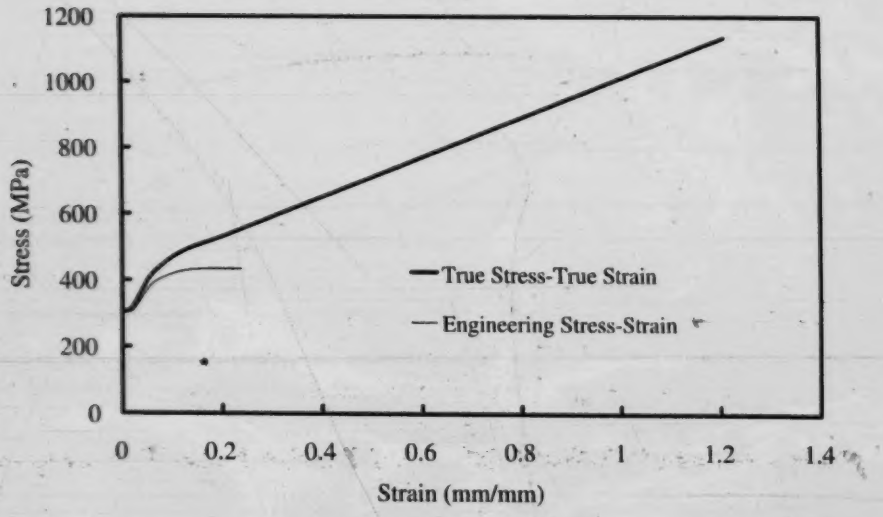

Figure 4-21 Stress vs. strain curve used in the analysis of gusset plate 8U tested by Mullin (2002)

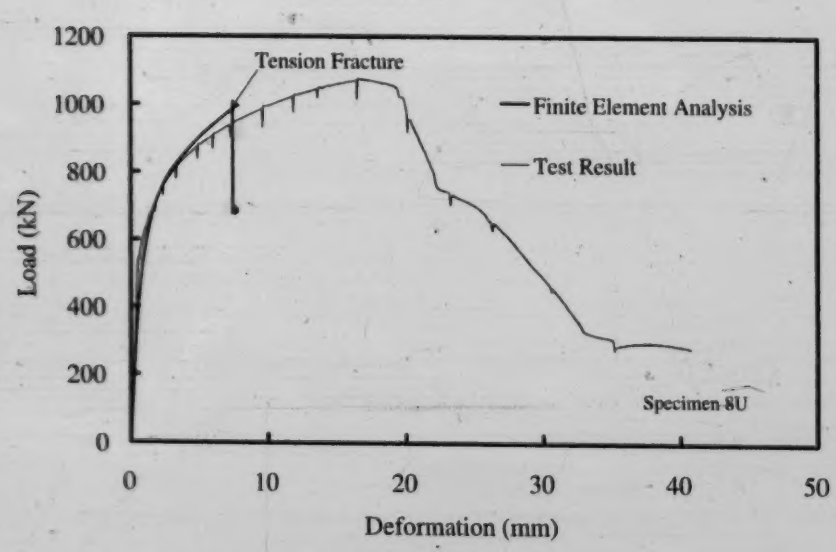

Figure 4-22 Load vs. deformation curve for 8U

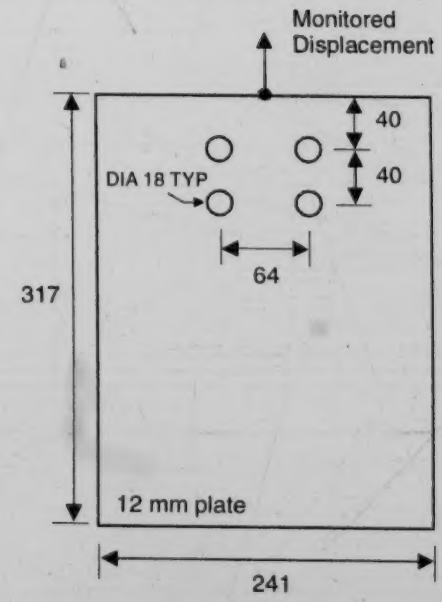

(a) Plate dimensions and bolt pattern

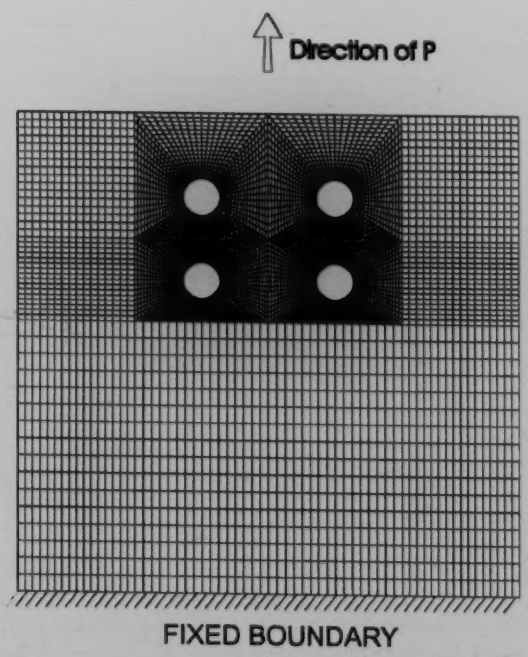

(b) Finite element mesh

Figure 4-23 Gusset plate 224.4 tested by Udagawa and Yamada (1998)

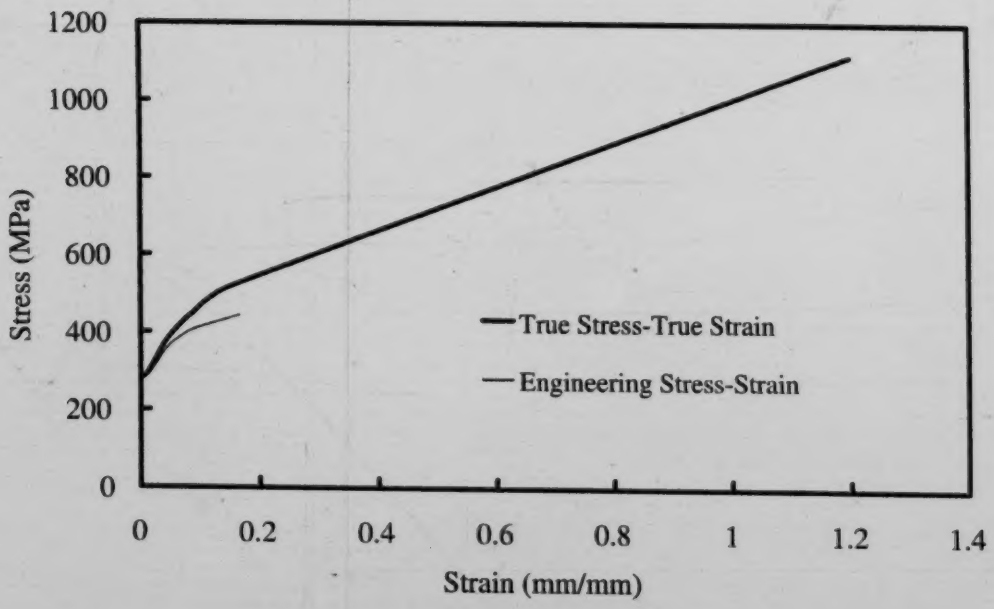

Figure 4-24 Stress vs. strain curve used in the analysis of gusset plate 224.4 tested by Udagawa and Yamada (1998)

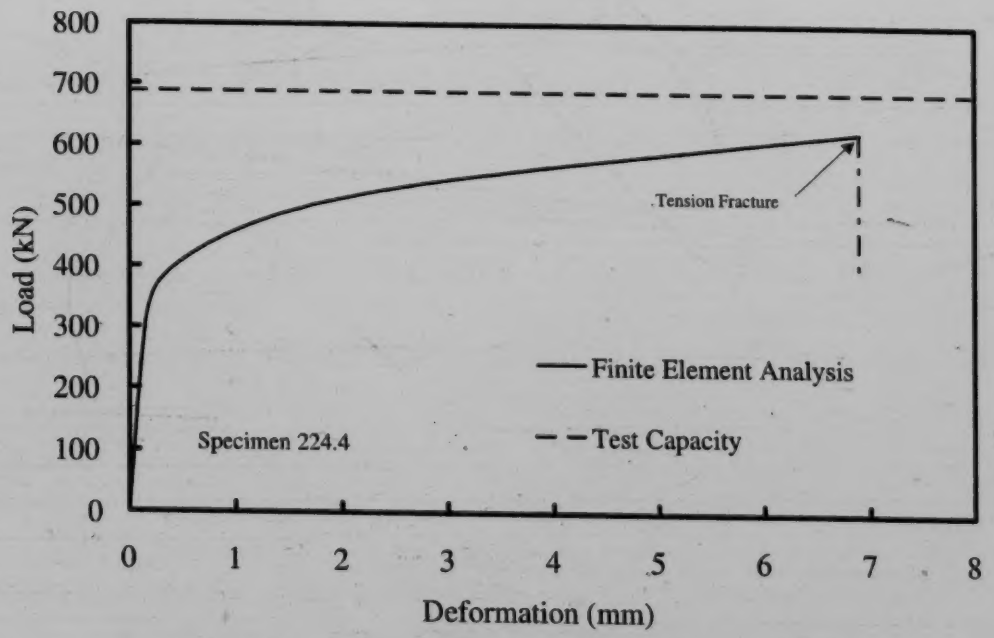

Figure 4-25 Load vs. deformation curve for gusset plate 224.4

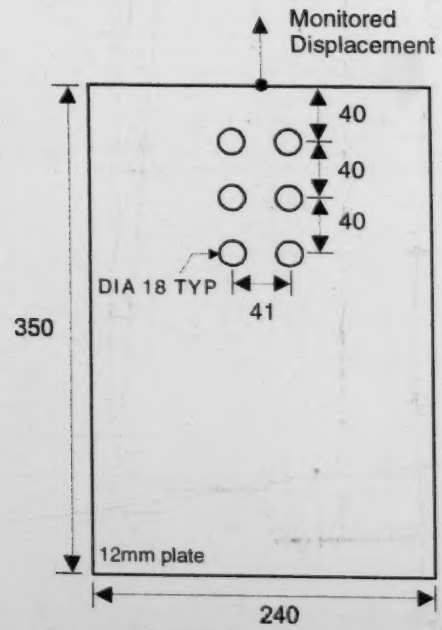

(a) Plate dimensions and bolt pattern

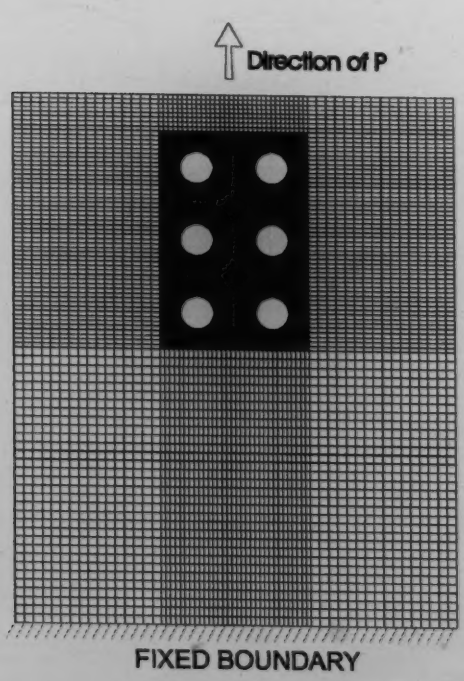

(b) Finite element mesh

Figure 4-26 Gusset plate 23F.4 tested by Udagawa and Yamada (1998)

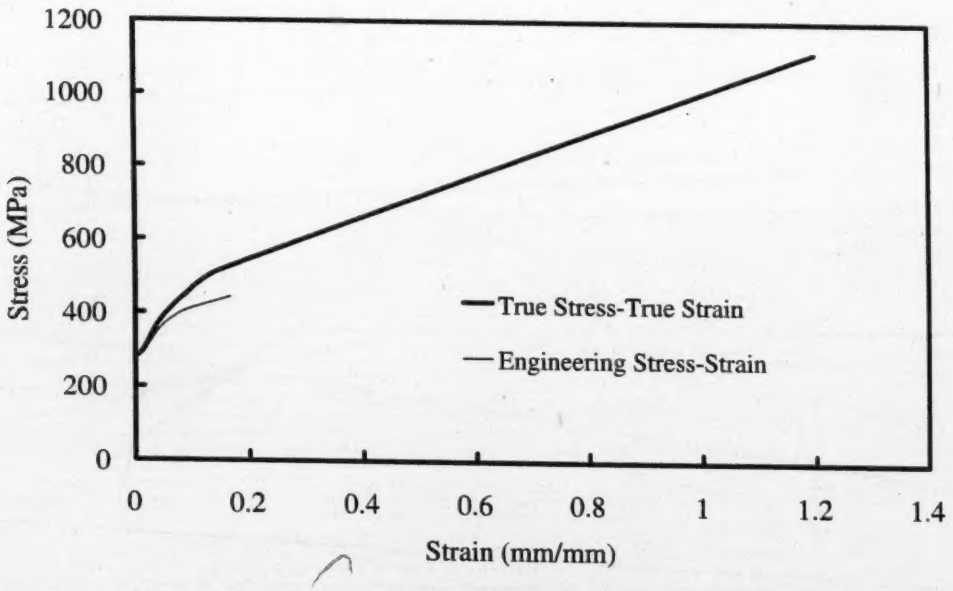

Figure 4-27 Stress vs. strain curve used in the analysis of gusset plate 23F.4 tested by Udagawa and Yamada (1998)

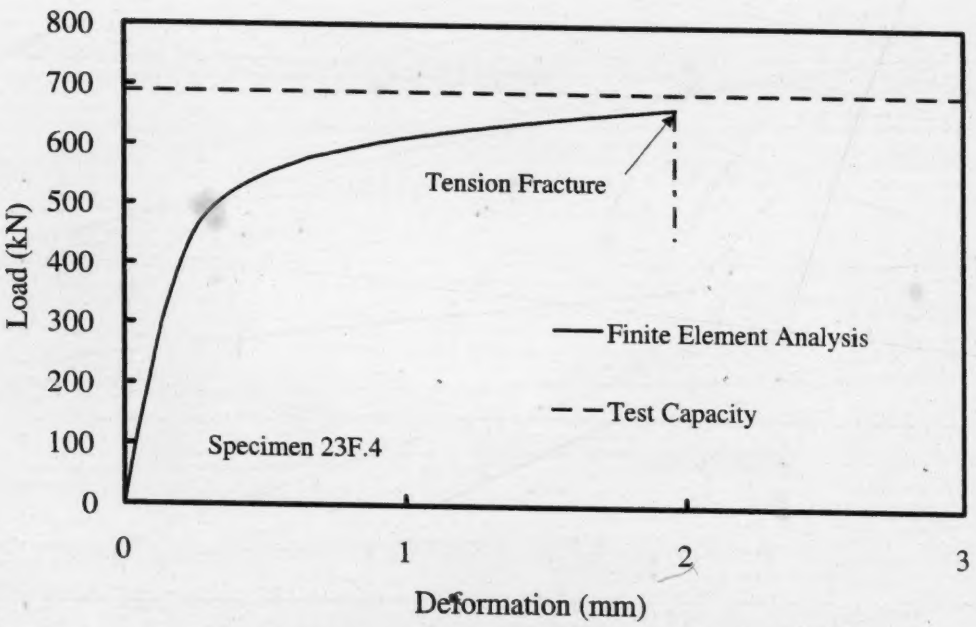

Figure 4-28 Load vs. deformation curve for gusset plate 23F.4

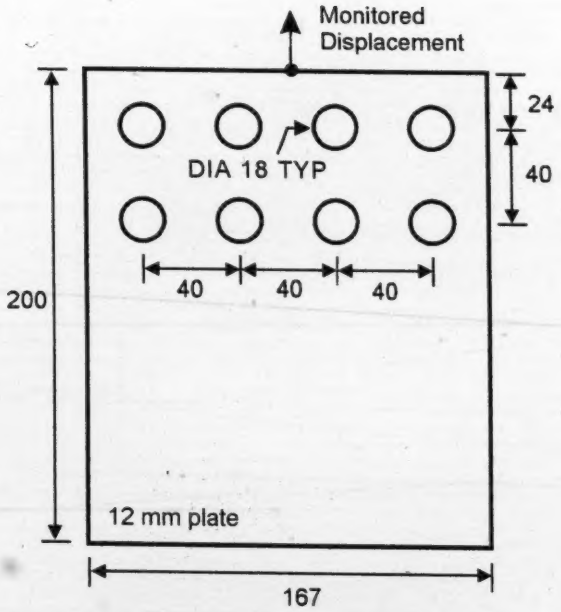

(a) Plate dimensions and bolt pattern

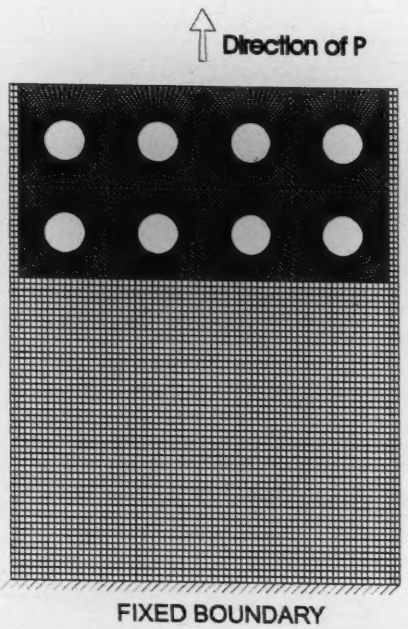

(b) Finite element mesh

Figure 4-29 Gusset plate 423.4 tested by Udagawa and Yamada (1998)

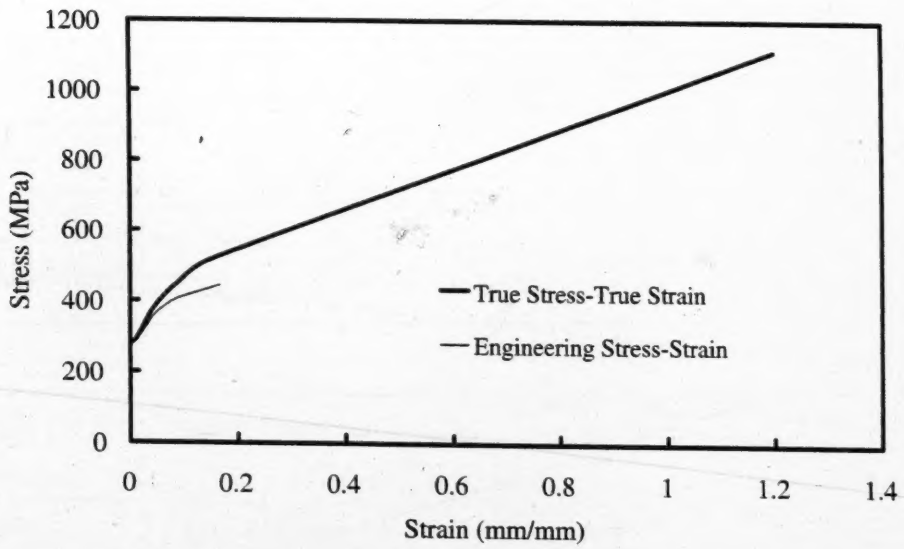

Figure 4-30 Stress vs. strain curve used in the analysis of gusset plate 423.4 tested by Udagawa and Yamada (1998)

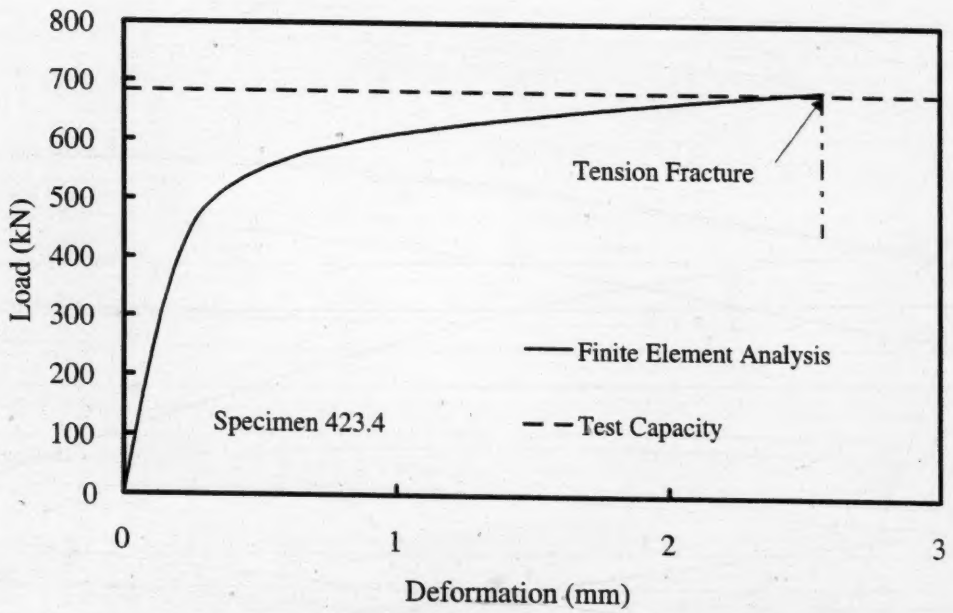

Figure 4-31 Load vs. deformation curve for gusset plate 423.4

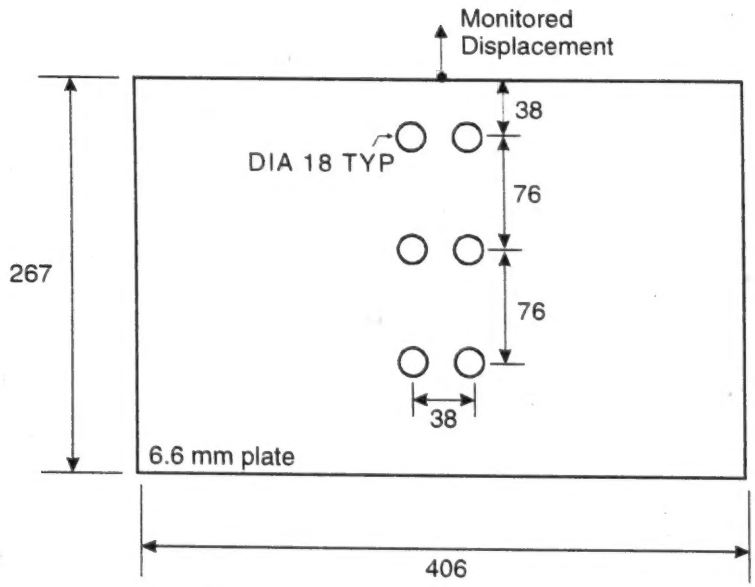

(a) Plate dimensions and bolt pattern

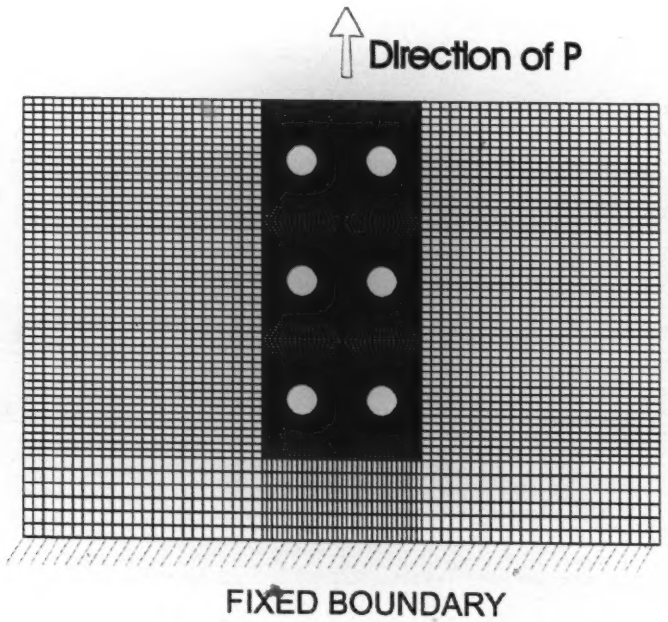

(b) Finite element mesh

Figure 4-32 Gusset plate T1 from current investigation

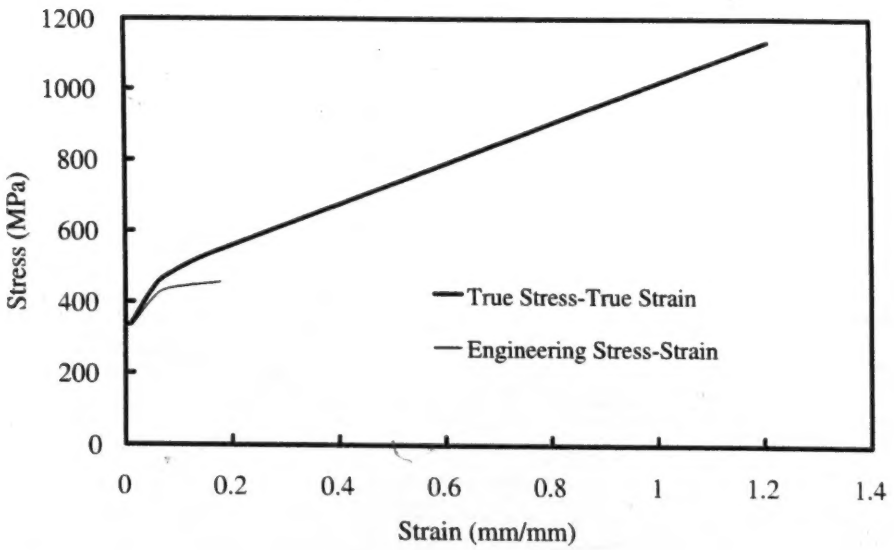

Figure 4-33 Stress vs. strain curve used in the analysis of gusset plate T1 from current investigation

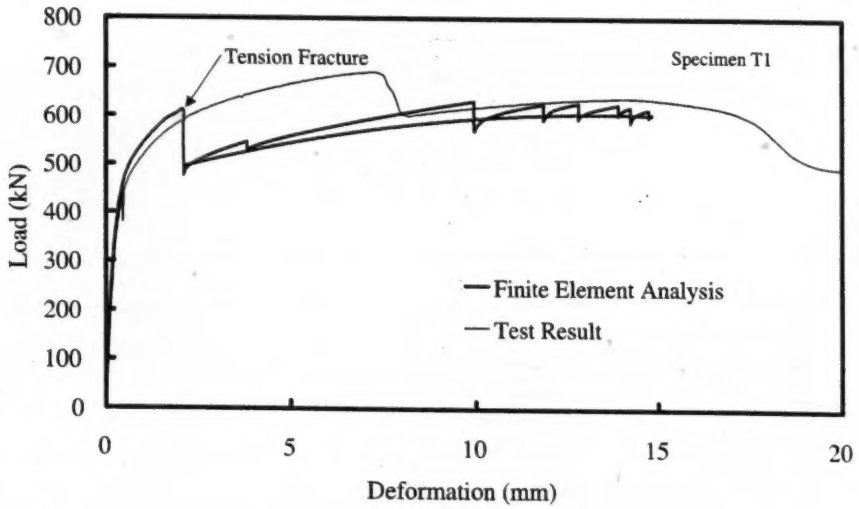

Figure 4-34 Load vs. deformation curve for T1

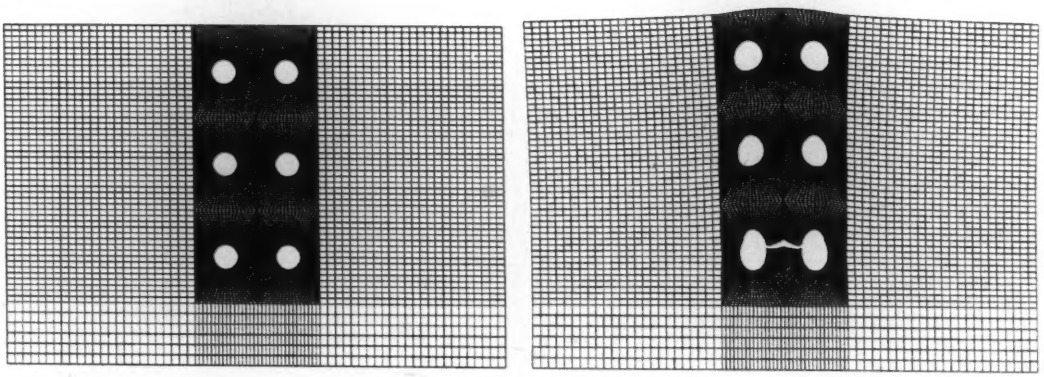

(a) Original mesh

(b) At 4 mm deformation

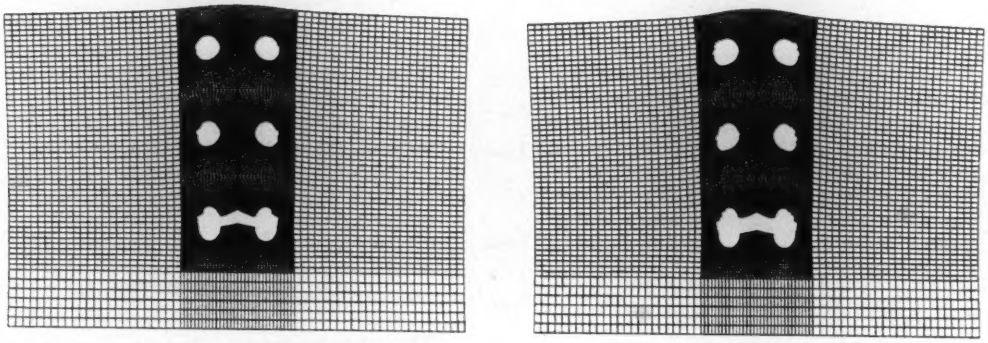

(c) At 10 mm deformation

(d) At 15 mm deformation

Figure 4-35 Progression of block shear failure in gusset plate T1 from current investigation

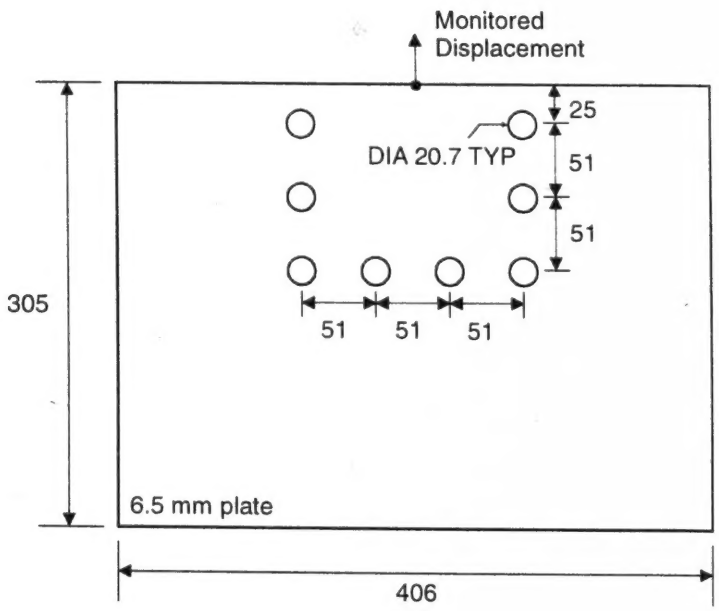

(a) Plate dimensions and bolt pattern

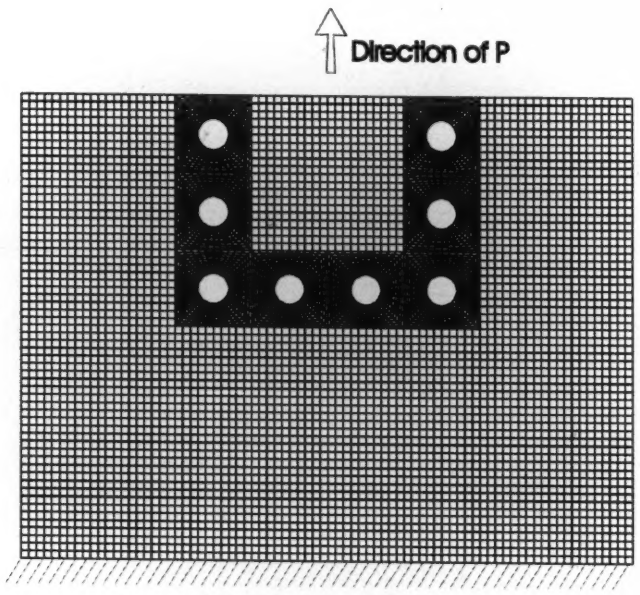

(b) Finite element mesh

Figure 4-36 Gusset plate T2 from current investigation

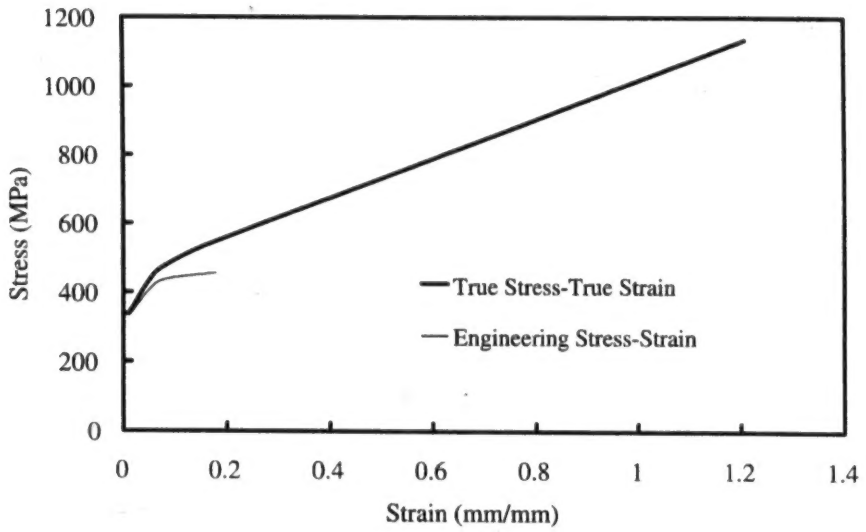

Figure 4-37 Stress vs. strain curve used in the analysis of gusset plate T2 from current investigation

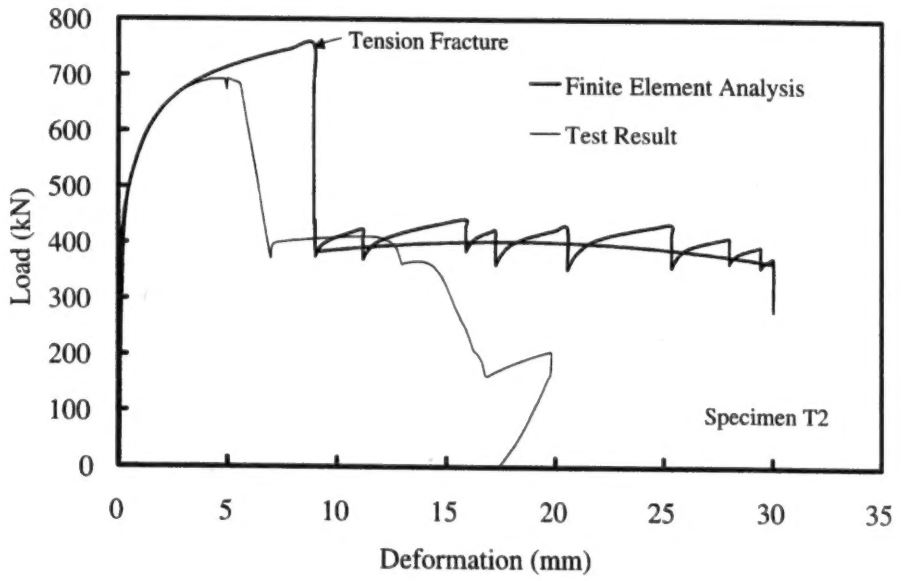

Figure 4-38 Load vs. deformation curve for T2

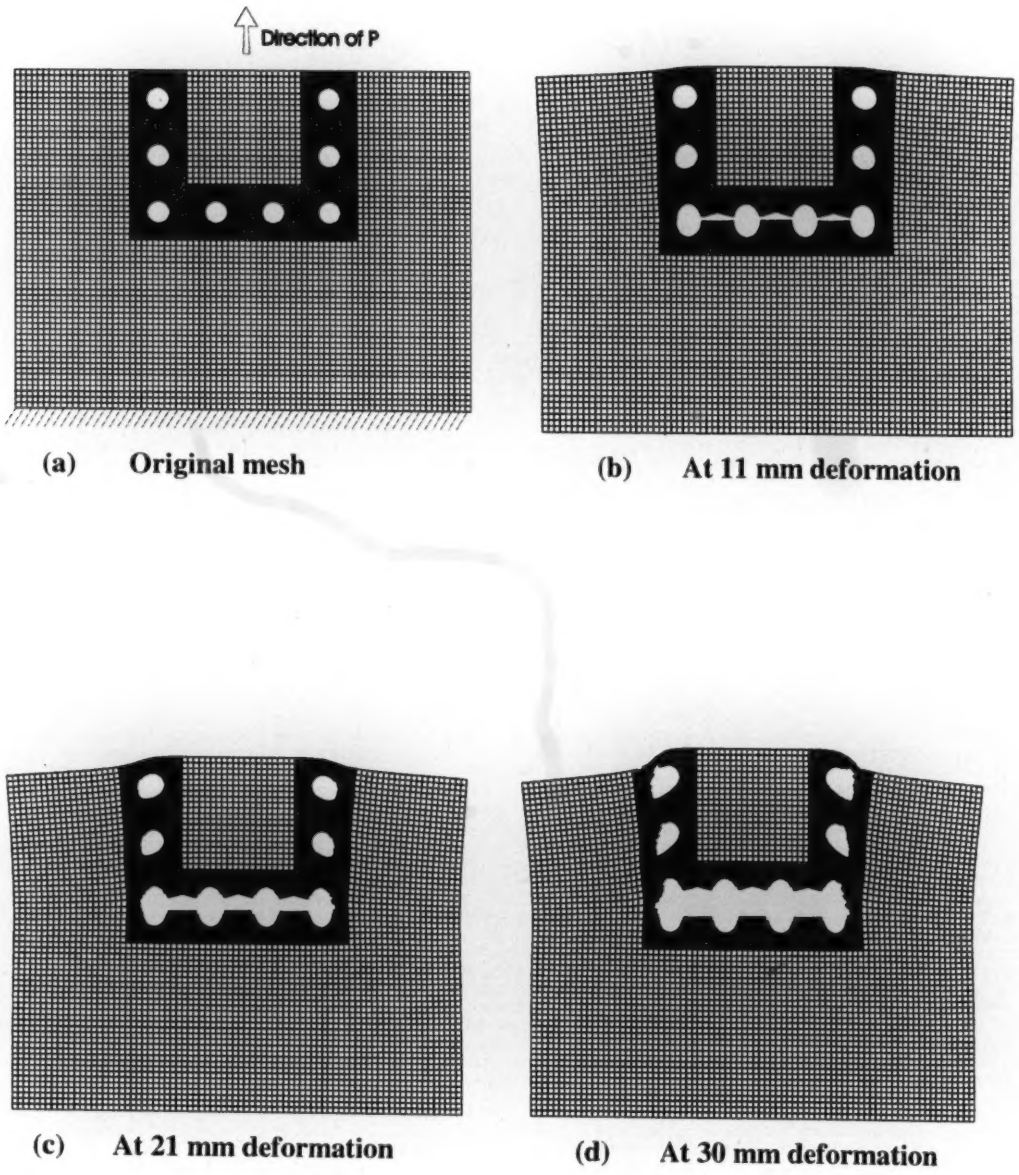

Figure 4-39 Progression of block shear failure in gusset plate T2 from current investigation

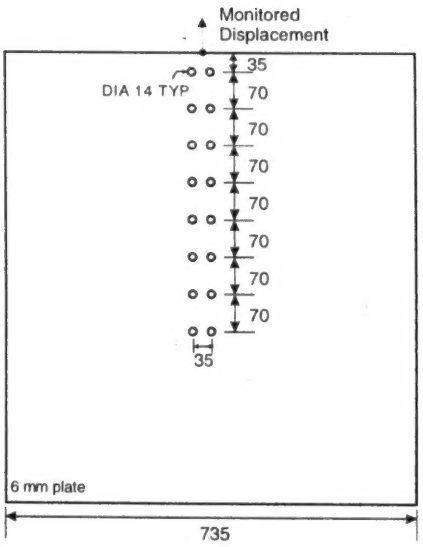

(a) Plate dimensions and bolt pattern

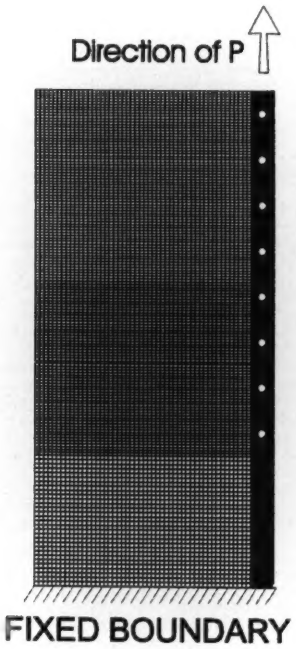

(b) Finite element mesh

Figure 4-40 Gusset plate 1 from the parametric study

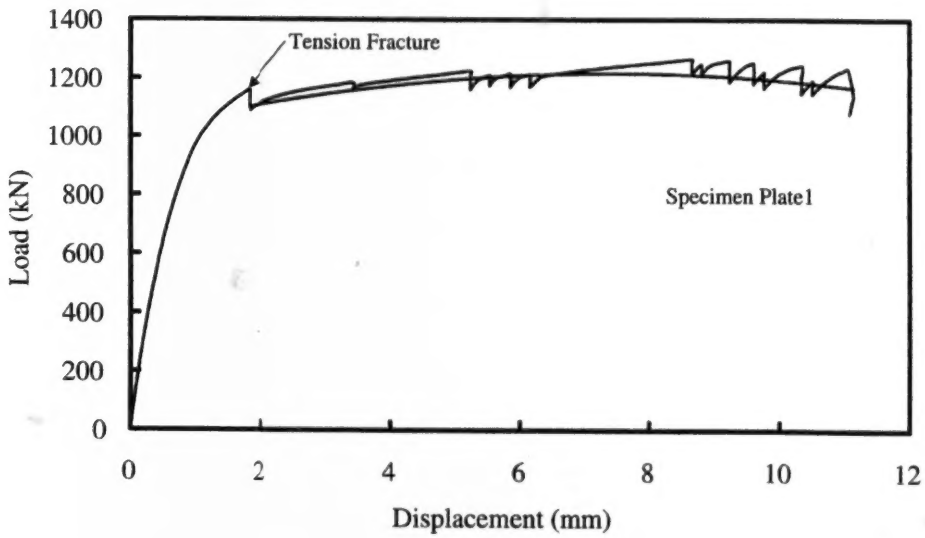

Figure 4-41 Load vs. deformation curve for gusset plate 1 (Finite Element Analysis)

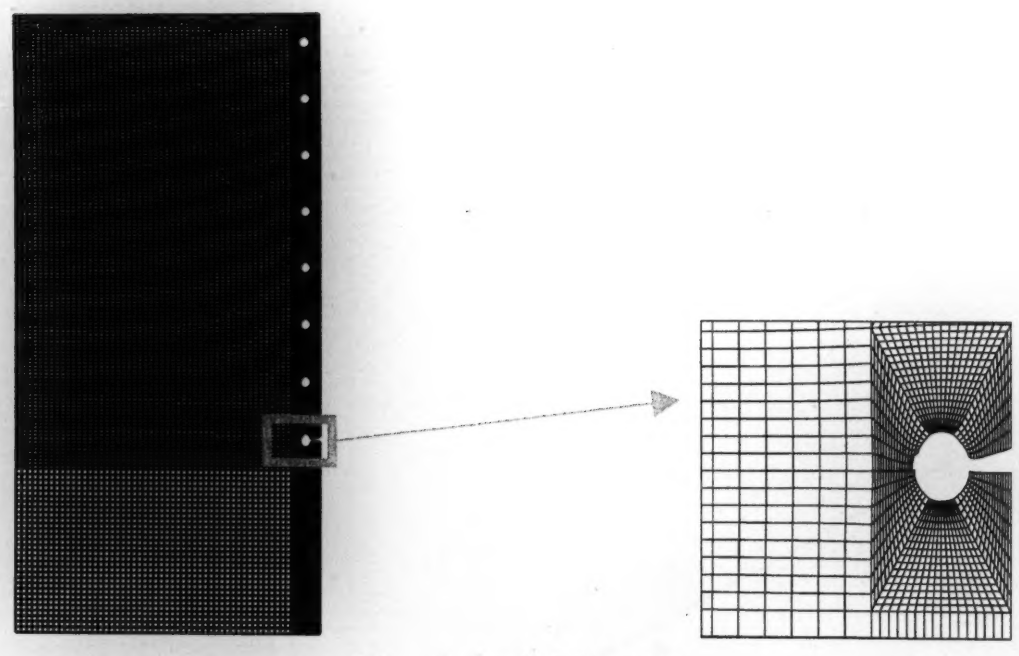

(a) At 5 mm deformation

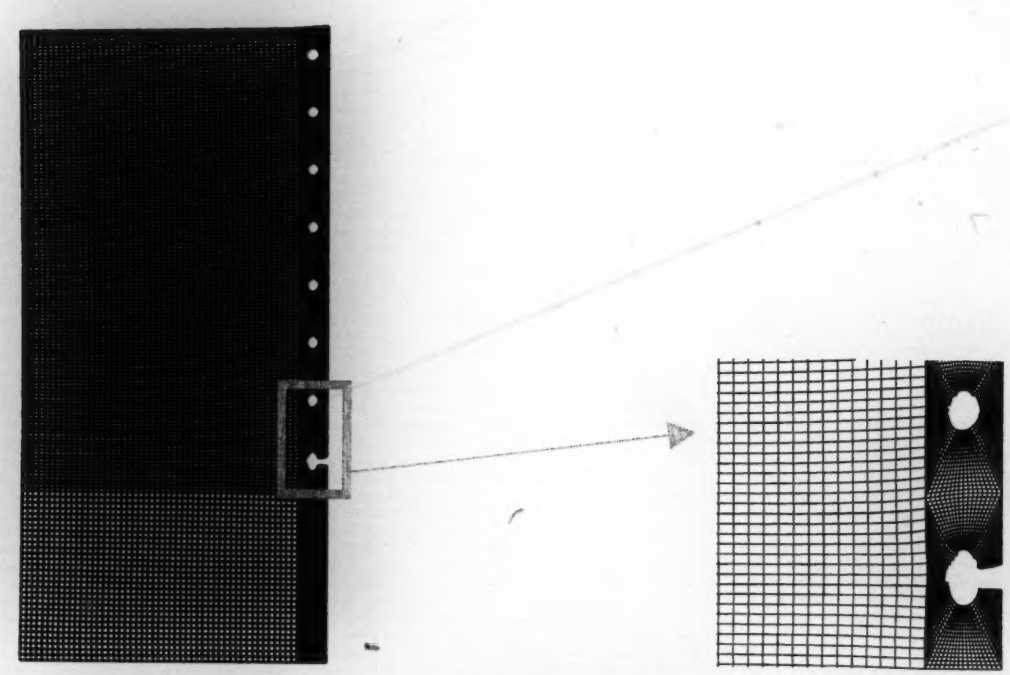

(b) At 9 mm deformation

Figure 4-42 Progression of block shear failure in gusset plate 1 from the parametric study

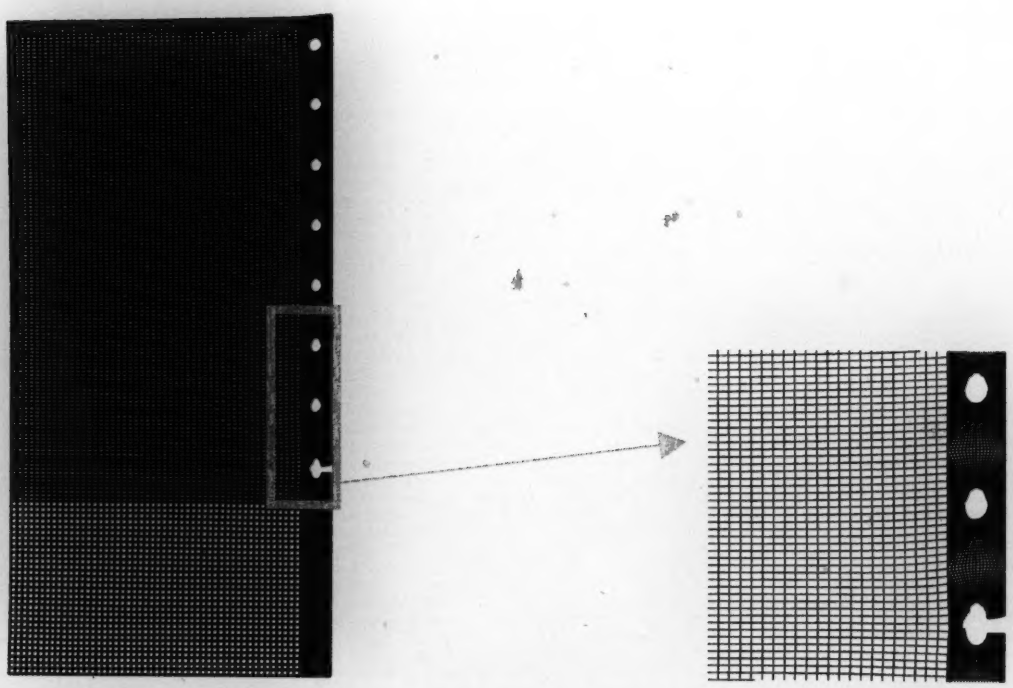

c) At 11 mm deformation

Figure 4-42 Cont'd

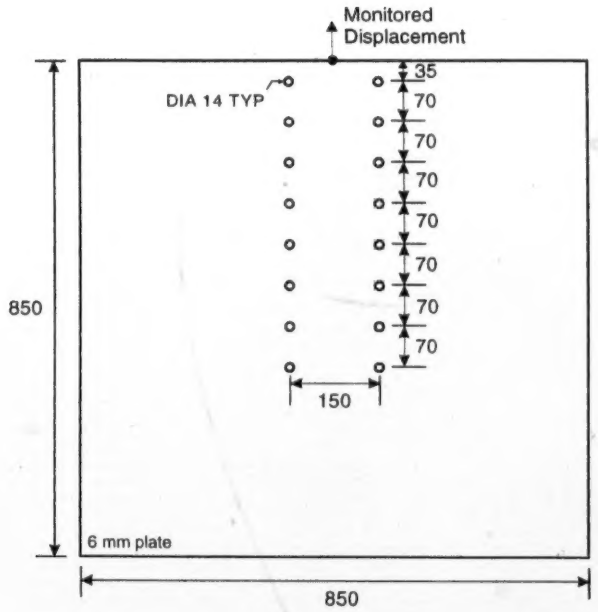

(a) Plate dimensions and bolt pattern

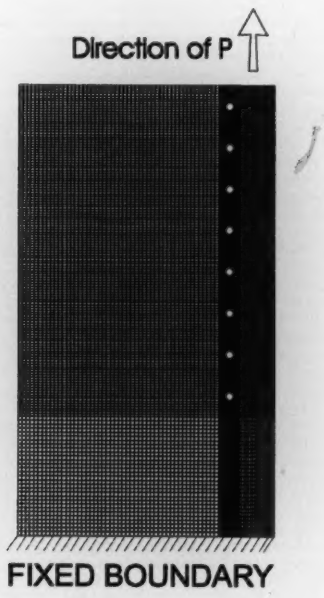

(b) Finite element mesh

Figure 4-43 Gusset plate 2 from the parametric study

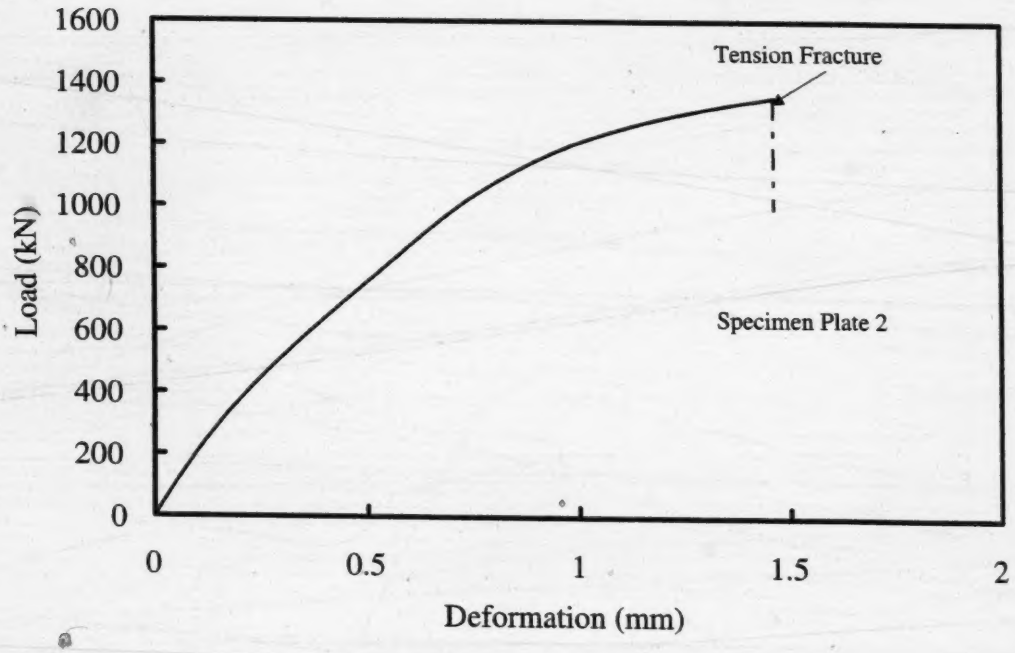

Figure 4-44 Load vs. deformation curve for gusset plate 2 (Finite Element Analysis)

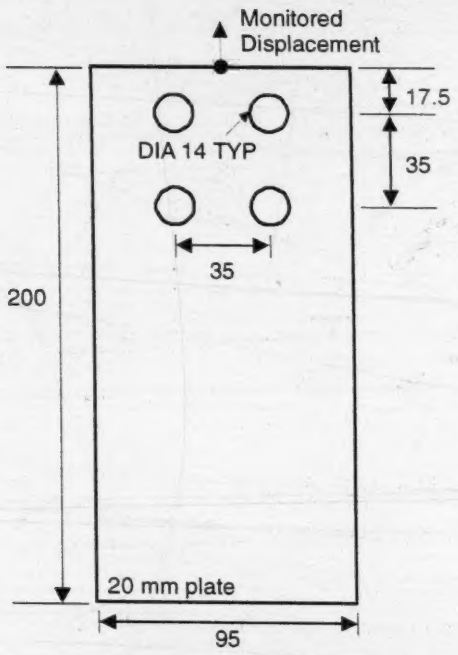

(a) Plate dimensions and bolt pattern

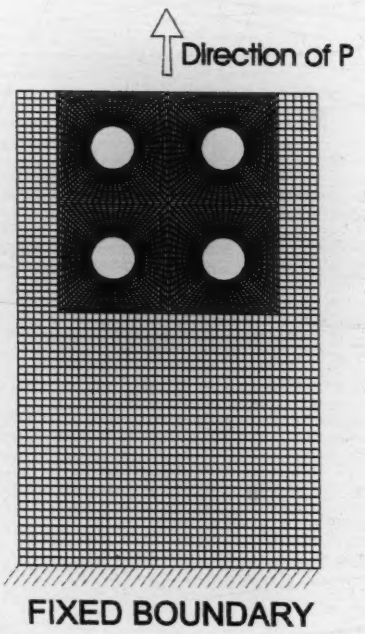

(b) Finite element mesh

Figure 4-45 Gusset plate 3 from the parametric study

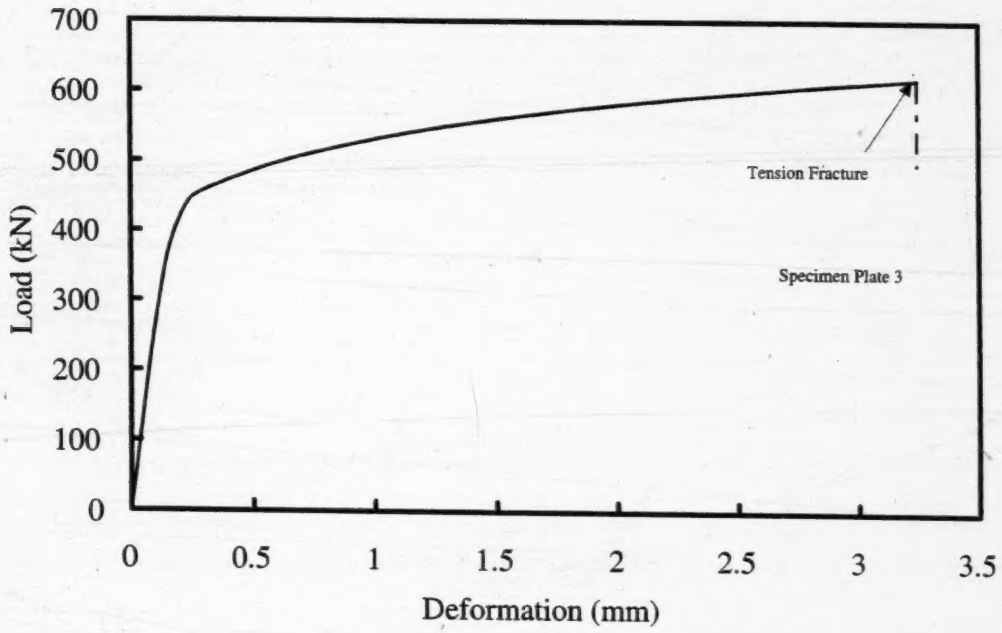

Figure 4-46 Load vs. deformation curve for gusset plate 3 (Finite Element Analysis)

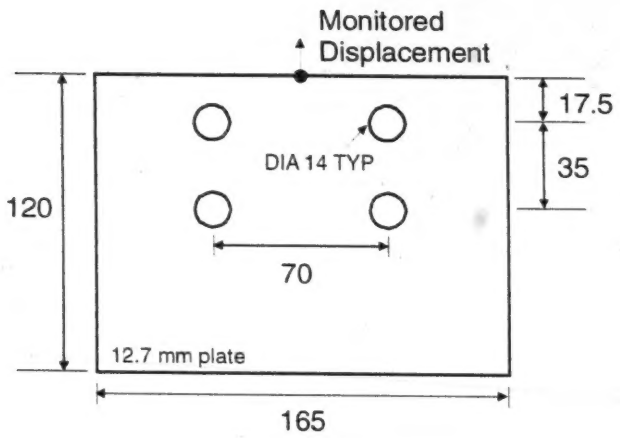

(a) Plate dimensions and bolt pattern

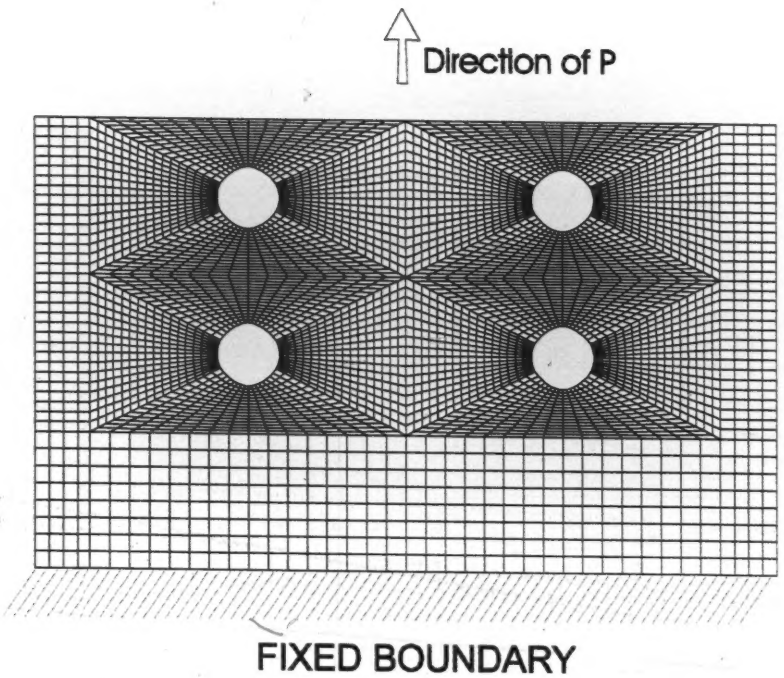

(b) Finite element mesh

Figure 4-47 Gusset plate 4 from the parametric study

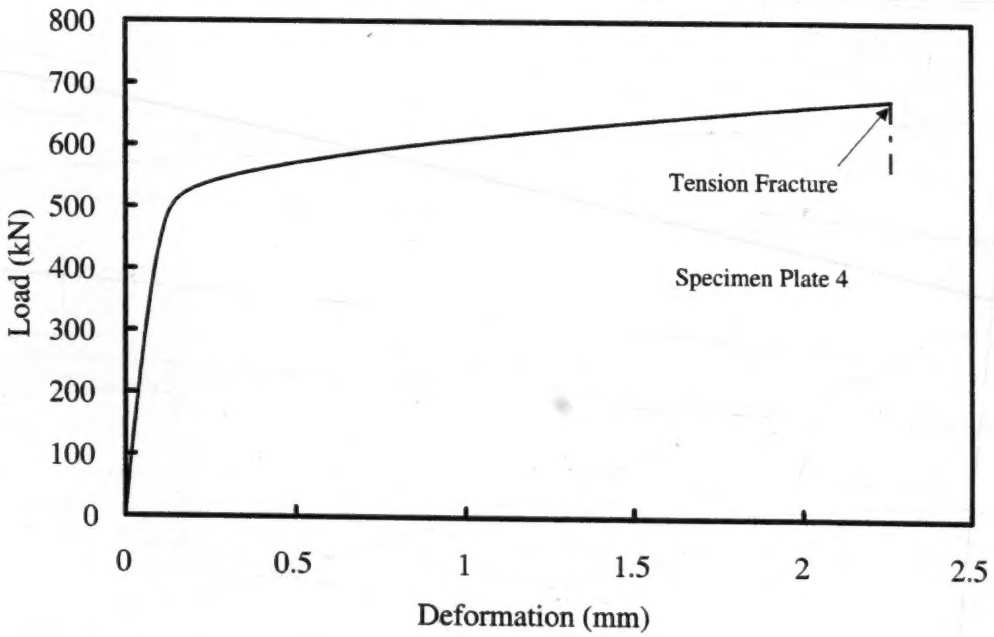

Figure 4-48 Load vs. deformation curve for gusset plate 4 (Finite Element Analysis)

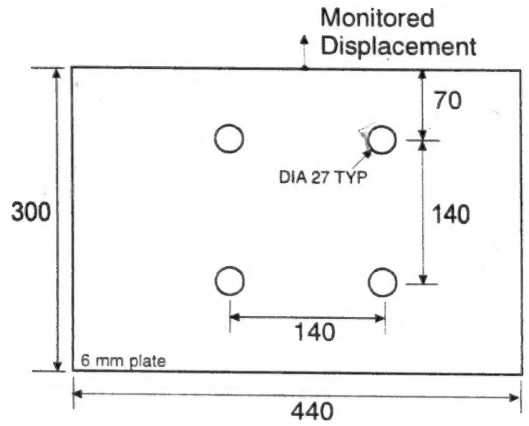

(a) Plate dimensions and bolt pattern

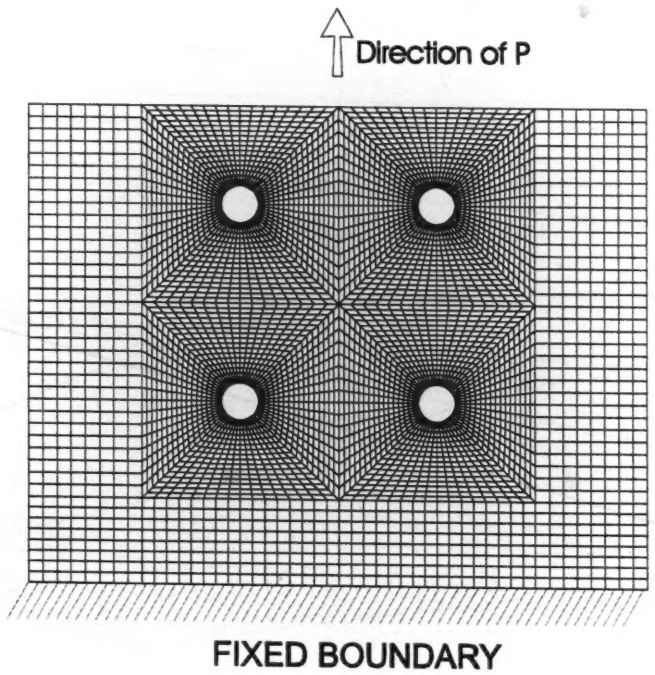

(b) Finite element mesh

Figure 4-49 Gusset plate 5 from the parametric study

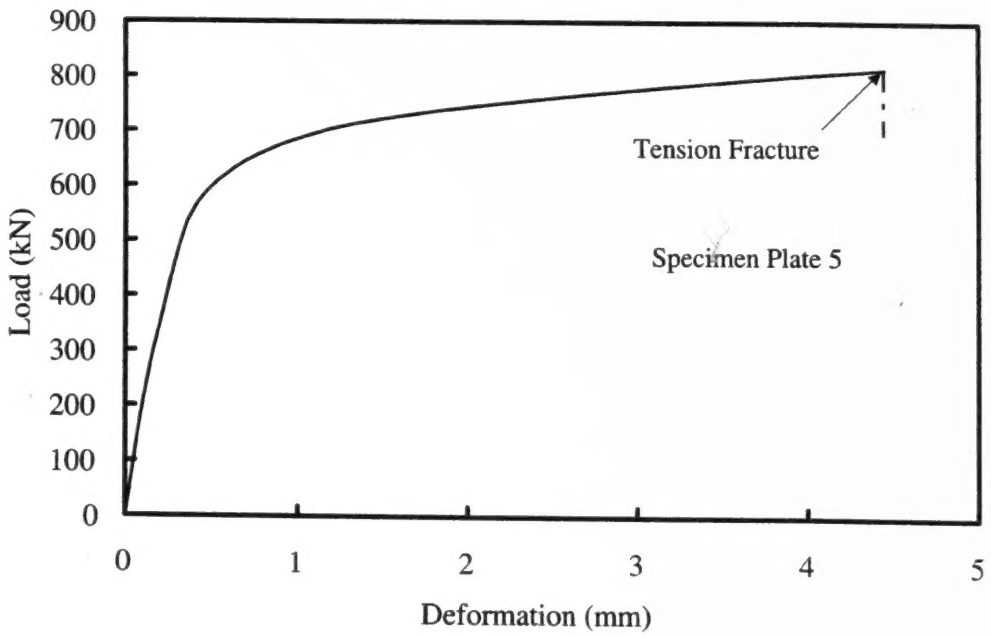

Figure 4-50 Load vs. deformation curve for gusset plate 5 (Finite Element Analysis)

CHAPTER 5

STATISTICAL ANALYSIS OF TEST RESULTS

5.1 Introduction

A large database of test results on block shear failure of gusset plates exists. An examination of this database revealed that the range of parameters that define the capacity of gusset plates in block shear could be expanded to include some practical connection layouts that have not been investigated experimentally. The database of test results was therefore expanded using the results of finite element analysis models as described in Chapter 4. In this chapter, this database of test results and finite element analysis results is used to evaluate commonly used prediction models for block shear failure from a limit states design point of view. Finally, a design equation that provides a better fit of the database will be proposed along with the appropriate values of the resistance factor to achieve various levels of safety.

5.2 Background to Limit States Design

Limit states design is a design method in which the factored resistance shall be equal to or greater than the effect of the factored loads and is represented by the equation (Galambos and Ravindra, 1977)

$$\phi R \geq \Sigma \alpha_i S_i . \tag{5-1}$$

where ϕ is the resistance factor, R is the nominal resistance, α is the load factor, and S is the specified load effect.

The resistance factor and load factors are chosen to provide a small probability of failure. The resistance factor, ϕ, takes into account the fact that the actual strength of the member may be less than anticipated due to variability of material properties, dimensions and workmanship and the uncertainty in the prediction model used to calculate the nominal resistance. The resistance factor can be expressed as (Galambos and Ravindra, 1977)

$$\phi = \rho_R \, e^{-0.55\beta V_R} \tag{5-2}$$

where ρ_R is the bias coefficient for the resistance, V_R is the coefficient of variation associated with ρ_R, and β is the safety index.

As the value of β increases, the probability of failure decreases. The target safety index for steel members is generally 3.0, but can increase to 4.5 for connections. A higher safety index is used for connections because of their generally less ductile failure mode to ensure that they are stronger than the parts being joined in order to give sufficient warning before failure. Since Equation 5-2 was derived for a safety index of 3.0, an additional factor, Φ_β, is included in Equation 5-2 to account for values of the safety index other than 3.0. The modified equation is expressed as follows (Franchuk *et al.*, 2002)

$$\phi = \Phi_\beta \, \rho_R \, e^{-0.55\beta V_R} \tag{5-3}$$

where Φ_β is the correction factor, which can be expressed as (Franchuk *et al.*, 2002)

$$\Phi_\beta = 0.0062\beta^2 - 0.131\beta + 1.338 \tag{5-4}$$

The bias coefficient for the resistance, ρ_R, and its coefficient of variation, V_R, are given by the expressions:

$$\rho_R = \rho_P \rho_M \rho_G \tag{5-5}$$

$$V_R = \sqrt{V_P^{\,2} + V_M^{\,2} + V_G^{\,2}} \tag{5-6}$$

where ρ_P is the mean value of the professional factor, taken as the measured capacity divided by the predicted capacity using measured geometric and material properties, ρ_M is the material factor, ρ_G is the geometric factor and represents the ratio between measured and expected tension and shear areas in the block shear equation. The parameters V_P, V_M and V_G are the coefficients of variation for the professional factor, material factor, and the geometric factor, respectively.

5.3 Professional Factor

The professional factor represents the ability of a model to predict the block shear capacity of gusset plates. The ratio of the measured capacity, obtained either by

laboratory testing or from a validated finite element analysis, to the capacity predicted by the equation is used as a measure of predictability. Many equations have been proposed to predict block shear capacity of gusset plates. These equations are presented below along with statistics (obtained using experimental data from a large number of tests summarized in Appendix A) for the professional factor.

5.3.1 CAN/CSA–S16.1–94

The equation adopted in the previous edition of the Canadian standard CAN/CSA–S16.1–94 is based on the assumption that ultimate tensile strength of the net tension area and the ultimate shear strength of the net shear area are reached simultaneously:

$$P_u = F_u A_{nt} + 0.6 F_u A_{nv} \tag{5-7}$$

where F_u is the tensile strength of the material and A_{nt} and A_{nv} are the net tension area and the net shear area, respectively. The constant 0.6 is a factor that converts the tensile strength into shear strength. The equation in CAN/CSA–S16.1–94 also includes a resistance factor of 0.85 ϕ, where the ϕ factor is taken as 0.9. The 0.85 reduction factor is added to reduce the probability of reaching the ultimate limit state expressed by Equation 5-7, which is based on the ultimate tensile strength.

The test data from other researchers, presented in Appendix A, the data presented in Chapter 3, and the finite element analysis results presented in Chapter 4, were used to calculate the ratio of the test or finite element analysis results to the predicted capacity using Equation 5-7. Calculated test-to-predicted ratios for 128 test results and five finite element analysis results are presented in Table B-2 of Appendix B. The bias coefficient of the professional factor is 1.18 and the associated coefficient of variation is 0.071. A plot of the test capacity versus predicted capacity using Equation 5-7 is presented in Figure 5-1. As indicated by the bias coefficient and the low coefficient of variation for the professional factor, the data show little dispersion and most of the data points lie above the diagonal line that represents a test-to-predicted ratio of 1.0.

5.3.2 CSA–S16–01

The current edition of the Canadian design standard, CSA–S16–01, provides two equations for the prediction of block shear capacity:

$$P_u = F_u A_{nt} + 0.6 F_Y A_{gv} \tag{5-8}$$

$$P_u = F_u A_{nt} + 0.6 F_u A_{nv} \tag{5-9}$$

where F_Y is the yield strength of the material and A_{gv} is the gross shear area. Equation 5-8, proposed by Kulak and Grondin (2001), is based on the observation that rupture on the tension plane occurs before rupture on the shear planes. This is supported by several test programs, including the test program presented in Chapter 3. In addition, CSA–S16–01 limits the capacity of the shear planes to the rupture strength of the net shear area, as expressed in Equation 5-9. Although all the presented experimental evidence does not support this limitation, Equation 5-9 was adopted to provide a sufficient level of safety with a resistance factor of 0.9, which is used with Equations 5-8 and 5-9. Fracture on the shear planes is well known to take place on an area larger than the net area. The test-to-predicted ratio for Equations 5-8 and 5-9 using all the available test and finite element analysis data is presented in the third column of Table B-2. The resulting bias coefficient of the professional factor is 1.18 and the corresponding coefficient of variation is 0.065. A plot of the test capacity versus predicted capacity using Equations 5-8 and 5-9 is presented in Figure 5-2. Once again, the data fit tightly together and most of the data points lie above the diagonal line that represents test-to-predicted ratios of 1.0.

5.3.3 AISC 1999 Specification

The block shear provisions in the AISC LRFD 1999 Specification make use of two equations, the use of which is dependent on the relative strength of the net tension and shear areas of the connection:

when $F_u A_{nt} \geq 0.6 F_u A_{nv}$

$$P_u = F_u A_{nt} + 0.6 F_Y A_{gv} \leq F_u A_{nt} + 0.6 F_u A_{nv} \tag{5-10}$$

when $F_u A_{nt} < 0.6 F_u A_{nv}$

$$P_u = F_Y A_{gt} + 0.6 F_u A_{nv} \leq F_u A_{nt} + 0.6 F_u A_{nv} \tag{5-11}$$

where A_{gt} is the gross tension area. The specification uses a resistance factor of 0.75, which is approximately equivalent to the combined factor used in CAN/CSA–S16.1–94. Equation 5-10, which combines the ultimate tensile strength on the net tension area and the yield strength on the gross shear area, is logical, but the qualifying statement effectively precludes it from being used most of the time. In 108 out of 133 times Equation 5-11 was used to calculate the block shear capacity, although rupture on the tension face was reported to occur before rupture on the shear area. Equation 5-11 combines the yield strength on the gross tension area with ultimate on the shear area, which has not been observed in any of the 133 tests reported in Appendix A. The bias coefficient of the professional factor, shown in Table B-2, is 1.19 and the corresponding coefficient of variation is 0.071. A plot of the test capacity versus predicted capacity using Equations 5-10 and 5-11 is presented in Figure 5-3. A tight distribution of data is again observed and most of the data lie above the diagonal line. Although Equation 5-11 governed in 80% of the cases investigated, the bias coefficient and coefficient of variation are similar to those obtained with the other models because of the limitation imposed on the strength of the tension area, which is not allowed to exceed the ultimate tensile strength on the net tension area. This condition made Equation 5-11 equivalent to Equation 5-7 in 60% of the cases. In the remaining 40% of cases, the difference between the tensile strength on the net section and the yield strength on the gross tension area was small (about 12% on average).

5.3.4 Hardash and Bjorhovde (1984)

Hardash and Bjorhovde (1984) proposed an equation to calculate the block shear capacity of gusset plates. Based on experimental observations, the proposed equation assumes that the capacity is the sum of the ultimate strength of the net tension area plus an effective shear strength on the gross shear area. This effective shear strength is a function of the connection length and the yield and ultimate strengths of the material. The equation is as follows:

$$P_u = F_u S_{net} t + 1.15 F_{eff} L t \tag{5-12}$$

where

$$F_{eff} = (1 - C_L) F_Y + C_L F_u \tag{5-13}$$

$$C_L = 0.95 - 0.047L \qquad (5\text{-}14)$$

Although Equation 5-14 was derived from an analysis of their own test data, Equation 5-12 has the advantage of offering a model that is supported by experimental observations, namely, tension fracture takes place before shear failure, and shear failure does not take place on the net shear area. The test–to–predicted values obtained from Equation 5-12 and all the available block shear data are presented in Table B-2. The bias coefficient for the professional factor is 0.95 and the corresponding coefficient of variation is 0.074. A plot of the test capacity versus predicted capacity using Equation 5-12 is shown in Figure 5-4. As expected from the low professional factor, a significant number of data points lie below the diagonal line.

5.3.5 Kulak and Grondin (2001)

Kulak and Grondin (2001) proposed an equation for block shear capacity based on the observation that block shear failure in gusset plates takes the form of rupture on the net tension area and yield on the gross shear area. The proposed equation is therefore Equation 5-8. The test-to-predicted ratios obtained using Equation 5-8 alone are presented in the sixth column of Table B-2. The resulting bias coefficient for the professional factor is 1.07 and the corresponding coefficient of variation is 0.099. A plot of the test data versus predicted capacities shown in Figure 5-5 indicates that the model proposed by Kulak and Grondin provides a better fit of the test data than the other models presented above with a comparable amount of scatter. It is less conservative than the model adopted in the current design standard.

5.3.6 Proposed New Equation

Although the equations presented above generally give a good prediction of the block shear resistance of gusset plates, not all equations describe well the block shear failure phenomenon. The equation proposed by Hardash and Bjorhovde attempts to provide a more realistic estimate of the stresses on the failure surfaces. It does predict a stress on the tension face equal to the tensile strength of the material, and an effective shear stress between yield and ultimate on the gross shear area. The proposed equation, however, was derived for gusset plates and does not apply to other members such as coped beams. Another equation, which is consistent with the block shear equation proposed by

Franchuk *et al.* (2002) for coped beams and simpler in form than the Hardash and Bjorhovde equation, is proposed. The equation takes the following form:

$$P_u = R_t A_{nt} F_u + \frac{1}{\sqrt{3}} A_{gv} \left(\frac{F_Y + F_u}{2} \right) \tag{5-15}$$

where R_t is a constant used to account for the uniformity of normal stresses on the tension area. The second term on the right hand side of Equation 5-15 indicates that the shear area is taken as the gross area and the effective stress is the average of the yield strength and the tensile strength. If the constant R_t is taken as 1.0, the resulting bias coefficient for the professional factor is 0.98 and the associated coefficient of variation is 0.075. Figure 5-6 shows a plot of the test capacity versus predicted capacity. Of all the models investigated, Equation 5-15 fits the data the best.

5.4 Material Factor

The material factor reflects the difference between the nominal material strength (yield or ultimate) and the measured strength. The bias coefficient and the coefficient of variation for the material properties were obtained from Schmidt and Bartlett (2002). The data analysed by Schmidt and Bartlett consisted of 1470 tension tests from plates ranging in thickness from 10 mm to 29.9 mm. Although Schmidt and Bartlett presented data for plate thicknesses up to 49.9 mm, only the statistics for plates up to 29.9 mm thick are used here since this thickness is assumed to be a practical upper bound for gusset plates. The data presented by Schmidt and Bartlett consist of static yield and tensile strengths for 350W steel. Since the CAN/CSA–S16.1–94 block shear equation uses only the ultimate tensile strength, the statistical data for F_u is used for this equation. The bias coefficient and coefficient of variation reported by Schmidt and Bartlett (2002) are 1.19 and 0.034, respectively. When evaluating the other equations, which make use of the yield strength (F_Y) and the ultimate strength (F_u), the statistical data for F_Y are used since it is more conservative than the data for the ultimate strength. The bias coefficient and coefficient of variation of the yield strength are reported as 1.11 and 0.054, respectively.

5.5 Geometric Factor

The geometric factor accounts for the difference between nominal and actual plate thickness specified and actual plate dimensions and bolt hole layout. This is representative of the geometric accuracy of the component in question. Since insufficient data exist to evaluate the geometric factors, the bias coefficient and the coefficient of variation for the geometric factor proposed by Hardash and Bjorhovde (1984) was used. The bias coefficient, ρ_G, and the coefficient of variation, V_G, were taken as 1.0 and 0.05, respectively. These values are more conservative than the values derived by Franchuk *et al.* (2002) ($\rho_G = 1.017$ and $V_G = 0.039$) based on measured dimensions on coped beam connections and data reported by Kennedy and Gad Aly (1980).

5.6 Calculation of Resistance Factor

There are three primary reasons for including resistance factors in structural design (MacGregor, 1976): (a) the strengths of material or elements may be less than expected, (b) overloads may occur, and (c) the consequences of a failure may be very severe. These three reasons must be considered when selecting the safety index, β, applicable to a given situation and the decision is somewhat subjective. Members are usually assigned a safety index of about 3.0, while connections are assigned a value of approximately 4.5 (Galambos and Ravindra, 1978). The resistance factor for each prediction equation presented above was calculated for three values of safety index, namely, 3.5, 4.0, and 4.5. Table 5-1 summarizes the calculations for all six prediction equations.

The results presented in Table 5-1 show that the capacity equations in CAN/CSA–S16.1–94, CSA–S16–01 and AISC 1999 are quite conservative. It should be remembered, however, that the AISC 1999 equations do not predict the correct failure mode in most cases. It is also noted that CSA–S16–01 provides a safety index of 4.5 with the current resistance factor of 0.9. The AISC specification, however, provides a much more conservative prediction of the block shear capacity since the specification uses 0.75 compared to 0.9 required to achieve a safety index of 4.5. For this latter case, the safety index provided with a resistance factor of 0.75 is in excess of 5.0.

The equations proposed by Hardash and Bjorhovde (1984) and Kulak and Grondin (2001) require a resistance factor of 0.71 and 0.76, respectively, to obtain a safety index of 4.5. The proposed Equation 5-15 requires a resistance factor of 0.73 to obtain a safety index of 4.5. Equation 5-15 seems to have an advantage over the other two models. It fits the test data more closely than the model proposed by Kulak and Grondin, and it is a simpler model than the one proposed by Hardash and Bjorhovde. It is also consistent with the equation proposed by Franchuk *et al.* (2002) for coped beams. A resistance factor of 0.75 would provide an adequate safety index at 4.4.

Table 5-1

Calculation of resistance factor

	CAN/CSA S16.1-94	CSA S16-01	AISC 1999	Hardash and Bjorhovde (1984)	Kulak and Grondin (2001)	New Equation
ρ_p	1.18	1.18	1.19	0.95	1.07	0.98
V_p	0.071	0.065	0.071	0.074	0.099	0.075
ρ_m	1.19	1.11	1.11	1.11	1.11	1.11
V_m	0.034	0.054	0.054	0.054	0.054	0.054
ρ_G	1.00	1.00	1.00	1.00	1.00	1.00
V_G	0.05	0.05	0.05	0.05	0.05	0.05
ρ_R	1.40	1.31	1.32	1.06	1.19	1.09
V_R	0.0931	0.0980	0.1021	0.1044	0.1233	0.1053
	Correction Factor, Φ_β					
Φ_β For $\beta = 3.5$	0.96	0.96	0.96	0.96	0.96	0.96
Φ_β For $\beta = 4.0$	0.91	0.91	0.91	0.91	0.91	0.91
Φ_β For $\beta = 4.5$	0.87	0.87	0.87	0.87	0.87	0.87
	Resistance Factor, ϕ					
ϕ For $\beta = 3.5$	1.12	1.04	1.04	0.83	0.89	0.85
ϕ For $\beta = 4.0$	1.04	0.97	0.97	0.77	0.83	0.79
ϕ For $\beta = 4.5$	0.97	0.90	0.90	0.71	0.76	0.73

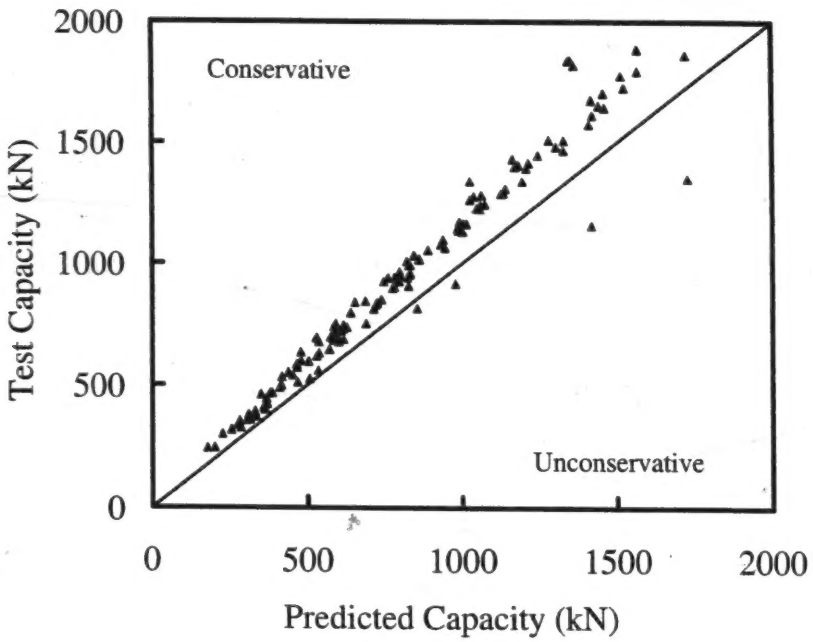

Figure 5-1 Test capacity vs. predicted capacity based on CAN/CSA–S16.1–94

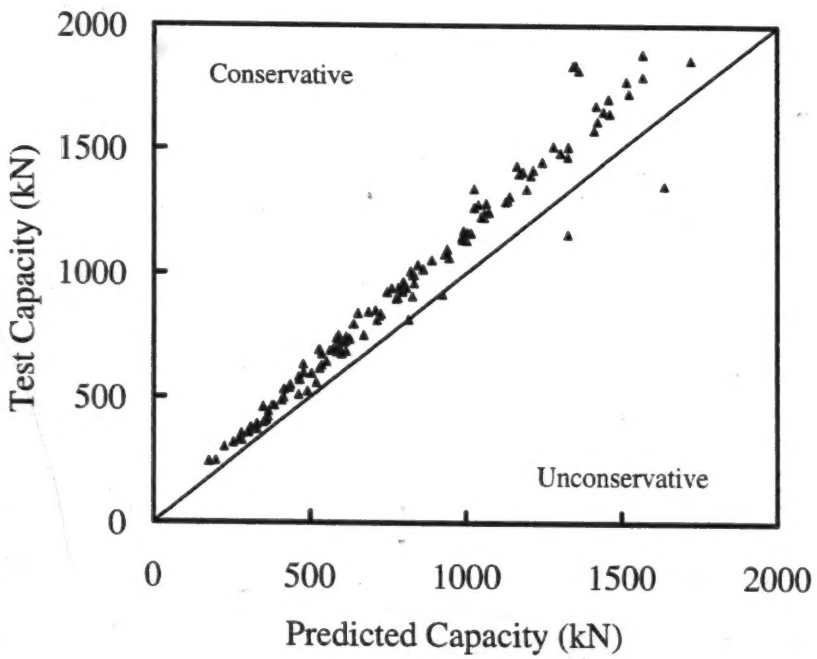

Figure 5-2 Test capacity vs. predicted capacity based on CSA–S16–01

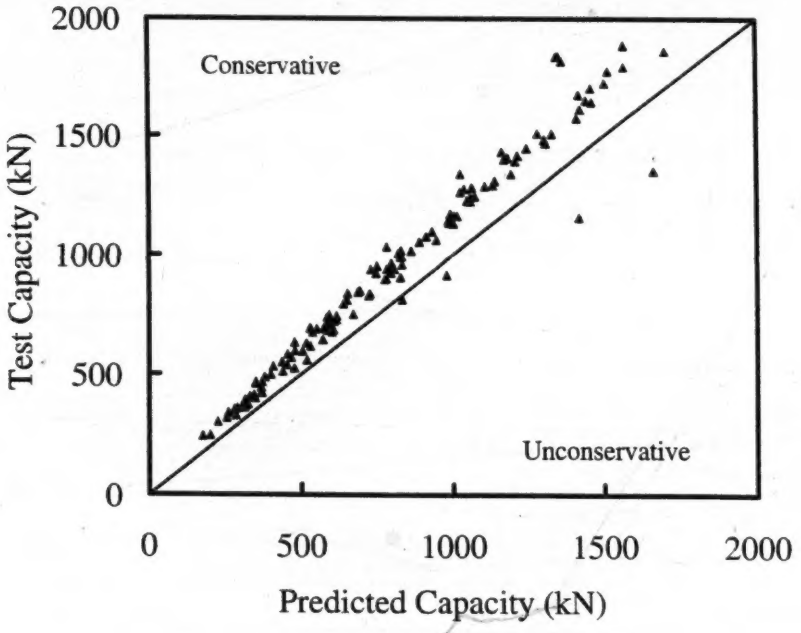

Figure 5-3 Test capacity vs. predicted capacity based on AISC 1999

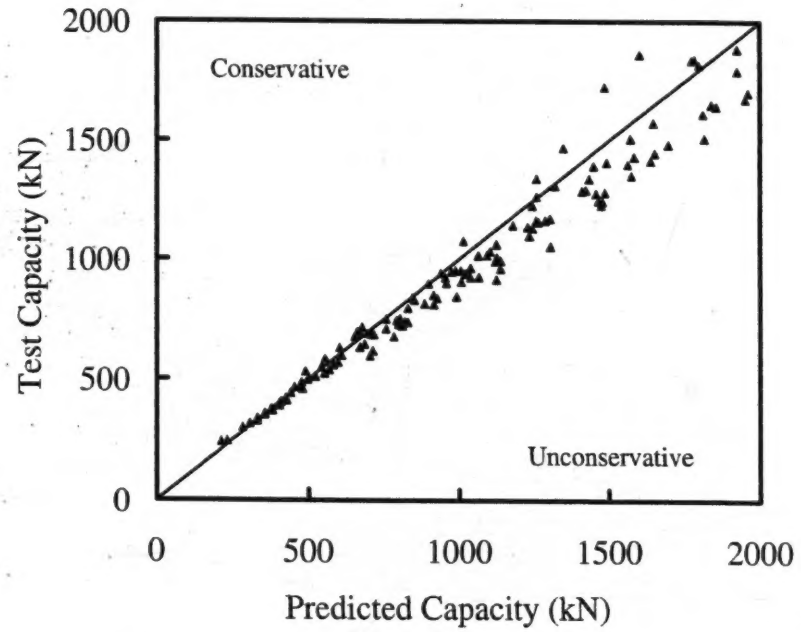

Figure 5-4 Test capacity vs. predicted capacity based on Hardash and Bjorhovde (1984)

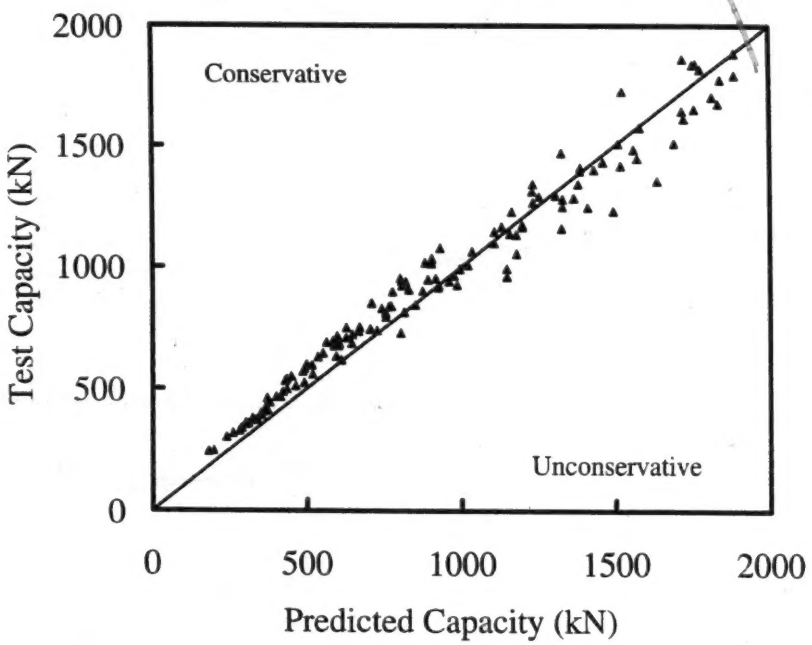

Figure 5-5 Test capacity vs. predicted capacity based on Kulak and Grondin (2001)

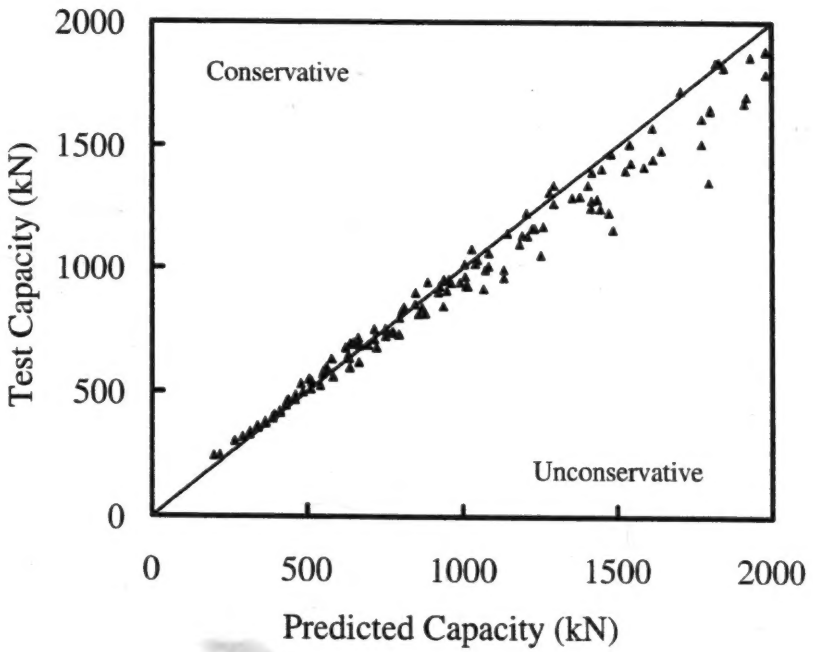

Figure 5-6 Test capacity vs. predicted capacity based on proposed new equation

CHAPTER 6

SUMMARY, CONCLUSIONS AND RECOMMENDATIONS

6.1 Summary

A review of the literature on block shear in gusset plates has revealed that although several experimental programs have been conducted to investigate block shear in gusset plates, the exact failure sequence is not well understood. A finite element procedure, using the commercial finite element analysis software ABAQUS, was developed to investigate the rupture sequence in a block shear failure mode. A mesh refinement study indicated that convergence of strains occurs with a much finer mesh than previously used in other similar research projects. A mesh size that consisted of 32 elements between bolt holes provided satisfactory convergence. A blunt crack approach was implemented to model block shear failure. In this approach, rupture on the tension and shear faces of the block shear failure surface was modelled by removing elements once the maximum localized shear strain had reached a magnitude of 130%. This critical rupture strain is substantiated by the results of tension coupon tests. Close examination of four gusset plate specimens tested as part of this research indicated that tension fracture occurs over most of the tension area at once, whereas shear fracture occurs gradually. The finite element analysis simulated this fracture progression by removing all the elements along the tension plane once the critical strain was reached at the edge of the end bolt holes and removing elements along the shear faces as the critical strain was attained.

A total of ten gusset plates were analysed to compare test results with the load response obtained using the proposed finite element analysis. Good correlation was observed between the predicted and the measured load resistance. The finite element model was able to predict deformations accurately only in a limited number of cases.

A review of the literature indicated that although a large number of tests had been conducted on gusset plates where block shear failure was the observed failure mode, the range of gauge distances, bolt pitch, and number of bolts in a line was fairly limited. The validated finite element procedure was therefore used to expand the database of test

results to increase the range of the parameters that were identified to be limited in the test programs. Five gusset plates of different bolt patterns were analyzed for the parametric study.

The augmented database of test results was used to assess a number of strength prediction equations for block shear failure using a reliability analysis. The following presents some of the conclusions drawn from this analysis.

6.2 Conclusions

The behaviour of block shear failure of gusset plates under tensile loading was investigated using both finite element analysis and experimental program. The following conclusions can be drawn:

1. A finite element procedure whereby ductile fracture was modelled by removing elements as a critical maximum shear strain of 130% is reached provides a good prediction of block shear capacity. Although tension fracture occurred earlier in the finite element analysis, there are strong resemblances to the failure progression observed in test specimens.

2. For the majority of cases examined, the peak capacity was reached at the time tension fracture took place. In all cases examined at least 95% of the shear capacity had been mobilized by the time tension fracture occurred.

3. Current design standard CSA–S16–01 provides a safety index of 4.5 for block shear failure in gusset plates.

4. AISC Specification failed to predict the correct failure mode in 106 out of 133 cases investigated.

5. The design equation proposed by Kulak and Grondin (2001), which consists of net tension area rupture plus gross shear area yield, provides a safety index of 3.46 when a resistance factor of 0.9 is used.

6.3 Recommendations

Many equations have been proposed to predict block shear capacity of gusset plates. These equations include the CAN/CSA–S16.1–94 equation, CSA–S16–01 equation, AISC equation, Hardash and Bjorhovde's equation and Kulak and Grondin's equation. A comparison of predicted capacities with a large number of test results showed that these equations can predict the block shear capacity quite well, with an average test to predicted ratio from 0.95 to 1.19. Only the equations proposed by Hardash and Bjorhovde (1984) and by Kulak and Grondin (2001) use the gross cross-sectional area exclusively on the shear planes as the effective shear failure area. All other models are based on the assumption that rupture on the net shear area is a possible failure mode. This assumption is not supported by test observations. Based on the experimental and numerical analysis investigations presented, the following design equation, which is identical to the equation proposed by Franchuk *et al.* (2002) for coped beams, is recommended:

$$P_r = \phi R_t A_{nt} F_u + \phi A_{gv} \left(\frac{F_Y + F_u}{2\sqrt{3}} \right) \tag{6-1}$$

where R_t is taken as 1.0 and ϕ is taken as 0.75. This equation is consistent with the observed block shear failure mechanism and provides a safety index of 4.4.

The finite element analysis conducted in this research program was not capable of accurately predicting the full load vs. deformation behaviour of gusset plates. Although the load carrying capacity was predicted accurately and the overall load response was predicted well, the predicted deformation response did not match the test results well. It is expected that a crack model that accounts for the stress intensity in the crack tip region and a ductile fracture model would likely lead to a more accurate representation of the displacement response. It is also expected that these improvements to the model would provide a more robust model that can be applied to block shear problems in eccentrically loaded members such as coped beams and structural tees.

REFERENCES

Aalberg, A. and Larsen, P. K. (1999) "Strength and Ductility of Bolted Connections in Normal and High Strength Steels," Department of Structural Engineering, Norwegian University of Science and Technology, N-7034, Trondheim, Norway.

American Institute of Steel Construction, (1995) "Load and Resistance Factor Design Specification," Chicago, Illinois.

American Institute of Steel Construction, (1999) "Load and Resistance Factor Design Specification," Chicago, Illinois.

ASTM 370-97a, (1997) Standard test methods and definitions for mechanical testing of steel products. American Society for Testing and Materials, Philadelphia, PA.

Birkemoe, P. C. and Gilmor, M. I. (1978) "Behaviour of Bearing Critical Double-Angle Beam Connections," Engineering Journal, AISC, Vol. 15, No. 4, Fourth Quarter, pp. 109-115.

Bjorhovde, R. and Chakrabarti, S. K. (1985) "Tests of Full-Size Gusset plate Connections," Journal of Structural Engineering, ASCE, Vol. 111, No. 3, pp. 667-684.

CAN/CSA–G40.21–98, (1998) "General Requirements for Structural Quality Steels," Canadian Standards Association, Toronto, Ontario.

CAN/CSA–S16.1–M89, (1989) "Limit States Design of Steel Structures," Canadian Standards Association, Toronto, Ontario.

CAN/CSA–S16.1–M94, (1994) "Limit States Design of Steel Structures," Canadian Standards Association, Toronto, Ontario.

CSA–S16–01, (2001) "Limit States Design of Steel Structures," Canadian Standard Association, Toronto, Ontario.

Davis, C. S. (1967) "Computer Analysis of the Stresses in a Gusset Plate," Master of Science Thesis, University of Washington, Seattle.

Epstein, H. I. and Chamarajanagar, R. (1996) "Finite Element Studies for Correlation with Block Shear Tests," Computers and Structures, Vol. 61, No. 5, pp. 967-974.

Fisher, J. W. and Struik J. H. A. (1974) "Guide to Design Criteria for Bolted and Riveted Structural Joints," John Wiley & Sons, New York, N.Y.

Franchuk, C. R., Driver, R. G. and Grondin, G. Y. (2002) "Block Shear Behaviour of Coped Steel Beams," Structural Engineering Report 244, Department of Civil and Environmental Engineering, University of Alberta, Edmonton.

Galambos, T. V. and Ravindra, M. A. (1977) "The Basis for Load and Resistance Factor Design Criteria of Steel Building Structures," Canadian Journal of Civil Engineering, Vol. 4, No. 3, pp. 178-189.

Galambos, T. V. and Ravindra, M. A. (1978) "Properties of Steel for Use in LRFD," ASCE Journal of Structural Engineering, Vol 104, No. ST, pp. 1459-1468.

Hardash, S. G. and Bjorhovde, R. (1984) "Gusset Plate Design Utilizing Block-Shear Concepts," The Department of Civil Engineering and Engineering Mechanics, University of Arizona, Tucson, Arizona.

Hardin, B. O. (1958) "Experimental Investigation of the Primary Stress Distribution in the Gusset Plates of a Double Plane Pratt Truss Joint with Chord Splice at the Joint," Bulletin No. 49, Engineering Experiment Station, University of Kentucky, September.

Hibbitt, Karlsson and Sorensen (1998) ABAQUS Version 5.8, ABAQUS/Standard User's Manual: Volumes 1, 2, and 3.

Hu, S. Z. and Cheng, J. J. R. (1987) "Compressive Behaviour of Gusset Plate Connections," Structural Engineering Report 244, Department of Civil and Environmental Engineering, University of Alberta, Edmonton.

Irvan, W. G. (1957) "Experimental Study of Primary Stresses in Gusset Plates of a Double Plane Pratt Truss," Bulletin No. 46, Engineering Experiment Station, University of Kentucky, December.

Kennedy, D. J. L. and Gad Aly, M. (1980) "Limit States Design of Steel Structures-Performance Factors," Canadian Journal of Civil Engineers, Vol. 7, pp. 45-77.

Khoo, H. A. Cheng, J. J. R. and Hrudey, T. M. (2000) "Ductile Fracture of Steel," Structural Engineering Report No. 232, Department of Civil and Environmental Engineering, University of Alberta, Edmonton, Alberta.

Kulak, G. L., Fisher, J. W. and Struik, J. H. (1987) "Guide to Design Criteria for Bolted and Riveted Joints, Second Edition," John Wiley and Sons, Inc. New York, pp. 44-49.

Kulak, G. L. and Grondin, G. Y. (2001) "Block Shear Failure in Steel Members – A Review of Design Practice," Engineering Journal, American Institute of Steel Construction, Vol. 38, No. 4, pp. 199-203.

MacGregor, J. G. (1976) "Safety and Limit States Design for Reinforced Concrete," Canadian Journal of Civil Engineering, Vol. 3, No. 4. pp. 484-513.

Menzemer, C. C., Fei, L. and Srivatsan, T. S. (1999) "Failure of Bolted Connections in an Aluminium Alloy," Journal of Materials Engineering and Performance, Vol. 8, No. 2, pp. 197-204.

Mullin, D. (2002) Unpublished test data. Department of Civil and Environmental Engineering, University of Alberta, Edmonton, Alberta.

Nast, T. E., Grondin, G. Y. and Cheng, J. J. R. (1999) "Cyclic Behaviour of Stiffened Gusset Plate-Brace Member Assemblies," Structural Engineering Report 229, Department of Civil and Environmental Engineering, University of Alberta, Edmonton, Alberta.

Research Council on Riveted and Bolted Structural Joints (1976), "Specification for Joints Using ASTM A325 or A490 Bolts," Chicago, Illinois.

Rabinovitch, J. S. and Cheng J. J. R. (1993) "Cyclic Behaviour of Steel Gusset Plate Connections," Structural Engineering Report 191, Department of Civil Engineering, University of Alberta, Edmonton, Alberta.

Ricles, J. R. and Yura, J. A. (1983) "Strength of Double-Row Bolted Web Connections," Journal of Structural Division, ASCE, No.ST1, Vol.109, January, pp. 126-142.

Schmidt, B. J. and Bartlett, F. M. (2002) "Review of Resistance Factor for Steel: Data Collection," Canadian Journal of Civil Engineering, Vol. 29, pp. 98-108.

Swanson, J. A. and Leon, R.T. (2000) "Bolted Steel Connections: Tests on T-Stub Components," Journal of Structural Engineering, ASCE, Vol. 126, No. 1, pp. 50-56.

Udagawa, K. and Yamada, T. (1998) "Failure Modes and Ultimate Tensile Strength of Steel Plates Jointed with High-Strength Bolts," Journal of Structural and Construction Engineering, Architectural Institute of Japan, No. 505, pp. 115-122.

Varsarelyi, D. D. (1971) "Test of Gusset Plate Models," Journal of Structural Division, ASCE, Vol. 97, No. ST2, February, pp. 665-678.

Walbridge, S. S., Grondin, G. Y. and Cheng, J. J. R. (1998) "An Analysis of the Cyclic Behaviour of Steel Gusset Plate Connections," Structural Engineering Report 225, Department of Civil and Environmental Engineering, University of Alberta, Edmonton, Alberta.

Whitmore, R. E. (1952) "Experimental Investigation of Stresses in Gusset Plates," Bulletin No. 16, Engineering Experiment Station, University of Tennessee, May.

Yam, C. H. M. and Cheng, J. J. R. (1993) "Experimental Investigation of the Compressive Behaviour of Gusset Plate Connections," Structural Engineering Report No. 194, Department of Civil and Environmental Engineering, University of Alberta, Edmonton, Alberta.

Yura, J. A., Birkemoe, P. C. and Ricles, J. M. (1982) " Double Angle Beam Web Connections: An Experimental Study," Journal of the Structural Division, ASCE, Vol. 108, No. ST2, February, pp. 311-325.

APPENDIX A

Published Gusset Plate Test Results

APPENDIX A

A summary of gusset plates that have been tested by various researchers and have failed in block shear is presented in this appendix. Table A-1 presents the dimensions of the gusset plates and bolt patterns, which include plate thickness, bolt end distance, edge distance, pitch and gauge dimensions, hole diameter, the number of bolt lines, the number of bolts per line, the yield and ultimate tensile strength of the gusset plate, and the reported test capacity. The dimensions presented in Table A-1 are defined in Figure A-1 for the three gusset plate geometries that have been tested.

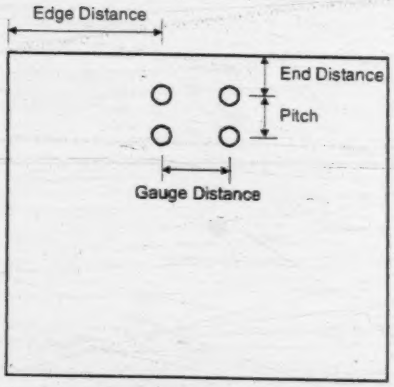

(a) Rectangular gusset plate

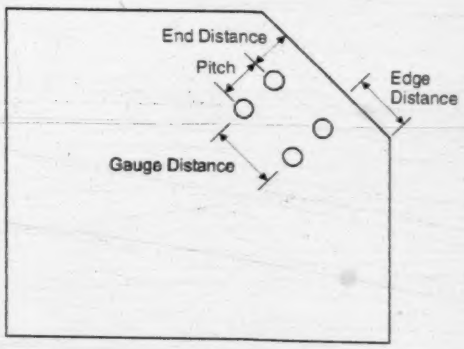

(b) Corner gusset plate

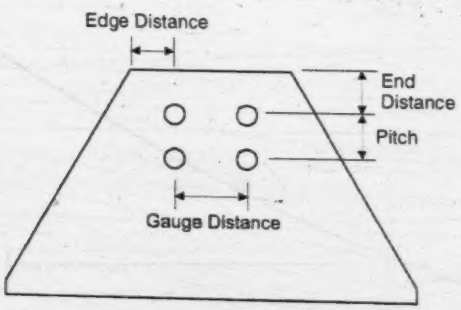

(c) Trapezoidal gusset plate

Figure A-1 Definition of dimensional parameters

Table A-1
Summary of gusset plate specimens

Specimen	Plate Thickness (mm)	End Distance (mm)	Edge Distance (mm)	Pitch (mm)	Hole Diameter (mm)	Gauge (mm)	Number of Bolt Lines	Number of Bolts Per Bolt Line	Yield Stress (MPa)	Ultimate Stress (MPa)	Test Capacity (kN)
Hardash and Bjorhovde (1984) - *Rectangular gusset plate*											
1	6.0	28	104	38	14	51	2	2	229	323	243
2	6.0	38	104	38	14	51	2	2	229	323	246
3	6.0	25	114	38	14	51	2	3	229	323	301
4	6.0	25	161	51	14	51	2	3	229	323	327
5	6.0	38	161	38	14	51	2	3	229	323	318
6	6.0	38	161	51	14	51	2	3	229	323	361
7	6.0	25	161	38	14	76	2	3	229	323	339
8	6.0	25	161	51	14	76	2	3	229	323	371
9	6.0	38	161	38	14	76	2	3	229	323	359
10	6.0	38	161	51	14	76	2	3	229	323	400
11	6.0	25	161	38	14	102	2	3	229	323	375
12	6.0	41	171	38	14	102	2	3	229	323	407
13	6.0	25	161	38	14	51	2	4	229	323	354
14	6.0	25	161	51	14	51	2	4	229	323	423
15	6.0	38	161	38	14	51	2	4	229	323	379
16	6.0	38	169	51	17	51	2	4	229	323	444
17	6.0	25	161	38	14	76	2	4	229	323	392
18	6.4	25	218	51	14	76	2	4	341	445	687
19	6.0	38	171	38	14	76	2	4	229	323	413
20	6.0	38	217	51	17	76	2	4	229	323	532
21	6.0	25	218	38	14	102	2	4	229	323	467
22	6.0	25	218	51	14	102	2	4	229	323	511
23	6.0	38	218	38	14	102	2	4	229	323	488
24	6.0	42	221	51	14	102	2	4	229	323	525
25	6.0	25	218	38	14	76	2	5	229	323	468
26	6.0	25	217	51	17	76	2	5	229	323	584
27	6.0	38	218	38	14	76	2	5	229	323	498
28	6.0	38	228	51	14	76	2	5	229	323	559

Table A-1
Cont'd

Specimen	Plate Thickness (mm)	End Distance (mm)	Edge Distance (mm)	Pitch (mm)	Hole Diameter (mm)	Gauge (mm)	Number of Bolt Lines	Number of Bolts Per Bolt Line	Yield Stress (MPa)	Ultimate Stress (MPa)	Test Capacity (kN)
Udagawa and Yamada (1998) - *Rectangular gusset plate*											
221.4	12.0	23	101	40	18	40	2	2	278	443	461
222.4	12.0	40	101	40	18	40	2	2	278	443	540
223.4	12.0	24	88	40	18	64	2	2	278	443	598
224.4	12.0	40	88	40	18	64	2	2	278	443	691
23E.4	12.0	24	100	40	18	40	2	3	266	452	596
23F.4	12.0	40	99	40	18	41	2	3	280	444	677
23G.4	12.0	24	87	40	18	65	2	3	280	452	737
23H.4	12.0	40	88	40	18	64	2	3	266	444	852
23I.4	12.0	24	79	40	18	81	2	3	280	452	812
23J.4	12.0	40	80	40	18	81	2	3	266	452	954
241.4	12.0	24	24	40	18	64	2	4	278	443	940
242.4	12.0	40	40	40	18	64	2	4	278	443	1018
243.4	12.0	24	24	40	18	80	2	4	278	443	1034
321.4	12.0	23	23	40	18	40	3	2	278	443	571
322.4	12.0	40	40	40	18	40	3	2	278	443	645
323.4	12.0	32	32	40	18	64	3	2	278	443	899
324.4	12.0	39	39	40	18	64	3	2	278	443	942
325.4	12.0	23	23	40	18	64	3	2	278	443	830
336.4	12.0	24	24	40	18	40	3	3	278	443	722
337.4	12.0	24	24	40	18	64	3	3	278	443	1016
422.4	12.0	40	40	40	18	40	4	2	278	443	752
423.4	12.0	24	24	40	18	40	4	2	278	443	685
435.4	12.0	64	64	40	18	40	4	3	278	443	916
438.4	12.0	24	24	40	18	40	4	3	278	443	838
439.4	12.0	40	40	40	18	40	4	3	278	443	907

Table A-1
Cont'd

Specimen	Plate Thickness (mm)	End Distance (mm)	Edge Distance (mm)	Pitch (mm)	Hole Diameter (mm)	Gauge (mm)	Number of Bolt Lines	Number of Bolts Per Bolt Line	Yield Stress (MPa)	Ultimate Stress (MPa)	Test Capacity (kN)
Udagawa and Yamada (1998) Cont'd											
221.6	12.0	24	100	40	18	40	2	2	476	601	634
222.6	12.0	40	100	40	18	40	2	2	474	598	746
223.6	12.0	24	88	40	18	64	2	2	477	601	840
224.6	12.0	40	88	40	18	64	2	2	482	602	950
23E.6	12.0	24	100	40	18	40	2	3	459	616	845
23F.6	12.0	40	101	40	18	40	2	3	447	590	926
23G.6	12.0	24	88	40	18	64	2	3	447	590	993
23H.6	12.0	40	88	40	18	64	2	3	459	516	1164
23I.6	12.0	24	88	40	18	80	2	3	447	590	1099
23J.6	12.0	40	80	40	18	80	2	3	459	616	1289
241.6	12.0	24	88	40	18	64	2	4	481	605	1277
242.6	12.0	40	88	40	18	64	2	4	478	600	1401
243.6	12.0	24	80	40	18	80	2	4	486	607	1432
321.6	12.0	24	80	40	18	40	3	2	473	598	797
322.6	12.0	40	80	40	18	40	3	2	482	604	903
323.6	12.0	32	64	40	18	64	3	2	482	604	1226
324.6	12.0	40	64	40	18	64	3	2	486	612	1311
325.6	12.0	24	40	40	18	64	3	2	480	601	1144
336.6	12.0	24	80	40	18	40	3	3	472	595	1008
337.6	12.0	24	72	40	18	64	3	3	481	608	1409
422.6	12.0	40	60	40	18	40	4	2	482	608	1063
423.6	12.0	24	60	40	18	40	4	2	478	601	954
438.6	12.0	24	80	40	18	40	4	3	482	604	1171
439.6	12.0	40	80	40	18	40	4	3	479	603	1293

Table A-1
Cont'd

Specimen	Plate Thickness (mm)	End Distance (mm)	Edge Distance (mm)	Pitch (mm)	Hole Diameter (mm)	Gauge (mm)	Number of Bolt Lines	Number of Bolts Per Bolt Line	Yield Stress (MPa)	Ultimate Stress (MPa)	Test Capacity (kN)
Udagawa and Yamada (1998) Cont'd											
221.8	12.0	24	100	40	18	40	2	2	679	736	740
222.8	12.0	40	100	40	18	40	2	2	681	778	927
223.8	12.0	23	88	40	18	64	2	2	622	742	965
224.8	12.0	40	88	40	18	64	2	2	574	775	1163
23E.8	12.0	24	100	40	18	40	2	3	648	800	1055
23F.8	12.0	40	100	40	18	40	2	3	649	801	1247
23G.8	12.0	19	68	40	18	64	2	3	649	801	1283
23H.8	12.0	40	68	40	18	64	2	3	648	800	1484
23I.8	12.0	19	80	40	18	80	2	3	649	801	1417
23J.8	12.0	40	80	40	18	80	2	3	648	800	1644
241.8	12.0	24	88	40	18	64	2	4	619	749	1511
242.8	12.0	40	88	40	18	64	2	4	610	751	1703
243.8	12.0	24	80	40	18	80	2	4	620	746	1676
321.8	12.0	24	80	40	18	40	3	2	622	742	942
322.8	12.0	40	80	40	18	40	3	2	671	780	1132
323.8	12.0	32	64	40	18	64	3	2	650	761	1509
324.8	12.0	39	64	40	18	64	3	2	650	761	1575
325.8	12.0	24	40	40	18	64	3	2	620	741	1395
336.8	12.0	23	80	40	18	40	3	3	674	775	1244
337.8	12.0	24	72	40	18	64	3	3	631	742	1652
422.8	12.0	40	60	40	18	40	4	2	669	767	1340
423.8	12.0	24	60	40	18	40	4	2	613	742	1136
438.8	12.0	24	80	40	18	40	4	3	650	761	1448
439.8	12.0	40	80	40	18	40	4	3	650	761	1613

Table A-1
Cont'd

Specimen	Plate Thickness (mm)	End Distance (mm)	Edge Distance (mm)	Pitch (mm)	Hole Diameter (mm)	Gauge (mm)	Number of Bolt Lines	Number of Bolts Per Bolt Line	Yield Stress (MPa)	Ultimate Stress (MPa)	Test Capacity (kN)
Mullin (2002) - *Trapezodal gusset plate*											
12U	6.8	38	51	76	21	102	2	6	317	435	1469
14U	6.8	38	51	76	21	102	2	7	317	435	1725
8U	6.8	38	51	76	21	102	2	4	317	435	1078
4U	6.8	38	51	76	21	102	2	2	317	435	631
16U	6.8	38	51	76	21	102	2	8	317	435	1862
Nast *et al.* (1999) - *Corner gusset plate*											
T-2	9.6	50	56	70	27	70	2	5	424	491	1819
T-3	9.5	50	56	70	27	70	2	5	408	478	1837
T-4	9.5	50	56	70	27	70	2	5	409	484	1841
Swanson and Leon (2000) - *Rectangular gusset plate*											
TA	14.9	33	32	64	27	89	2	4	352	469	1776
Aalberg and Larsen (1999) - *Rectangular gusset plate*											
T7 S355	8.4	38	151	48	19	48	2	2	373	537	551
T8 Weldox	7.7	38	151	48	19	48	2	2	786	822	730
T9 S355	8.4	38	151	48	19	48	2	3	373	537	751
T10 Weldox	7.7	38	151	48	19	48	2	3	786	822	994
T11 S355	8.4	38	151	48	19	48	2	4	373	537	925
T12 Weldox	7.7	38	151	48	19	48	2	4	786	822	1229
T15 S355	8.4	38	131	48	19	48	2	3	373	537	710
T16 Weldox	7.7	38	131	48	19	48	2	3	786	822	961
Rabinovitch and Cheng (1993) - *Corner gusset plate*											
A-1	9.3	50	50	70	22	70	2	5	449	537	1794
A-2	6.2	50	50	70	22	70	2	5	443	530	1340
A-3	9.3	50	50	70	22	70	2	5	449	537	1884
A-4	6.2	50	50	70	22	70	2	5	443	530	1265
A-5	9.3	50	50	70	22	70	2	5	449	537	1887

Table A-1
Cont'd

Specimen	Plate Thickness (mm)	End Distance (mm)	Edge Distance (mm)	Pitch (mm)	Hole Diameter (mm)	Gauge (mm)	Number of Bolt Lines	Number of Bolts Per Bolt Line	Yield Stress (MPa)	Ultimate Stress (MPa)	Test Capacity (kN)
Current Investigation - *Rectangular gusset plate*											
T1A	6.5	38	178	76	21	51	2	3	336	450	696
T1B	6.6	38	178	76	21	51	2	3	336	450	691
T1C	6.6	38	178	76	21	51	2	3	336	450	716
T2B	6.5	25	127	51	21	51	4	3	336	450	691
T2C	6.5	25	127	51	21	51	4	3	336	450	693
Plate 1	6.0	35	350	70	14	35	2	8	336	450	1158
Plate 2	6.0	35	350	70	14	150	2	8	336	450	1354
Plate 3	20.0	18	30	35	14	35	2	2	336	450	618
Plate 4	12.7	18	30	35	14	70	2	2	336	450	676
Plate 5	6.0	70	150	140	27	140	2	2	336	450	815

APPENDIX B

Summary of Predicted Gusset Plate Capacities

APPENDIX B

Table B-1 summarizes the block shear capacity of the tested gusset plates and the associated predicted block shear capacity calculated using various equations, namely, CAN/CSA–S16.1–94, CSA–S16–01, AISC 1999, Hardash and Bjorhovde (1984), Kulak and Grondin (2001) and the equation recommended herein. Table B-2 presents the test–to-predicted ratios from the published test data presented in Appendix A. The predicted capacities were obtained using the equations presented in Chapter 5.

Table B-1

Summary of measured and predicted capacities of published test data

Specimen	Block Shear Capacity (kN)						
	Experimental	CAN/CSA S16.1-94	CSA S16-01	AISC 1999	Hardash and Bjorhovde (1984)	Kulak and Grondin (2001)	New Equation
Hardash and Bjorhovde (1984)							
1	243	175	175	174	211	180	198
2	246	199	197	198	232	197	217
3	301	225	225	224	283	239	266
4	327	284	281	283	332	281	315
5	318	255	255	254	307	260	290
6	361	314	302	313	356	302	339
7	339	274	274	259	332	289	316
8	371	334	331	318	381	331	364
9	359	304	304	289	357	310	340
10	400	363	352	348	405	352	389
11	375	324	324	324	381	338	365
12	407	359	359	329	411	363	394
13	354	281	281	280	356	302	339
14	423	370	365	369	425	365	412
15	379	310	310	309	379	323	364
16	444	367	367	367	441	380	431
17	392	330	330	315	405	352	389
18	687	615	615	605	710	645	695
19	413	360	360	344	428	373	413
20	532	417	417	407	491	429	480
21	467	379	379	350	454	401	438
22	511	468	464	439	524	464	511
23	488	409	409	379	478	422	462
24	525	507	491	477	553	491	543
25	468	386	386	370	474	415	462
26	584	465	465	455	555	492	553
27	498	415	415	400	497	436	486
28	559	534	520	518	582	520	584

Table B-1

Cont'd

Specimen	Block Shear Capacity (kN)						
	Experimental	CAN/CSA S16.1-94	CSA S16-01	AISC 1999	Hardash and Bjorhovde (1984)	Kulak and Grondin (2001)	New Equation
Udagawa and Yamada (1998)							
221.4	461	349	349	349	480	370	434
222.4	540	453	435	453	568	435	514
223.4	598	479	479	479	610	499	563
224.4	691	583	565	551	698	565	644
23E.4	596	504	504	504	703	518	637
23F.4	677	601	601	601	782	604	723
23G.4	737	626	626	594	829	667	770
23H.4	852	738	709	693	914	709	847
23I.4	812	714	714	650	916	754	857
23J.4	954	831	801	749	1007	801	939
241.4	940	760	760	728	1020	819	963
242.4	1018	861	861	830	1095	882	1042
243.4	1034	845	845	782	1105	904	1048
321.4	571	466	466	466	597	487	551
322.4	645	570	553	570	686	553	632
323.4	899	775	775	775	898	776	848
324.4	942	824	807	807	939	807	886
325.4	830	721	721	721	852	742	805
336.4	722	608	608	608	810	648	751
337.4	1016	863	863	863	1065	903	1007
422.4	752	689	670	670	803	670	750
423.4	685	585	585	585	716	606	669
435.4	916	980	925	980	1125	925	1068
438.4	838	725	725	725	927	765	868
439.4	907	827	827	827	1008	829	948
221.6	634	478	478	478	670	596	635
222.6	746	616	616	616	792	705	753
223.6	840	652	652	652	844	771	810
224.6	950	798	798	798	976	892	938
23E.6	845	686	686	686	992	850	937

Table B-1

Cont'd

Specimen	Block Shear Capacity (kN)						
	Experimental	CAN/CSA S16.1-94	CSA S16-01	AISC 1999	Hardash and Bjorhovde (1984)	Kulak and Grondin (2001)	New Equation
Udagawa and Yamada (1998) (Cont'd)							
23F.6	926	791	791	791	1067	928	1017
23G.6	993	828	828	828	1123	996	1074
23H.6	1164	1005	1005	1005	1289	1133	1234
23I.6	1099	940	940	931	1235	1108	1186
23J.6	1289	1127	1127	1109	1411	1255	1356
241.6	1277	1040	1040	1040	1458	1331	1418
242.6	1401	1171	1171	1171	1564	1433	1528
243.6	1432	1164	1164	1164	1585	1462	1546
321.6	797	639	639	639	829	755	795
322.6	903	780	780	780	959	874	921
323.6	1226	1059	1059	1059	1245	1167	1209
324.6	1311	1141	1141	1141	1321	1233	1282
325.6	1144	988	988	988	1180	1110	1147
336.6	1008	821	821	821	1127	1022	1085
337.6	1409	1183	1183	1183	1494	1388	1451
422.6	1063	946	946	946	1125	1037	1086
423.6	954	797	797	797	989	917	955
438.6	1171	993	993	993	1304	1201	1262
439.6	1293	1134	1134	1134	1424	1308	1381
221.8	740	585	585	585	819	726	776
222.8	927	796	796	796	1039	987	1011
223.8	965	798	798	798	1040	977	1008
224.8	1163	1016	1016	1016	1258	1201	1228
23E.8	1055	890	890	890	1306	1182	1254
23F.8	1247	1074	1074	1074	1467	1331	1415
23G.8	1283	1065	1065	1065	1487	1367	1436
23H.8	1484	1305	1305	1305	1697	1562	1645
23I.8	1417	1217	1217	1217	1640	1519	1589
23J.8	1644	1463	1463	1463	1855	1720	1803
241.8	1511	1282	1282	1282	1816	1694	1774

Table B-1

Cont'd

Specimen	Block Shear Capacity (kN)						
	Experimental	CAN/CSA S16.1-94	CSA S16-01	AISC 1999	Hardash and Bjorhovde (1984)	Kulak and Grondin (2001)	New Equation
Udagawa and Yamada (1998) (Cont'd)							
242.8	1703	1460	1460	1460	1961	1816	1920
243.8	1676	1419	1419	1419	1952	1836	1913
321.8	942	782	782	782	1024	960	992
322.8	1132	1003	1003	1003	1245	1182	1213
323.8	1509	1330	1330	1330	1573	1512	1541
324.8	1575	1413	1413	1413	1648	1582	1615
325.8	1395	1209	1209	1209	1450	1386	1418
336.8	1244	1060	1060	1060	1479	1412	1447
337.8	1652	1444	1444	1444	1840	1759	1803
422.8	1340	1196	1196	1196	1435	1381	1406
423.8	1136	989	989	989	1230	1160	1195
438.8	1448	1246	1246	1246	1653	1574	1617
439.8	1613	1423	1423	1423	1812	1725	1775
Mullin (2002)							
12U	1469	1329	1327	1308	1350	1327	1481
14U	1725	1526	1525	1506	1487	1525	1707
8U	1078	933	932	912	1016	932	1030
4U	631	537	537	516	602	537	579
16U	1862	1724	1723	1704	1604	1723	1933
Nast *et al.* (1999)							
T-2	1819	1364	1364	1364	1798	1779	1846
T-3	1837	1345	1345	1345	1774	1755	1821
T-4	1841	1352	1352	1352	1783	1764	1831
Rabinovitch and Cheng (1993)							
A-1	1794	1570	1570	1570	1924	1888	1982
A-2	1340	1027	1027	1027	1259	1235	1297
A-3	1884	1570	1570	1570	1924	1888	1982
A-4	1265	1027	1027	1027	1259	1235	1297
A-5	1887	1570	1570	1570	1924	1888	1982

Table B-1

Cont'd

Specimen	Block Shear Capacity (kN)						
	Experimental	CAN/CSA S16.1-94	CSA S16-01	AISC 1999	Hardash and Bjorhovde (1984)	Kulak and Grondin (2001)	New Equation
Swanson and Leon (2000)							
TA	1776	1517	1517	1517	2023	1842	2014
Aalberg and Larsen (1999)							
T7 S355	551	437	437	437	544	450	506
T8 Weldox	730	615	615	615	799	803	794
T9 S355	751	591	591	591	756	629	716
T10 Weldox	994	832	832	832	1139	1149	1134
T11 S355	925	746	746	746	955	807	925
T12 Weldox	1229	1049	1049	1049	1476	1495	1475
T15 S355	710	591	591	591	756	629	716
T16 Weldox	961	832	832	832	1139	1149	1134
Current Investigation							
T1A	696	575	575	575	662	586	649
T1B	691	583	583	583	671	594	658
T1C	716	588	588	588	677	600	664
T2B	691	531	531	531	663	600	642
T2C	693	528	528	528	659	596	638
Plate 1	1158	1419	1328	1419	1266	1328	1487
Plate 2	1354	1730	1639	1665	1576	1639	1798
Plate 3	618	530	530	530	713	613	666
Plate 4	676	537	537	537	653	589	623
Plate 5	815	855	814	832	885	814	878

Table B-2

Test to predicted ratios for various resistance equations

Specimen	Test/Predicted Ratio					
	CAN/CSA S16.1-94	CSA S16-01	AISC 1999	Hardash and Bjorhovde (1984)	Kulak and Grondin (2001)	New Equation
Hardash and Bjorhovde (1984)						
1	1.39	1.39	1.39	1.15	1.35	1.23
2	1.23	1.25	1.24	1.06	1.25	1.13
3	1.34	1.34	1.34	1.06	1.26	1.13
4	1.15	1.16	1.16	0.99	1.16	1.04
5	1.25	1.25	1.25	1.03	1.22	1.09
6	1.15	1.19	1.15	1.01	1.19	1.06
7	1.24	1.24	1.31	1.02	1.17	1.07
8	1.11	1.12	1.17	0.97	1.12	1.02
9	1.18	1.18	1.24	1.00	1.16	1.05
10	1.10	1.14	1.15	0.99	1.14	1.03
11	1.16	1.16	1.16	0.98	1.11	1.03
12	1.13	1.13	1.24	0.99	1.12	1.03
13	1.26	1.26	1.27	0.99	1.17	1.04
14	1.14	1.16	1.15	0.99	1.16	1.02
15	1.22	1.22	1.23	1.00	1.17	1.04
16	1.21	1.21	1.21	1.01	1.17	1.03
17	1.19	1.19	1.25	0.97	1.11	1.01
18	1.12	1.12	1.14	0.97	1.07	0.99
19	1.15	1.15	1.20	0.96	1.11	1.00
20	1.28	1.28	1.31	1.09	1.24	1.11
21	1.23	1.23	1.34	1.03	1.16	1.07
22	1.09	1.10	1.17	0.98	1.10	1.00
23	1.19	1.19	1.29	1.02	1.16	1.05
24	1.04	1.07	1.10	0.95	1.07	0.97
25	1.21	1.21	1.26	0.99	1.13	1.01
26	1.26	1.26	1.28	1.05	1.19	1.06
27	1.20	1.20	1.25	1.00	1.14	1.02
28	1.05	1.08	1.08	0.96	1.08	0.96

Table B-2

Cont'd

Specimen	Test/Predicted Ratio					
	CAN/CSA S16.1-94	CSA S16-01	AISC 1999	Hardash and Bjorhovde (1984)	Kulak and Grondin (2001)	New Equation
Udagawa and Yamada (1998)						
221.4	1.32	1.32	1.32	0.96	1.24	1.06
222.4	1.19	1.24	1.19	0.95	1.24	1.05
223.4	1.25	1.25	1.25	0.98	1.20	1.06
224.4	1.18	1.22	1.25	0.99	1.22	1.07
23E.4	1.18	1.18	1.18	0.85	1.15	0.94
23F.4	1.13	1.13	1.13	0.87	1.12	0.94
23G.4	1.18	1.18	1.24	0.89	1.10	0.96
23H.4	1.15	1.20	1.23	0.93	1.20	1.01
23I.4	1.14	1.14	1.25	0.89	1.08	0.95
23J.4	1.15	1.19	1.27	0.95	1.19	1.02
241.4	1.24	1.24	1.29	0.92	1.15	0.98
242.4	1.18	1.18	1.23	0.93	1.15	0.98
243.4	1.22	1.22	1.32	0.94	1.14	0.99
321.4	1.22	1.22	1.22	0.96	1.17	1.04
322.4	1.13	1.17	1.13	0.94	1.17	1.02
323.4	1.16	1.16	1.16	1.00	1.16	1.06
324.4	1.14	1.17	1.17	1.00	1.17	1.06
325.4	1.15	1.15	1.15	0.97	1.12	1.03
336.4	1.19	1.19	1.19	0.89	1.11	0.96
337.4	1.18	1.18	1.18	0.95	1.13	1.01
422.4	1.09	1.12	1.12	0.94	1.12	1.00
423.4	1.17	1.17	1.17	0.96	1.13	1.02
435.4	0.93	0.99	0.93	0.81	0.99	0.86
438.4	1.16	1.16	1.16	0.90	1.10	0.96
439.4	1.10	1.10	1.10	0.90	1.09	0.96
221.6	1.33	1.33	1.33	0.95	1.06	1.00
222.6	1.21	1.21	1.21	0.94	1.06	0.99
223.6	1.29	1.29	1.29	0.99	1.09	1.04
224.6	1.19	1.19	1.19	0.97	1.06	1.01
23E.6	1.23	1.23	1.23	0.85	0.99	0.90

Table B-2

Cont'd

Specimen	Test/Predicted Ratio					
	CAN/CSA S16.1-94	CSA S16-01	AISC 1999	Hardash and Bjorhovde (1984)	Kulak and Grondin (2001)	New Equation
Udagawa and Yamada (1998) (Cont'd)						
23F.6	1.17	1.17	1.17	0.87	1.00	0.91
23G.6	1.20	1.20	1.20	0.88	1.00	0.92
23H.6	1.16	1.16	1.16	0.90	1.03	0.94
23I.6	1.17	1.17	1.18	0.89	0.99	0.93
23J.6	1.14	1.14	1.16	0.91	1.03	0.95
241.6	1.23	1.23	1.23	0.88	0.96	0.90
242.6	1.20	1.20	1.20	0.90	0.98	0.92
243.6	1.23	1.23	1.23	0.90	0.98	0.93
321.6	1.25	1.25	1.25	0.96	1.06	1.00
322.6	1.16	1.16	1.16	0.94	1.03	0.98
323.6	1.16	1.16	1.16	0.99	1.05	1.01
324.6	1.15	1.15	1.15	0.99	1.06	1.02
325.6	1.16	1.16	1.16	0.97	1.03	1.00
336.6	1.23	1.23	1.23	0.89	0.99	0.93
337.6	1.19	1.19	1.19	0.94	1.01	0.97
422.6	1.12	1.12	1.12	0.95	1.03	0.98
423.6	1.20	1.20	1.20	0.96	1.04	1.00
438.6	1.18	1.18	1.18	0.90	0.98	0.93
439.6	1.14	1.14	1.14	0.91	0.99	0.94
221.8	1.27	1.27	1.27	0.90	1.02	0.95
222.8	1.17	1.17	1.17	0.89	0.94	0.92
223.8	1.21	1.21	1.21	0.93	0.99	0.96
224.8	1.15	1.15	1.15	0.93	0.97	0.95
23E.8	1.18	1.18	1.18	0.81	0.89	0.84
23F.8	1.16	1.16	1.16	0.85	0.94	0.88
23G.8	1.21	1.21	1.21	0.86	0.94	0.89
23H.8	1.14	1.14	1.14	0.87	0.95	0.90
23I.8	1.16	1.16	1.16	0.86	0.93	0.89
23J.8	1.12	1.12	1.12	0.89	0.96	0.91
241.8	1.18	1.18	1.18	0.83	0.89	0.85

Table B-2

Cont'd

Specimen	Test/Predicted Ratio					
	CAN/CSA S16.1-94	CSA S16-01	AISC 1999	Hardash and Bjorhovde (1984)	Kulak and Grondin (2001)	New Equation
Udagawa and Yamada (1998) Cont'd						
242.8	1.17	1.17	1.17	0.87	0.94	0.89
243.8	1.18	1.18	1.18	0.86	0.91	0.88
321.8	1.20	1.20	1.20	0.92	0.98	0.95
322.8	1.13	1.13	1.13	0.91	0.96	0.93
323.8	1.13	1.13	1.13	0.96	1.00	0.98
324.8	1.12	1.12	1.12	0.96	1.00	0.98
325.8	1.15	1.15	1.15	0.96	1.01	0.98
336.8	1.17	1.17	1.17	0.84	0.88	0.86
337.8	1.14	1.14	1.14	0.90	0.94	0.92
422.8	1.12	1.12	1.12	0.93	0.97	0.95
423.8	1.15	1.15	1.15	0.92	0.98	0.95
438.8	1.16	1.16	1.16	0.88	0.92	0.90
439.8	1.13	1.13	1.13	0.89	0.93	0.91
Mullin (2002)						
12U	1.11	1.11	1.12	1.09	1.11	0.99
14U	1.13	1.13	1.15	1.16	1.13	1.01
8U	1.16	1.16	1.18	1.06	1.16	1.05
4U	1.17	1.17	1.22	1.05	1.17	1.09
16U	1.08	1.08	1.09	1.16	1.08	0.96
Nast *et al.* (1999)						
T-2	1.33	1.33	1.33	1.01	1.02	0.99
T-3	1.37	1.37	1.37	1.04	1.05	1.01
T-4	1.36	1.36	1.36	1.03	1.04	1.01
Rabinovitch and Cheng (1993)						
A-1	1.14	1.14	1.14	0.93	0.95	0.91
A-2	1.30	1.30	1.30	1.06	1.08	1.03
A-3	1.20	1.20	1.20	0.98	1.00	0.95
A-4	1.23	1.23	1.23	1.00	1.02	0.98
A-5	1.20	1.20	1.20	0.98	1.00	0.95

Table B-2

Cont'd

Specimen	Test/Predicted Ratio					
	CAN/CSA S16.1-94	CSA S16-01	AISC 1999	Hardash and Bjorhovde (1984)	Kulak and Grondin (2001)	New Equation
Swanson and Leon (2000)						
TA	1.17	1.17	1.17	0.88	0.96	0.88
Aalberg and Larsen (1999)						
T7 S355	1.26	1.26	1.26	1.01	1.22	1.09
T8 Weldox	1.19	1.19	1.19	0.91	0.91	0.92
T9 S355	1.27	1.27	1.27	0.99	1.19	1.05
T10 Weldox	1.19	1.19	1.19	0.87	0.86	0.88
T11 S355	1.24	1.24	1.24	0.97	1.15	1.00
T12 Weldox	1.17	1.17	1.17	0.83	0.82	0.83
T15 S355	1.20	1.20	1.20	0.94	1.13	0.99
T16 Weldox	1.16	1.16	1.16	0.84	0.84	0.85
Current Investigation						
T1A	1.21	1.21	1.21	1.05	1.19	1.07
T1B	1.19	1.19	1.19	1.03	1.16	1.05
T1C	1.22	1.22	1.22	1.06	1.19	1.08
T2B	1.30	1.30	1.30	1.04	1.15	1.08
T2C	1.31	1.31	1.31	1.05	1.16	1.09
Plate 1	0.82	0.87	0.82	0.91	0.87	0.78
Plate 2	0.78	0.83	0.81	0.86	0.83	0.75
Plate 3	1.17	1.17	1.17	0.87	1.01	0.93
Plate 4	1.26	1.26	1.26	1.04	1.15	1.08
Plate 5	0.95	1.00	0.98	0.92	1.00	0.93

	CAN/CSA S16.1-94	CSA S16-01	AISC 1999	Hardash and Bjorhovde (1984)	Kulak and Grondin (2001)	New Equation
Mean	1.18	1.18	1.19	0.95	1.07	0.98
C.O.V	0.071	0.065	0.071	0.074	0.099	0.075